PHD THESIS

FROM HYDROCARBONS TO CARBON NANOSTRUCTURES: A THEORETICAL ANALYSIS OF SURFACE-CATALYSED CYCLODEHYDROGENATION

DEPARTAMENTO DE FISICA TEORICA DE LA MATERIA CONDENSADA

FACULTAD DE CIENCIAS

UNIVERSIDAD AUTONOMA DE MADRID

Author:
GIULIO BIDDAU

Thesis Supervisor:
RUBEN PEREZ

ALL HUMAN BEINGS ARE BORN FREE AND EQUAL IN DIGNITY AND RIGHTS. THEY ARE ENDOWED WITH REASON AND CONSCIENCE AND SHOULD ACT TOWARDS ONE ANOTHER IN A SPIRIT OF BROTHERHOOD.

United Nations General Assembly resolution 217 A (III) of 10 December 1948

Acknowledgements (Giulio's Version)

My adsorption on C-V (now C-05) room 503 has reached is stable configuration, but time has reached to diffuse further than the saddle point achieved today that these lines are read. Tomorrow the space will be explored in different configurations towards the synthesis of an appropriate life configuration.

This thesis has no dedication, it would have been too obvious to dedicate to my family, they have been essential all along and they know that. I decided then to put one statement I always felt extremely significant and, in particular in these days.

By the way, this thesis, the huge work behind, all the things that I had no time or even space to include... all this amount of data, terabytes of data, sometimes repeated across the directories.. all these would have not been possible without one person. People may expect me to read some cheesy stuffs now, thanking my wife, my a-priori condition of life, my heart's desire [cite: Barney Panofsky]. This is not the case, when I try to tell her what I do, she crushes aslept.... Therefore I want to thank Ruben to have accepted me to work with him long time ago; through all these years many things happened, Italy got the fourth star as world champion, I married, the DEA, the Nature, the conferences, NCAFM2008, collegues and friends came and go away, the JAIST and now this doctorate. Thanks to have shown me the path (MEP perhaps?) and supported when things didn't seem to turn out properly. Time passes, things are thrown, simulations become obsolete, data formatted, but human relations synthesize the men we are. Thanks for that.

This bring me to thank to Prof. Ozaki, for his essential contribution to this study, his help has been more than important, for his openess to discussions and his time with me in the three months at JAIST.

Experimental Results I want to tribute a special mention to two persons who made this result possible: the dr. José Angel Martin Gago and the dr Gonzalo Otero. I deeply enjoy the time spent on the work on these molecules understanding your results and trying to find inspiration to save my computational time. Talking to you opened my mind to the dark side of the science, the experiments. It's an experience I deeply suggest anyone to do. Without you this would have not been possible. Without your contributions, as you can see in this thesis, I would have lost the way.

Computational Details I want to thank the clusters in the departments, AFM may you RIP and uamc11/spmthpc13/cls1 with your identity problems may you RunInPeace, now once for all! The cluster of the centro de computacion, Poseidon and Terpsichore... the computer facilities in Japan, abacus2, chopin2 almost always empty as the desert, and the superfast and not so crowded Cray XT5 (and the father XT3).

And I thank Mandriva to have made my pc stable with the same version without any single problem for all these years, and Suse/Windows not to have came across. Slackware I miss you!

Interaction Human-Human Many interactions have characterized the phenomenas related (and not) to this thesis. Therefore I need, and want now more than ever, to thank environment by environment the people I came across. Let me therefore start with the short range interactions, the people of the 503. A special thank must be addressed here, to my friends of such long journey, Alfonso, Dani y Miguel, cuya compañia ha sido fundamental, y por las leciones de cultura y politica española (Alfonsopedia) y de castellano (Dani corregido por Miguel). Alfonso, de la copañia de los anillos, thanks so much for all the tricks and tips, thanks porque gracias a ti ahora Lem es parte de mi biblioteca. Gracias a Dani porque sin su adicion a la chatarras no me hubiera montado un beowulf en casa y pagado una pasada de luz, bromas a parte gracias por todo, por xeo y por tu amistad. Tu ya has cogido el tren y esta vez no es para EEUU. Ahora es mi tren, y no es para Japon. Gracias a Miguel, por los viajes divertentes, al limite del "pero

esto esta pasando de verdad?", claro divertentes ahora... I will miss our time in the cafeteria of Psicologia. Juan, gracias, no nos hemos visto mucho pero me parece que eres un buen chaval, suerte con el piso!

Ma qui non posso mancare di ringraziare un caro amico, da lunghissimo tempo (20 anni ci pensi?), grazie al quale ho conosciuto la morte del tango, grazie Dimitri perché un'amicizia sincera vale piú di molte altre cose. Dovunque ci porteranno le nostre strade, so che potró sempre contare su di te.

Therefore I cannot forget to thanks all members past and present for all interesting discussions, on physics and on other matters that made these years in the group extremely pleasant. As it would be extremely unfair to mention all of them in any order, I randomly list them here.. and if I forget someone, please don't be upset. Thanks for the last year of talks and advices to Delia and Miliça, to Pablo Pou for all these years I had to teach him what real football is and, meanwhile someone can think it is strange, to Yannick Dappe, apart from football it's a pleasure to discuss with you, and thanks to Laura Cano which help in these last months has been essential. Thanks to Wojciech (good luck with the babies!), I am still waiting for you in Sardinia and thanks to *I need a vowels in the name* Krzystof. Thank you to Lucia, to take now the heavy weight I leave....

I should thank all people I had interaction with in these years, but the list would be too long, therefore let me be patriotic and thank Linda, Emiliano, Francesca and Filippo.

Y no puedo no agradecer a Laura, mi querida secretaria favorita. El echo que sea la sola secretaria es verdaderamente segundario, ha echo mi estancia en el departamento mucho mas sencilla de lo que temia, por los asuntos burocraticos y por el lado umano. Un muchissimas gracias Laura.

A special thank to both Huang and Toyoda which made my period in the most rural area of Japan, much easier in practical terms. I enjoyed any moment over there tasting every single difference I could, because you helped me when I needed. Thanks to Prof. Terakura, the weekly talks on all possible topics, the discussions on Japanese society characteristics, structure etc have been absolutely amazing and I deeply miss them.

Last but not least I want to thank here three persons, Kaijs, Fabio and Antonio, because they made one of the most strange period of my life in one of the nicest adventures, thanks to have helped me there and to have become my friends.

Ed infine un grazie particolare anche ai miei genitori e a mia sorella, ai miei amici e conoscenti, vari ed eventuali, conosciuti alcuni da sempre alcuni lungo questo percorso dottorale, grazie ad Enrico per i pomeriggi passati a mangiarci il fegato per una squadra che non lo meriterebbe e a tutti gli altri. E grazie anche a tutti quegli amici che da un pó ovunque hanno deciso di venire a visitarmi e a quelli, mandroni, che non lo hanno fatto.

Conclusions Once a great person said

> *"An eye for an eye makes the whole world blind."*
> *(Mahatma Gandhi)*

Science may open those eyes.

Bibliography Here I want to mention three of the most interesting books I have read, my own personal bibliography, from rubbish beach books to Nobel prizes.

Orhan Pamuk, Istanbul.

Mordechai Richler, Barney's Version

Stanislav Lem, Futurological Congress

Shahriyar Mandanipour, Censoring and Iranian Love Story

Giuseppe Garibaldi, Le Memorie

enddo

Abstract

The synthesis of carbon nanostructures represents an important technological task of modern nanotechnology, to allow new insight in the physics of such materials, to develop new compounds and, indeed, new industrial applications which, potentially, spread from biological application to quantum computing.

In this thesis the focus is a new synthesis process, developed in collaboration with experimental groups, for fullerenes and nitrogen doped fullerenes (triazafullerenes) from appropriate polycyclic aromatic hydrocarbons (PAHs), and which may open the path to the formation of new heterofullerenes and which methodological approach is now considered for the formation of a wide range of carbon nanostructures. The overall process, of deposition and adsorption of the molecular precursors, of the final synthesis products, and of phenomenas involved in the annealing process, the cyclodehydrogenation, is here characterized theoretically by DFT ab initio plane waves and localized orbitals methods.

In particular, the adsorption of the molecular precursors is discussed structurally and electronically in terms of their components, of their preferential adsorption behavior, and along with dependence on doping and hydrogenation. The enantioselectivity obtained upon adsorption is characterized and explained in terms of substrate molecule structural matching that uniquely determine the ground state and its multiplicities, essential for the subsequent cyclodehydrogenation. Experimental and theoretical disagreement on STM images is also explained as merely apparent for structural and electronic reasons.

The study of the fullerene adsorption on Pt(111) is discussed for a wide range of configurations, considering also the possible formation of surface defects (vacancy), to explain the experimental findings of different domains and different molecular orientation with the increase of deposition and temperature. Similar approach is considered for the characterization of the triazafullerene, to understand effects of doping in the adsorption of this new molecule.

The cyclodehydrogenation is discussed in both gas phase and on the platinum surface; in particular, in the gas phase the aim is to understand the efficiency limits of the process in such condition and the structural effects of both doping and hydrogenation. On surface the description is qualitative for computational cost limits related to complexity of the phenomena, following different possible paths to understand the difference respect to the same process in the gas phase.

This thesis is then organized as follows: definition of objective and motivations can be found in chapter 1, the theoretical approach in chapter 2, the adsorption of the molecular precursors in chapters 3 and 4), of the (triaza)fullerene in chapter 5), of the cyclodehydrogenation process in chapter 6 and finally the conclusions and future developments are in chapter 7.

Resumen

La síntesis de nanoestructuras de carbono representa una importante tarea de la moderna nanotecnología, para permitir una nueva visión de la física de materiales, para desarrollar nuevos compuestos y, de hecho, nuevas aplicaciones industriales que, potencialmente, incluyen tanto aplicaciónes biológica como por la computación cuántica.

En esta tesis el enfoque es un nuevo proceso de síntesis, desarrolado en colaboracion con grupos esperimentales, para fullerenos y fullerenos dopados con nitrógeno (triazafullerenos) desde adecuados hidrocarburos policíclicos aromáticos, que pueda abrir el camino a la formación de nuevos heterofullerenos, nuevos enfoques metodológico y que ahora se considera para la formación de diferentes nanoestructuras de carbono. El proceso de la deposición y adsorción de los precursores moleculares, de los productos finales de la síntesis, y de los fenómenos implicados en el proceso de annealing, la ciclodeshidrogenacion, aquí se caracterizan teoricamente con la teoria del funcional de la densidad, por métodos dem ondas planas y de orbitales localizados.

En particular, la adsorción de los precursores moleculares se discute estructuralmente y electrónicamente en términos de sus componentes, de su comportamiento de adsorción preferencial, y junto con la dependencia sobre el dopaje y la hidrogenación. La enantioselectividad obtenida en la adsorción se caracteriza y explica en términos de afinidad electronica y estructural de las interaciones moléculas sustrato y que determina el estado fundamental y sus multiplicidades, esencial para la posterior ciclodeshidrogenacion. El desacuerdo teórico y esperimental en las imágenes STM se explica también como sólo aparente, por razones estructurales y electrónicas.

El estudio de la adsorción de fullerenos sobre Pt (111) trata de una amplia gama de configuraciones, considerando también la posible formación de defectos en la superficie (vacantes), para explicar los resultados experimentales de formacion de agregados y la diferente orientación molecular con el aumento de la deposición y temperatura. Se considera un enfoque similar para la caracterización de los triazafullerenos, para entender los efectos del dopaje en la adsorción de esta nueva molécula.

La ciclodeshidrogenacion se discute tanto en fase gaseosa que en la superficie de platino; en particular, en la fase gaseosa, el objetivo es comprender los límites de la eficiencia del proceso en tal condición y los efectos estructurales, tanto de dopaje que de la hidrogenación. En la superficie la descripción es cualitativa debido al coste computacional de los calculos, relacionado con la complejidad de los fenómenos, y siguen diferentes caminos posibles para entender la diferencia respecto a el mismo proceso en la fase gaseosa.

Esta tesis sigue entonces la siguiente estructura: la definición de objetivos y de las motivaciones se puede encontrar en el capítulo 1, el enfoque teórico en el capítulo 2, la adsorción de los precursores moleculares en los capítulos 3 y 4, de los (triaza)fullerenos en el capítulo 5, del proceso de ciclodeshidrogenacion en el capítulo 6 y, finalmente, las conclusiones y los desarrollos futuros están en el capítulo 7.

Contents

List of Figures

List of Tables

Chapter 1

Motivations and Outline of the Thesis

This chapter introduces briefly the motivations of this study and gives an outline of the steps followed along the thesis. In particular the fullerene[1] molecule is here introduced (section 1.1), then its possible cage modifications (section 1.2) with special attention to the azafullerene (subsection 1.2.1), the state-of-art of their synthesis methods (section 1.3), the dehydrogenation as a methodology with great potentials (section 1.4) are discussed and, finally, provides an overview of a method for the efficient synthesis of fullerenes and triazafullerenes on metallic surface (section 1.5).

1.1 Fullerene

The carbon nanostructures science has always been considered as one of the icon of nanotechnology, but while many other technologies developed, carbon based applications, and in particular the fullerene based, did not or, at least, not as much as industrially required. The main reason behind such delay is the synthesis, and the costs coming from its intrinsic difficulties.

The major obstacle to a proper development of fullerene technologies is that the synthesis process fails to produce isomeric pure samples; along with such ability, the prices rise, up to thousands of times the same amount of gold. Strongly affected are then the industrial and the experimental study of this molecule and its derivatives. Still, huge interests and expectations remain, due to the large number of potential applications, that spread across many fields, from nano-bio-electronics, drug delivery, spintronics, solar cell applications and many others. Therefore the synthesis of fullerene, and of its carbon cage modified structures, is, today, a key technological issue, which costs and efficiency are among the main problems toward applications in the real world. It can be said then, that the main issue to obtain a fullerene based technology is to rely on an easy synthesis process.

By IUPAC definition, fullerenes is a polyhedral closed cage made up entirely of n three-coordinated carbon atoms and having 12 pentagonal and (n/2-10) hexagonal faces, where n is equal or greater than 20. When such definition is not applicable, the molecules are called *quasi* fullerene. Among the many component of the large family, the focus given here is on the C_{60} (fig. 1.1 left).

After almost a quarter of century since fullerenes have been identified by Kroto[1], no clear path has been identified to achieve an easy, cheap and therefore industrial applicable synthesis. In fact, at the current market rate, any real industrial application is precluded by the high cost, that, depending on purification, oscillates between \$45 and \$1000 per gram (gold is \$10 per gram). Never the less, research on fullerene continues, for fundamental knowledge of the carbon physics and chemistry, for technological issues and for potential therapeutic applications.

1.2 Cage modifications

Considering that the fullerene itself has extraordinary potential applications, those related to cage modified fullerenes are expected to be much more. Among these molecules, three main categories rationalize the eventual doping: hetero-

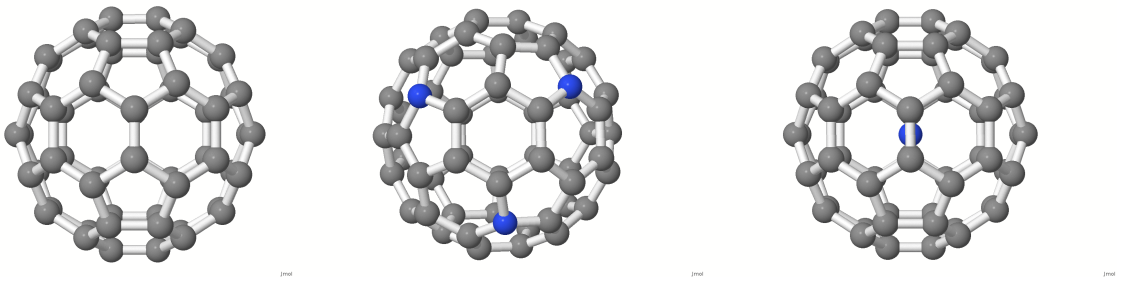

Figure 1.1: Fullerene cage (left), triazafullerene (centre) and endohedral fullerene (right)

fullerenes[2, 3, 4, 5] (fig. 1.1 centre), endohedral[6, 7, 8](fig. 1.1 right) and exohedral fullerenes[9, 10, 11], in which dopant atoms are respectively substituted, introduced in, and externally bonded to the carbon cage.

Among the applications, it worths mentioning that the PCBM, an exohedral fullerene is regarded as essential in solar cells, that the magnetic hetero-fullerenes are so for the potential in molecular electronics and spintronics, that some endohedral fullerenes are superconductors and that the fullerene itself has also important medical applications which include anti HIV-protease activity, photo-dynamic DNA cleavage, free radical scavenger, antimicrobial action and as diagnostic agents. It is then logical that toward the development of a true fullerene-based nanotechnology, a preceding requirement is a synthesis process which may enable also the structural modifications, and now, more than ever, molecular electronics, spintronics and solar cells technologies require innovative approaches which could allow their implementations in real world. Among the different problems that blocked these three fields to be part of daily life efficient technologies, it is important to mention that most of the proposed molecules either has a short lifetime, strictly related to their "strength", or, for solar cells related technology, have a low conductivity. Fullerene based technology had offered a solution in all these three fields, but it has been limited in the synthesis of carbon cage with proper characteristics.

In this sense the procedures proposed and used, are many and of various complexity. Therefore, for the carbon cage modified fullerenes, additional difficulties have to be summed to the pre-existing for fullerene, increasing the costs and representing an huge obstacle even to theit scientific characterization. Sometimes, such difficulties prevent the synthesis of molecules, whose properties remain merely in the theory, and promising new materials and applications remain inaccessible.

To open up these material science branches, the synthesis is, as mentioned, a preceding requirement. Indeed, such synthesis should be preferably cheap, controlled and efficient. The actual problem faced by fullerene science is that these three essential properties do not occur contemporary because they are related to the isomeric purity of the sample. The more pure a sample is required to be, to avoid useless or even dangerous contamination, more difficult and accurate its synthesis is or more cleaning procedures must be applied. Such precision in the production is an essential requirement, for example, for the potential application of fullerene technology to biomedical science, as some carbon nanostructures (and the fullerene itself) have been reported to be carcinogens.

1.2.1 Azafullerenes

The functionalization of fullerene cage, has been the focus of most studies on important physical and chemical properties related to these "hybrid" materials, mostly derived by partial replacement of some carbon atoms by nitrogen, boron, silicon etc.

By definition, an heterofullerene, generally indicated as $C_{60-n}X_n$, is a fullerene in which one or more carbon atoms have been substituted by an equal number of atoms of another specie (heteroatoms), and which effects are related to the electric charge redistribution. Since the beginning[2] such molecules have been considered of extreme interest as made possible a significant selection of geometry, chemical functionality and electronic character of the samples, with great expectation in the ability to pre select such properties.

In this work, we focus attention on nitrogen doped heterofullerenes, simply labeled as azafullerene $C_{60-n}N_n$. The first member of such large family is the monoazafullerene $C_{59}N$, that for the nitrogen tri-valency is an highly unstable radical. The open shell configuration leaves a dangling bond on the adjacent atom with a resonant structure and it is has been observed as an open shell monomer at room temperature[12]. Nevertheless, at early stage, its effective synthesis and not of its hydroazafullerene[13] has been often unclear.

From 1995 certain exohedrally nitrogen-containing fullerene derivatives showed efficient formation of azafullerene in the gas[11, 14], and one year later methods for production in bulk quantities have been developed[15, 16]. Since then, with the chemical modification of the fullerene cage with addition of azides, two efficient gas phase methods make the synthesis of monoazafullerene possible in bulk quantities. The first method starts from non-azafullerene precursors and the second from the dimer $(C_{59}N)_2$. In the first case efficiency is under 50%[17] and slightly inferior for the second[18].

Theoretically, molecular structure, binding energies, electronic properties, optical and magnetic properties have been studied not only for monoazafullerene, monomer and dimer, but also for many other different azafullerenes as not blocked by any synthesis procedure[4, 5, 19, 20, 21, 22, 23, 24], in order to address further experiments toward more interesting molecules.

Interestingly only $C_{60-2n}N_{2n}$ azafullerene synthesis is obtained by contact arc vaporization of graphite in presence of pyrrole, while no isolation of azafullerene with an odd numbers of nitrogen atoms, apart from monoazafullerene, have been yet obtained. A remarkable result showed the stability of $C_{48}H_{12}$[25] compound, which bring the azafullerenes near to carbon-nitride compounds, which are, anyway, obtained with different methods[26, 27] and which properties are extremely interesting.

As seen, azafullerene "zoology" is today merely limited to the mono, the di azafullerenes, and the $C_{48}H_{12}$; the first monomeric only on Si(111) surface and the second addressed as "elusive". Such limitation is strictly related to the synthesis processes, that, based on modification of fullerene cage, also rely on the intrinsic difficulties to obtain only required fullerene. The isomeric purity of the sample increases, and not linearly, with the price of the synthesis procedures.

1.3 Looking for an efficient synthesis: molecular precursors

Since the discovery of fullerene, scientists had problems in producing sufficient amount of fullerenes, usually it was less than 10-15 g. Such condition remained so until 5 years later, when a new high yielding method for fullerenes has been developed[28]. Now, plain fullerenes are obtained industrially from graphite in high yield, while latest scientific advances show that it is possible to obtain directly from graphene sheets[29], and from polycyclic aromatic hydrocarbons (PAHs) via flash vacuum pyrolytic methods (FVP)[30]; all these procedures are, never the less, expansive, uncontrolled or inefficient.

Meanwhile graphite vaporization still represents the main path to obtain fullerenes, various attempts have been made to rationalize such process. Particular importance and hopes have been on curved PAHs and their combination.

1.3.1 Fullerenes from PAHs

In details, much has been done in the recent year in terms of analysis of polycyclic aromatic hydrocarbons (PAHs) to understand cyclization and bonding process to obtain fullerenes. The polycyclic aromatic hydrocarbons are a category of molecules that are studied in astrophysics[31, 32], biology, oil industry, medicine and are regarded to have played an important role in the evolution of pre-biotic life forms. Their abundance in nature in various forms is a key point.

The main idea was to obtain fullerene from already curved PAHs. Therefore different molecules, parameters, inversion barriers and indeed methodologies, have been tried to figure the path for a "self-reorganization" of one or more PAHs to form fullerene or, at least, part of it.

The first molecule resembling part of a fullerene, aside from the benzene, is the corannulene; mainly obtained via flash vacuum pyrolysis (FVP), is composed by a central pentagon and five hexagons. Its synthesis methodologies show that insertion of vinylidenes formed by isomerization of alkynes into aromatic C-H bonds are essential for the formation of C-C bonds. Other bowl-shaped hydrocarbons, larger than corannulene, are still obtained with FVP methods[33, 34, 35], while the sumanene through organic synthetic methods[36]. It was expected that fullerene formation from PAHs was possible only through a combination of classical organic synthesis and FVP methodologies. One of the major problem in this path is that, in general, along with the complexity of the PAHs,a strong behavior to form planar structures is reported[33].

An important point among these various techniques considered for the synthesis of the bowl-shaped aromatic molecules[33, 34, 35, 37, 38, 39, 40, 41, 42], was to to pave the path for the synthesis without undesired residual contaminants[30, 43, 44, 45].

The idea to obtain fullerenes from already curved hydrocarbons[46, 47], has been based on respect of IP rule[48] of the bowl-shaped hydrocarbons[48, 49, 50, 51] and on extensive studies of their inversions barriers[52]. Such approach has been proof to be misleading with the synthesis of polyarene $C_{60}H_{30}$[44], a polycyclic aromatic hydrocarbon that has the proper number of carbon atoms of the final fullerene, and by the experiments of Scott[30] on such PAH, that have shown that it was not anymore necessary to complicate further the synthesis of curved PAH and the fullerene obtained from not bowl shaped precursor.

The idea proposed by Scott and collaborators[30] was to produce isolable amounts of the fullerene through the dehydrogenation of an appropriate molecular precursors, obtained from commercially available materials; process that requires 12 steps from the starting materials by rational chemical methods. The fullerene candidate molecular precursor, subjected to flash vacuum pyrolysis at 1100°C formed the expected buckyball. Unfortunately, the efficiency of dehydrogenation and cyclization in the gas phase is only about 1%. Still the process seemed to own a great potential. In the meantime, triaza analogue of polyarene had been synthesized, the heteropolyarene $C_{57}H_{33}N_3$[45], which aimed to ease the way to form heterofullerene, showing flexibility of doping of the fullerene molecular precursor, in both amount and species. The process proposed occurred through dehydrogenation, a new approach for carbon nanostructures, and that shows an amazing potential in solving the problems of the isomeric purity of the sample and in becoming a base for the synthesis of heterofullerenes.

1.4 Dehydrogenation

The idea of the dehydrogenation of carbon nanostructures as a bottom-up method, is to break selectively some C-H bonds to guide the "self-reassembly" towards the formation of pre-chosen structures. Such procedure may open synthesis of new molecules with relevant technological applications, as they would merely depend on the precursors and their much easier synthesis. Meanwhile regarded as a methodology with extraordinary potential it has not been considered for technological difficulties.

In such sense various methodological approaches have been tried, such as laser beams, temperature, scanning probe microscopy selective stimulation (STM, AFM), but all these attempts, in the gas phase as much as on surface, have shown one difficulty: lack of ability in targeting proper bond in the correct order. In particular, in gas phase, appropriate dehydrogenation temperature effects indiscriminately all similar bonds[30, 43] while on surface, lack of precision in topology prevents ad-hoc in situ dehydrogenation.

Until now, no effective improvements have been achieved to obtain a selective/controlled dehydrogenation in carbon nanostructures, and therefore it was adopted only for the synthesis of CNT caps[53].

1.5 Surface Catalyzed Cyclodehydrogenation: a controlled and efficient synthesis method

On one side expansive uncontrolled synthesis processes were the scientific and industrial standard, while on the other side, a new methodology was cheap, controllable but not efficient[30]. It seemed possible to improve this last methodology, through the active aid of metallic surfaces.

The "solution" to the problem of an efficient and controlled synthesis process, is discussed along this thesis as developed in collaboration with experimental groups, leaded by Dr. José Angel Martin-Gago and Dr. Berta Gomez-Lor at the Instituto de Ciencia de Materiales (ICMM-CSIC) and by Dr. Antonio Echavarren at the Insitute of Chemical Research of Catalonia (ICIQ), and with the RCIS theoretical group at Japan Advanced Institute of Science and Technology (JAIST) leaded by prof. Ozaki. Such multidisciplinary approach allowed a comprehensive analysis of the problem and therefore brought to the relevant results that are here theoretically analyzed.

As previously mentioned, the cyclodehydrogenation of PAHs from commercially available components, carried huge potential but lacked of efficiency[30]. To improve the synthesis rate, focus has been on methods to trigger progressively the dehydrogenation and to alternate such process with cyclization steps. To "tune" the process it has been decided to deposit the two molecular precursors, for fullerene the polyarene $C_{60}H_{30}$[44] and for the triazafullerene the heteropolyarene $C_{57}H_{33}N_3$[45], on metallic substrates. The attempts proceeded first on Au(111), where no significant difference from gas phase results[30] was obtained, and then on the more reactive Pt(111) surface.

In details, after deposition at room temperature (RT), the adsorption of molecular precursor shows low and high diffusion barriers respectively on gold and platinum. When Pt(111) is considered as substrate, the molecule is well anchored to the surface at room temperature. Indeed, the strong molecule-surface interaction is an evidence that, experimentally, neither long-range ordered molecular structures nor preferential adsorption at step edges have been found, indicating a reduced mobility of the molecule on the Pt surface, preventing any molecular networking formation.

The polyarene $C_{60}H_{30}$ and the heteropolyarene $C_{57}H_{33}N_3$ deposited on the Pt(111) surface present a total apparent height in the STM images independent on the bias voltage and a triangular shape. After annealing the sample at 750K, the triangular molecules imaged on the surface are transformed into rounded-shaped molecules, which linear dimension are compatible with values obtained for fullerenes on other surfaces and in particular on Pt(110); analogously the electronic analysis of the density on states and molecular orbitals are consistent with what scientifically reported on Si and other metallic surfaces. No benchmark was possible for triazafullerene, because this work synthesized it for the first time. The reported low adsorption height of both fullerene and triazafullerene is due to covalent interaction with the substrate and that the molecule tries to maximize the number of bonds, in agreement with known results which associate the behaviour to a substrate vacancy formation[54].

The characterization of the process, represented in fig. 1.2, has been published in

- G. Otero, G. Biddau, C. Sanchez-Sanchez, R. Caillard, M. F. Lopez, C. Rogero, F.J. Palomares, N. Cabello, M.A. Basanta, J. Ortega, J. Mendez, A.M. Echavarren, R. Perez, B. Gomez-Lor and J. A. Martin-Gago, *Fullerenes from aromatic precursors by surface-catalysed cyclodehydrogenation* Nature 454, 865-869 (2008)

In addition a remarkable behavior is observed when the adsorption of the molecular precursors has been considered on Pt(111): the landing side of the molecule induces two chiral molecular forms on the surface. The substrate recognizes the landing side of each molecule, becoming enantioselective. Each molecule adsorbs with a well defined, and opposite in sign, angle respect to crystallographic direction and, therefore, the angular distance between two different landing sides is constant, as the symmetry of the molecule (120º) is a multiple of the (111) surface geometry (60º).

The study of the enantioselectivity of the molecular precursors and their characterization is chapters 3 and 4 and has been published in

- G. Otero, G. Biddau, T. Ozaki, B. Gomez-Lor, J. Mendez, R. Perez and J.A. Martin-Gago, *Spontaneous discrimination of PAH enantiomers on a metal surface* Chemistry A European Journal, accepted (2010)

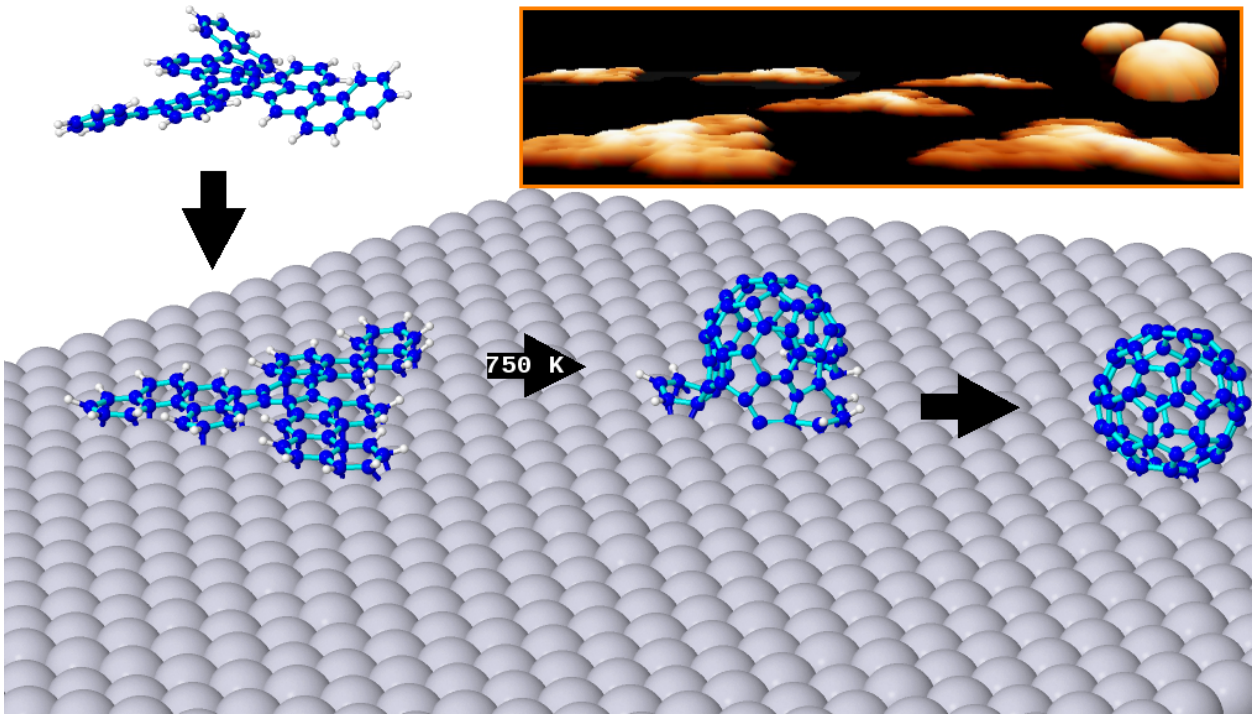

Figure 1.2: Artistic representation of the deposition of molecular precursors, subsequent cyclodehydrogenation process and formation of fullerene. Inset: theoretical STM images of adsorbed precursors and fullerenes

- G. Biddau, T. Ozaki, G. Otero, J.A. Martin-Gago, and R. Perez, *Understanding the bonding of large polycyclic aromatic hydrocarbons on reactive metal surfaces*, Physical Review B, submitted (2010)

The adsorption of fullerene, in different conditions of deposition, domain formations and along with formation of surface defects, is discussed in details in chapter 5 with the adsorption of triazafullerene.

The process occurring during the annealing that forms the spherical (triaza)fullerene from the adsorbed triangular molecular precursors, is a progressive cyclodehydrogenation, catalyzed by the metallic surface. Such selectivity in the process is one of the keys of the efficiency of the cyclodehydrogenation on platinum, compared to the poorly efficient process in the gas phase, and is analyzed in details in chapter 6 in both gas phase and on the surface.

Theoretically the challenge offered by such systems is indeed relevant, as involves carbon structures interaction with a reactive transition metal substrate, which, for the presence of *d* orbitals, may be of difficult convergence, may require an increasing number of layers and therefore of the computational costs, limiting the explorable configurations. Meanwhile the adsorption of fullerenes and nitrogen doped fullerenes, and of their molecular precursors, is of extre,e interest for technological applications and for fundamental understanding of the metallorganic interaction, for technical limitations has not been yet extensively addressed by any DFT study.

Then, this thesis aims to understand and characterize the synthesis of (triaza)fullerenes from polycyclic aromatic hydrocarbons (PAHs), with a detailed analysis of all steps involved and to understand the possibility to extend the process to other systems and to new molecules.

Chapter 2

Theoretical Methods

In this chapter the theoretical approach to the problems of the surface catalysed cyclodehydrogenation is discussed with a brief introduction on the density functional theory DFT (section 2.1), on the different exchange correlations functionals considered (section 2.2) and on the choice of LDA (subsection 2.2.1); the description of core electrons is discussed through the various pseudopotential approaches (section 2.3), then are resumed the electronic wavefunction expansion methods (section 2.4), the supercell approach to simulations and the Brillouin space sampling (section 2.5) and the methods to determine barriers between ground states (section 2.6). In the last part (section 2.7) the local orbitals approach adopted along this thesis is discussed, the specific basis sets and its energetic, structural and electronic benchmarks.

Introduction

The Schrodinger equation in a system of interacting particles is impossible to be solved analytically, except some extremely simple cases. For this reason, the methods developed to solve such problem, make use of approximations.

The most accurate way to describe the physics of a system is to treat in terms of wavefunctions through the Schrodinger equation. The problem, through various approximations can be reduced to the knowledge of a the exchange correlation term, which itself can be related to the charge density. The so called ab-initio, or first principle, method, solves the Schrodinger equations without any parameter, apart from the physical constants. This category includes Hartree Fock (HF) methods, subsequent developments, and the actually most used methods based on the Density Functional Theory.

As previously stated, the ab-initio methods are accurate, but this still implies huge computational cost. For this reason, to approach systems which complexity is particularly high, alternative approaches have been developed, so simulation of more complex structures like DNA, proteins or macro systems, which involve tens of thousands of atoms and/or their development in time, are possible only with other approximations; among these methods is important to note the tight binding and the semi empirical methods, which make use of experimental values to shorten the calculation time.

Frequently used are the mixed methods, in which only a part of the system studied is treated ab-initio; these methods give a good approximation when quantomechanical properties are required for a part of a particularly complicated system (high number of atoms, evolutions in time etc).

If otherwise was possible to solve the Schrodinger equation for system with high number of particles, the calculations would generate an untreatable amount of data. The most famous example is provided by the simple atomic oxygen (8 electrons, therefore each wavefunction would depends on 24 coordinates), which proper description would include 10 “entries” per coordinate and 1 byte per entry, so 10^{24} bytes, that would require $2x10^{14}$DVD, which weight is of 10g each. So, to describe a simple O molecule, more than 20^9 tons of DVD would be necessary.

2.1 Density Functional Theory

The density functional theory, or DFT, allows the study of properties of complex aggregates, such as atoms and molecules, reducing the quantistic problem of many bodies interaction to an equivalent problem of no-interacting particles, substituting the charge density variable in the electronic many bodies wave function, conjugating accuracy of the results and computational cost.

To describe a system with atoms and nuclei, is necessary to solve the Schrodinger equation

$$H(R_i, r_j)\psi(R_i, r_j) = E\psi(E_i, r_j)$$

where the Hamiltonian is made by two parts, the first is the kinetic contribution (T_e e T_n) and the second represent the potential (U_{ee}, U_{en} e U_{nn}) part,

$$H(R_i, r_j) = T_n(R_i) + U_{nn}(R_i) + T_e(r_j) + U_{ee}(r_j) + U_{en}(R_i, r_j)$$

where the index e and n refer respectively to electrons and to nuclei. The potential part includes a first term of interaction electrons nuclei U_{en}, a second term of interaction of electrons, U_{ee}, and a term for the exchange correlation energy term that in density functional theory is a functional of the new variable, the electronic charge density.

The use of the density as fundamental variable, has been firstly demonstrated by Hohenberg and Kohn[55], and is valid for the ground state of the system; they showed that there is a one to one correspondence between the ground state electronic density of a system and the external potential $V(r)$ that, in most cases is the interaction electron - ion.

To treat the problem, some approximations are necessary, first is the so called adiabatic separation of variables of the Schrodinger equation. Electrons and nucleus can be conceptually decoupled due to the huge mass difference and the time scale of the electronic motion. Under these assumptions electrons and nucleus have not been only decoupled, but a time dependent Schrodinger equation is now time independent. Adiabatic approximation and assumption that nucleus motion can be treated as semi classical are the Born-Oppenheimer approximation.

The DFT generates an input guess (density), constructs an Hartree potential, solves the Kohn and Sham equations[56] and from them obtains the densities, then if these values do not matches the criteria, the DFT restarts with the density guess step.

This statement and the variational principle allow to define an universal functional *F[n]* so that the following E[n]

$$E[n] = F[n] + \int n(r)V(r)dr$$

is minimum for the ground state, and contemporary the F[n] is minimum.

To be computationally implemented, is then necessary to go further with the Kohn and Sham method[56]. The process reduces the problem from many body wavefunction depending to 3N (where N is the number of atoms) electronic density, now position dependent.

When electrons are not interacting, *F[n]* is equal to the kinetic energy of the system T_s*[n]*, so that

$$F[n] = T_s[n] + \frac{e^2}{2}\int \frac{n(r)n(r')}{|r-r'|} + E_{xc}[n]$$

that is a sum of three terms, $T_s[n]$ is the kinetic energy functional for the equivalent non-interacting system with the same density, the second one ciontains the Coulomb interaction described by the charge density and the third $E_{xc}[n]$ for the exchange correlation functional, the non classical exchange effects .

The problem of knowing the terms is now confined. If we set to zero the variation of $E(n)$, the equation obtained is equivalent to one subject to a self consistent potential

$$V_{scf}(r) = V(r) + e^2\int \frac{n(r')}{|r-r'|} + V_{xc}(r)$$

when V_{xc} is the functional derivative of $E_{xc}[n]$ respect to the electronic density; under the condition of the conservation of the total number of particles. The many body problem of interacting electrons in an external potential[55] is replaced by and independent electron problem[56].

As an interacting system is reduced to a non interacting, the minimization of the energy functional gives now the ground states that must be the same as from the Slater determinant (that satisfies the Schrodinger equation)

$$H_{scf}\psi_n(r) \equiv -\left(\frac{\hbar^2}{2m}\nabla^2 + V_{scf}(r)\right)\psi_n(r) = \varepsilon_n\psi_n(r)$$

where ε_n and ψ_n are eigenvalues and eigenvectors of no interacting system.

The Hamiltonian now describes a non interacting electron gas subject to the effective potential. The charge density can be written now as

$$n(r) = \sum_i f_i|\psi_i(r)|$$

where i is the index for the single particle state, f_i is the Fermi-Dirac coefficient and $\psi_i(r)$ are the one particle wavefunctions; wavefunctions that are merely eigenstates of the system considered but are not wavefunction of the electrons in the real systems.

The following problem is the definition of the electronic charge density through approximations; the most commonly used are the local density approximation LDA, and the generalized gradient approximation GGA.

2.2 Exchange-correlation functionals

LDA Created to work in system where the electronic charge density is supposed smooth, such as metals and intrinsic semiconductors, the Local Density Approximation, LDA has provided good results also in covalent crystals.

The exchange correlation energy is as follow:

$$E_{xc}^{LDA}[n(r)] = \int \varepsilon_{xc}^{ug}[n(r)]n(r)dr$$

where ε_{xc}^{ug} is the energy of an uniform gas.

Being an approximation fails in a proper description of binding energy and the bond lengths are underestimated.

GGA The generalized gradient approximation represents a step towards a deeper precision in accounting the density contribution to the exchange correlation energy, including as a term, the gradient of the density, so that the previous formula becomes:

$$E_{xc}^{GGA}[n(r)] = \int \varepsilon_{xc}^{ug}[\nabla n(r), n(r)]n(r)dr$$

Limits of the GGA approach can be found in the definition of insulating state, properly predicted, but which gap is smaller than experimental values; furthermore, where LDA underestimates important parameters such as lattice constant, GGA overestimates. In transition metals its divergence respect to experiment is larger than in LDA.

2.2.1 The choice of LDA functional for the calculations

The suitability of functionals for the interaction of aromatic molecules with metal surfaces, is object of debate in the literature. As LDA is known to overestimate the bonding energies, GGA functionals are a priori the best option. However, GGA calculations give molecule-surface distances far larger than the ones determined from experiments for certain well studied cases like PTCDA on Ag(111). When van der Waals corrections are added to the GGA functional, the resulting structures and total energies tend to be quite close to the LDA results.

Nonetheless the adsorption of molecules on metallic surfaces, and so their orientations, is strictly related to the appropriate choice of the lattice constant of the substrate. In transition metals, is known that such parameter is much more similar to experimental values in LDA than in GGA (subsection 2.7.1.3), and the phenomenas involved in this thesis show that the "matching" between substrate and adsorbate is extremely important. On such assumptions, in this thesis, the chosen theoretical approximation for the exchange correlation functional is then the LDA approximation. Total energy differences between benchmark systems are maintained between plane waves, more accurate, and localized orbital, more efficient, methods for the LDA approximation, and the energy differences are maintained between LDA and GGA in plane wave approach, as shown in section 2.7. GGA functionals have not been considered for localized orbital methods, because the proper description of a still large lattice constant required a computationally demanding basis set with *f* orbitals.

2.3 Pseudopotentials

As seen, the DFT simplifies a description of interacting electrons onto one of non-interacting electrons in an effective potential. The obtained Schrodinger equation still faces difficulties related with the kinetic energy, one in the atomic region near the nucleus and another in the bonding region. A fine and accurate description is necessary to describe the rapid oscillations of the wave functions near the nucleus where kinetic energy is large, while out of the core region, requires a smoother wavefunction, for the smaller kinetic energy. In the attempt to develop a suitable method, many approaches have been developed; among them the pseudopotentials. Worth to mention the ones used in this thesis, like the Troullier-Martins pseudopotentials and the projector augmented wave method, or PAW. The simplest wave that can be used to describe the wavefunction is logically the plane wave. Nonetheless, in the nucleus, the oscillations are particularly complicated and the plane waves fail to achieve a proper description. To describe the core region in a smoother way, the pseudopotential methods are necessary, this is possible for the arbitrary of the wavefunction for $r < r_c$.

Describing the core wavefunction

In this way, the weak pseudopotential is used to design the core region, and produces a regular behavior in the wavefunctions, decreasing the number of plane waves necessary to describe it. In the core region, the pseudopotential is more regular than a coulombian one, while elsewhere is equivalent to the real potential. The eigenfunctions solution of the Schrodinger equation, written using the pseudopotentials, are pseudo-eigenfunctions, equivalent to real eigenfunctions only out of the core region, where chemical bonds take place.

While in the core region, the real eigenfunctions present nodes, the pseudo eigenfunctions are regular and without nodes; this characteristic allows the fast convergence of the calculations with clear computational advantages. Considering only the no core region, the method permits to consider only the valence electrons, ignoring the internal ones.

2.3.1 Limits of Pseudopotentials

To properly represent the wavefunctions with plane waves, it is necessary to smooth the core description, loosing information on charge density and wave functions nears the nucleus. Furthermore, when pseudopotentials are applied to first row elements of the Mendeleev's s table, or to system which valence electrons are *d* or *f*, they require either more plane waves than in other cases, or a localized basis for the wave functions expansion. This happens because the *p* states of atoms which Z<10 have not core states of same symmetry to be orthogonal to, tightening the states to the strongly attractive region of nuclear potential. Similar problems occur for transition metal, such as Cu and Pt, which *d* orbitals have almost the same energy of *s* states, so the electrons must be considered as part of the valence band; being much more localized, to be treated with a proper accuracy, they require an increased number of plane waves,

increasing the computational cost. The *ultrasoft* pseudopotentials of Vanderbilt are today a solution to the problem, as they are not norm-conserving as normal pseudopotentials.

2.3.2 Kleinman - Bylander separable form

The elements of the pseudopotential are independent on the plane wave basis and can be calculated for each type of pseudopotential once the expansion functions are known. To find the optimal basis set, Kleinman and Bylander[57] proposed to use single reference function per angular momenta, and the atomic reference obtained with the pseudopotential Hamiltonian as eigenfunction of the pseudo atom. This approximation is valid considering only small perturbations of the wavefunctions close to the atoms (atomic pseudo wavefunctions).

The use of Kleinman-Bylander (KB) pseudopotential may generate spurious states, called ghost states, below the valence states, as consequence of non locality of the approach. Ghost states may anyway avoided through accurate choice of cutoff radii in the semilocal pseudopotential.

2.3.3 Troullier-Martins pseudopotentials

The Troullier-Martins (T-M) approach extends the Kerker methods (and the HSC on which it is based on), where the pseudo wavefunctions, inside some cutoff radius, are changed to an analytic function that matches the all-electrons wavefunction at the cutoff radius. The T-M pseudopotentials make use of polynomials of higher order than in previous methods, smoothing the pseudopotentials using additional parameters (the coefficients of the higher terms in the polynomial).

The Troullier-Martins wavefunctions has the following form

$$\Phi_l(r) = r^{l+1} e^{p(r)} \quad r < r_c$$

where $p(r) = c_0 + c_2 r^2 + c_4 r^4 + c_6 r^6 + c_8 r^8 + c_{10} r^{10} + c_{12} r^{12}$ and c_n are norm conserving terms.

2.3.4 Ultrasoft psudopotentials

To make calculations faster it appeared necessary to smooth (soft) the pseudo wavefunctions and, still maintaining same accuracy, use an smaller number of plane-waves. In 1990, the ultrasoft pseudopotentials have been theorized by Vanderbilt [58], relaxing the norm-conservation constraint; the total valence density is written in two contributions hard and soft. In general the required number of plane waves scales as $E_{cutoff}^{3/2}$, where E_{cutoff} is half that of conventional norm-conserving pseudopotentials.

2.3.5 Projector Augmented Wave (PAW) Method

« The Projector Augmented-Wave method is an extension of augmented wave methods and the pseudopotential approach, which combine their traditions into a unified electronic structure method » says Blochl[59].

The basic concept of the method relies in using a smooth auxiliary wavefunction instead of the effective one. These auxiliary wavefunctions are the plane wave parts of the full wave functions, in a way that, to calculate a physical property through expectation value of a generic operator, this can be expressed in terms of either real or auxiliary wavefunctions.

If the auxiliary wavefunction is $|\psi_n^{\sim}>$ and the real wavefunction $|\psi_n> = T|\psi_n^{\sim}>$ where T is the transformation, the expectation value of operator A is

$$< A >= \sum_n f_n < \psi_n|A|\psi_n >= \sum_n f_n < \psi_n^{\sim}|T^{\dagger}AT|\psi_n^{\sim} >$$

and the total energy is

$$E\left([\tilde{\psi_n}],R_i\right) = E^{\sim} + \sum_R (E_R^1 - E_R^{\sim 1})$$

Wavefunctions, expectation values and total energies can be divided in three parts; the plane wave one, $E^{\sim}$ is the longest, computationally speaking, to be treated, as it's treated in real and reciprocal space, while remaining parts are calculated on radial grids in a spherical harmonics expansion. The so called augmentation part, $\triangle E = E^1 - E^{\sim 1}$, is a functional of one center density matrix.

2.4 Basis sets for expanding the wavefunctions

After a proper description on core electrons, the second step is to choose an accurate description for the valence electrons.

The single electron wavefunction can be written as

$$\psi_i(r) = \sum_{j=1,\infty} c_j \phi_j(r)$$

where $\phi_j(r)$ is then a complete set of functions. As infinite number of wavefunctions cannot be considered, the other possibility is to approximate with other functions which behavior resembles the real wavefunctions. The two possible expansion of the wavefunctions considered here, are through plane waves (subsection2.4.1) or via localized orbitals (subsection 2.4.2). Computationally, the first approach is much more expansive than the second, but more accurate.

2.4.1 Plane Waves: accurate but expensive (benchmarking with VASP)

The wavefunction can be written as product of two parts, the first $e^{i,k,r}$, is periodic, as consequence of the Bloch's theorem, and the second is the proper wavefunction $f_i(r)$

$$\psi_i(r) = e^{i,k,r} f_i(r)$$

if $f_i(r)$ is then expanded on a set of plane waves $f_i(r) = \sum_G c_{i,G} e^{i(k+G)r}$, where G are the reciprocal lattice vectors, the electronic wavefunction is

$$\psi_i = \sum_G c_{i,G} e^{i(k+G)r}$$

Therefore the number of plane waves considered is limited by the largest wave vector considered in the expansion, therefore to a cutoff energy, because the kinetic energy of an electron with wavevector k is

$$E_k = \frac{\hbar^2 |k|^2}{2m}$$

In general such kind of expansion has some advantages respect over Slater or Gaussian functions, as it can be used for all atomic species, its convergence toward completeness can easily be tested and because the plane waves, as they are independent on nuclear positions, do not require correction terms for the calculation of the forces, unlike localized basis sets. At the same time, such kind of expansion is much slower than other which bases on orbitals.

Vasp The Vienna Ab-initio Simulation Package, VASP[60, 61], is a complex software for DFT quantomechanical ab-initio simulations based on use of supercell approach, ultrasoft and PAW pseudopotentials. The code, originally built for total energy calculations, is now able to provide a wide range of material characteristics.

Main characteristic of the code is the calculation speed; in most of plane waves programs, the calculation time scale with N^3, when N is the number of atoms of the system, while VASP is faster due to the analysis of the non local contribution of pseudopotential in the real space and not in the reciprocal as it usually is.

2.4.2 Tight Binding and Localized Orbital basis sets

Tight Binding In the tight binding model, the Fourier transform of the Bloch function can be approximated by the Linear Combination of Atomic Orbital (LCAO), so that the band structure of solids can be calculated. The Hamiltonian is approximated by the Hamiltonian of an isolated atom centered at each lattice point. This assumption is valid when it is assumed that the eigenfunctions of the single atom Hamiltonian is negligible for distances larger to the proper lattice constant of the considered element, so that all lattice sites are almost independently treatable.

The atomic potential is taken in account but the variation can be appreciated only if atomic orbitals are small. The time independent single electron Schrodinger equation has solution Φ as linear combination of atomic orbitals Ψ_n

$$\Phi(r) = \sum_{n,R} b_{n,R} \Psi_n(r-R)$$

where n refers to the n-th energy level and R is an atomic site.

Local Orbitals The concept has its base on fact that wave functions describing the electron configurations of a given atom, can be assumed as basis set of functions. Once chemical reaction occurs, the shape of the electronic cloud is modified, so the orbital wavefunctions.

It is so possible to describe a molecular orbital ϕ_i as a linear combination of basis functions χ_r as:

$$\phi_i = \sum_r c_{ri} \chi_r$$

where c_{ri} is the coefficient that is basis function dependent. The choice is now on the basis set, which can be of different types, numerical, Gaussian etc.

Further approximation can be done through a minimal or a polarized basis sets. In a minimal basis set a single basis function is used per each orbital on the free atom; its limits are in proper description of first row elements in Mendeleev's table. Following step is to add other basis functions, theoretically indefinitely, but both efficiency and physical meaning can be lost. The most important addition to minimal basis set is a polarized function, that include additional nodes. In most case, such addition is necessary as polarized auxiliary functions take into account the d (or f) asymmetry; similarly the asymmetry of hydrogen atomic bonding can be properly described with additional contribution of an auxiliary polarized function. Other additional functional may have been considered to describe the shallow "tail" of anions orbitals.

The first basis set to be implemented were Slater orbitals, then these have been approximated with linear combination of Gaussian orbitals.

Simulation programs such as Siesta and Openmx provides a Kohn - Sham equation equivalent to a TB method, in which the potential are defined self consistently and the pseudo atomic orbitals are numerically confined, with a drastic increase of the computational speed respect to Gaussian type orbitals.

2.4.2.1 Fireball

Fireball[62, 63, 64] is a simulation program based on a self-consistent version of the Harris-Foulkes functional[65], where the input density of the energy functional is allowed to vary and determined self-consistently.

The confined pseudo atomic orbitals (basis set) determine the occupied eigenvalues and eigenvectors of the one-electron Hamiltonian. The fireball orbitals, introduced by Sankey and Niklewski[66] are obtained by solving the atomic problem. The orbitals are considered zero for distances larger than the cutoff radius The advantage of the

fireball basis set is that the Hamiltonian and the overlap matrix elements are quite sparse for large systems. The four-center integrals are not required for the calculation and all the two and three centers interactions are tabulated in advance, to which Hamiltonian make reference to.

For C, the optimized basis set considered a cutoff radii of .45 a.u. for the s and p orbitals, while for H it has been used a double-zeta basis with s symmetry cutoff at 4.1 a.u; for platinum, the cutoff is different depending on the orbital considered, 4.6 5.8 and 4.2 a.u. for s, p and d orbitals, respectively. Appropriate nitrogen basis set required a minimal basis (with s, p orbitals) plus polarization (with a d orbital) which cutoff are respectively 3.6, 4.1 and 5.2 a.u.

2.4.2.2 Openmx

Openmx[67, 68, 69] (Open source package for Material eXplorer) is a program package under GNU license developed by RCIS group leaded by prof Taisuke Ozaki at the research facilities of the Japan Advanced Institute of Science and Technology. Openmx is a DFT code based on norm-conserving pseudopotentials and pseudo-atomic localized basis functions; developed for large scale ab initio calculation, and its use is particularly performing on parallel computers. In particular, the code implements non-collinear DFT methods, collinear and non-collinear LDA+U methods.

Being N the number of atoms, the scaling time for the Hamiltonian matrix, the solution of the Poisson's equation, is $O(N)$ and $O(Nlog(N))$ for any eigenvalue solver; for diagonalization of the generalized secular equation, it is possible to choose between conventional diagonalization scheme that scales as $O(N^3)$ and a more efficient but less accurate $O(N)$ scaling method.

2.5 Supercell Method and K-sampling

With the so called supercell method, ab-initio calculations make use of Bloch's theorem even for a non-periodic system. In this method a large unit cell, the *supercell*, is periodically repeated in space. Eventually, to avoid undesired interaction between unit cells, vacuum is used as a spacer between. Strict requirements are necessary, among them the cell must be the smallest possible (to avoid unnecessary computational cost) to guarantee results invariant to small changes in the cell size. As a periodic system, the Bloch theorem can be applied to the supercell, the largest the smaller the Brillouin zone should be. The description of the charge density is done on the k point, which mesh must be appropriately chosen to obtain convergence of the results. In the Monkhorst and Pack[70] scheme, the k are distributed homogeneously in the Brillouin zone, while the Chadi and Cohen[71] scheme is based on the "shell"' analysis. The appropriate choice of the k space grid is therefore essential, minimized to avoid computationally expansive calculation but accurate enough to guarantee reliability of the results.

2.6 Beyond the ground state: the minimum energy path

In the study of dehydrogenation process, diffusivity and other phenomenas, it may be necessary to face the problem of the *minimum energy path*, or MEP, between two configuration. The *minimum energy path*, exploring the configurations space, identifies the saddle point as the potential energy maximum that defines the activation barrier for a considered process, an important value to understand the transition rate in the *harmonic state transition theory*. The methods proposed to achieve the saddle points are various. Starting from a local minimum representing the initial states, slowly describing a path of increasing energy configurations; or calculating the normal modes of a local armonic approximation of energy and to follow the modes till the required saddle point.

More recent method is the nudged Elastic Band (NEB)[72], in which a chain of images is generated between the starting and the ending points of the system. The images of this chain are hold together by spring forces and are relaxed together. At the end of the optimization process the chain will give the MEP. The number of images used depends by the transition process studied; logically, for computational efficiency it must be the lowest as possible. The spring force that holds the images doesn't interfere with the relaxation in the direction normal to MEP. The results

can be achieved with a certain freedom in the choice of the spring constants between the images. This method is then efficient in parallel calculations.

2.7 Testing Our Approach With Openmx

The choice of a proper methodology for the description of the theoretical problems studied here, has to consider some restrictive condition, such as the simulation unit cell of, at least, 10×10 atoms, the metallic nature of the substrate, the complex description of the relaxation with a minimum number of layers, the metallorganic interaction, the k space sampling, the cyclodehydrogenation of the molecule and so its possible extension on z axis. Therefore the only realistic methodological approach possible is through DFT ab initio LCAO methods. The choice of the appropriate basis set is then critical in terms of ratio between accuracy and time of the simulations. Due to the arbitrary in the choice of the basis set, an accurate benchmark with standard plane waves methods is neeed for basic properties, lattice parameter and bulk modulus, and specific characteristics considered in the problem, such as the total energy differences.

2.7.1 Basis set for H, C, N and Pt (atoms and molecules)

DFT calculations have been performed with the OPENMX code, that solves the Kohn-Sham equations in a local orbital basis. The wave functions are expanded as a linear combination of strictly localized pseudo-atomic orbitals (PAOs) centered on atomic sites. These PAOs are the solutions of the atomic Schrodinger equation with an additional confinement potential that enforces the wavefunction to go to zero at the cutoff radius. In the calculations reported here, basis chosen is labeled C5.0-s2p3 (C5.0-s52p53d51), H4.5-s1 (H4.5-s21), N5.0-s2p2d1 and Pt7.0-s2p2d2. The meaning of this notation is the following: atomic specie, cutoff radius (in Bohr), the number of orbitals with a l=s,p,d symmetry included in the basis. The values in parenthesis refer to the original set of primitive orbitals to which optimization was applied (e.g. p53 means that three optimal p orbitals have been generated from five p orbitals).

Troullier-Martins pseudopotentials in the Kleinman-Bylander separable form are used. The projector expansion method is employed in the calculation of three-center integrals for the deep neutral atom potentials. The criteria for electronic and ionic convergence are respectively differences in energy less than 10^{-6} Hartree ($2.7 * 10^{-5}$ eV) per atom and forces on each moving atom smaller than 10^{-4} Hartree/Bohr (10^{-2}eV/Å)

Our basis set for C and H has been optimized to reproduce the results of converged plane-wave calculations (using VASP) for (1) the C-C, C-H and C-Pt bond distances in a wide range of carbon rich materials including hydrocarbons (methane, acetylene, ethylene, ethane), benzene, pyridine, fullerenes, azafullerenes, nanotubes and graphene, and (2) total energy differences among a large number of configurations including aromatic rings with in different configuration that are relevant in the process of cyclization of dehydrogenated PAHs to form closed fullerenes. No optimization was performed for the Pt basis set. In the following part of this chapter a detailed description of benchmark results is provided in particular for benzene adsorption on Pt(111). Being an already widely studied systems, the comparison with known and accepted results, helps to validate the local orbital basis set obtained with Openmx.

2.7.1.1 Energetics

Optimized basis set energy differences respect to extended atoms are resumed in table 2.1, while in table 2.2 (left) we show bonding energies and distances for C_2, Pt_2, graphene and $C-Pt$ and the $C-C$ bonding energies for different hybridization in table 2.2 (right).

2.7.1.2 Hydrocarbons description

Computational Characterization of C-C bond One of the most important criteria considered along this work, for the selection of an appropriate basis set, is the description of C-C bond break between two aromatic rings, and subsequent formation of a 10 carbon atoms rings (fig. 2.1), that may occurs under certain particular conditions,

E_{atom} (eV)	Openmx LDA	Vasp LDA	Vasp GGA
C	-150.48 (+0.80)	-146.69	-147.47
H	-11.48 (+0.46)	-12.13	-12.53
Pt	-773.10 (+0.16)	-732.45	-730.04

Table 2.1: Energy difference between optimized basis set and extended orbital

	Openmx LDA	VASP LDA	VASP GGA
$C-Pt$	1.71 Å	-9.65 eV 1.67 Å	-8.91 eV 1.70 Å
C_2	-8.07 eV 1.26 Å	-9.64 eV 1.25 Å	-8.99 eV 1.26 Å
Pt_2	2.34 Å	-5.12 eV 2.29 Å	-4.52 eV 2.33 Å

	Openmx LDA	VASP LDA	VASP GGA
C_2H_2	-10.49 (2.56)	-11.71 (3.15)	-10.96 (3.00)
C_2H_4	-7.83 (3.2)	-8.56 (3.75)	-7.96 (3.63)
C_2H_6	-4.63	-4.81	-4.33
C_6H_6	-6.83	-7.24	-6.67
C_2	-8.07	-9.64	-8.91
CH_4	-6.56	-6.20	-6.03
graphene	-9.28		

Table 2.2: Left: Bonding energies (eV) and distances (Å) for biatomic molecules. Right: Carbon - Carbon bonding energy (eV) obtained assuming CH bond energy as 1/4 of methane total energy from C-H bonding energy of methane. In parenthesis the energy differences

avoided under others and also eventually heal. Through geometrical relaxation the bond lengths and total energy differences are shown in table 2.3.

Biatomic N-Pt molecule

Cohesive energy calculated for biatomic N-Pt molecule respect to its isolated components is -3.6 eV and distance is 1.82 Å. To understand levels shift in N-Pt bonds, we show in fig. 2.2 how the density of states of each atom is modified by interaction and how the biatomic molecules levels are, compared with the case of isolated atoms.

2.7.1.3 Platinum Surface

Platinum basis set is in good agreement with plane wave results (table 2.4). Surface energy per atom, defined as $E_{slab} - E_{bulk}$, for Openmx and Vasp is compared along $1 \times 1 \times n$ and $3 \times 3 \times n$ unit cells, and shows that it decreases similarly in LDA in both methods (table 2.5), and relaxation effects are negligible (not shown).

$C_{10}H_2$	Plane Waves				LCAO		
	VASP		CASTEP		Fireball		Openmx
	LDA	GGA	LDA	GGA	LDA	LDA*	LDA
$\triangle E_{tot}$	0.70	0.98	0.71	1.08	2.00	1.38	0.72
$C-C_{bond}$	1.57	1.58	1.58	1.58	1.62	1.6	1.58

Table 2.3: Energetic (eV) and bond lengths (Å) with different ab initio approaches (plane waves / localized orbitals) and simulation programs.

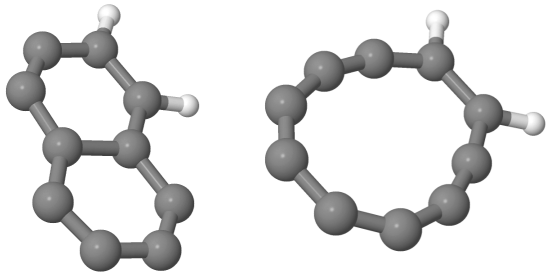

Figure 2.1: The $C_{10}H_2$ systems considered to test reliability of carbon basis set in the description of bond break

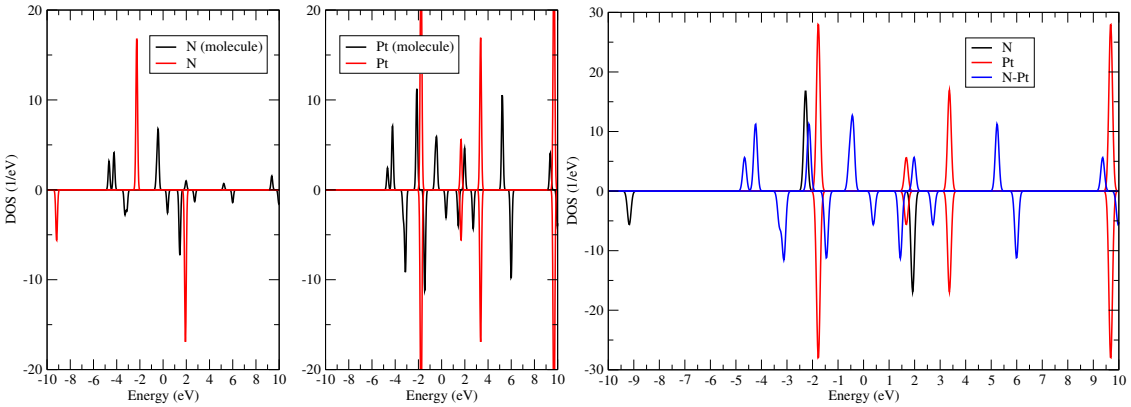

Figure 2.2: Up: comparison between DOS for nitrogen (left) and platinum atom (right), isolated and in the biatomic NPt molecule. Down: DOS of biatomic molecule and of the isolated single atoms.

Platinum	Openmx		Vasp	
	LDA	GGA	LDA	GGA
α (Å)	3.928	3.985	3.907	3.994
B_0 (mbar)	2.99		2.75	2.21
E_{bulk} (eV)	-7.21		-7.42	-6.02

Table 2.4: Bulk calculations parameters. Experimental lattice constant is 3.92 Å[73], Openmx basis set for GGA calculation required a basis set s3p3d3f2 to reproduce a Vasp-GGA like value.

Kgrid 551 2 layers free	Openmx LDA	Vasp LDA	Kgrid 12 12 1	Openmx LDA	Vasp LDA	Kgrid 551	Openmx LDA	Vasp LDA
1x1x3	0.74	0.69		0.58	0.54	3x3x3	0.59	0.54
1x1x4	0.59	0.54		0.42	0.41	3x3x4	0.41	0.38
1x1x6	0.42	0.41		0.27	0.25	3x3x6	0.27	
1x1x9	0.31	0.32		0.17	0.16			
1x1x12	0.26	0.27		0.12	0.11			

Table 2.5: Surface energy per atom (eV), defined as $E_{slab} - E_{bulk}$, for Openmx and Vasp. Bulk values are shown in table 2.4.

2.7.2 Adsorption of benzene on Pt(111)

The next step consisted in checking reliability of basis set in their mutual interaction. Therefore the choice of benchmark system has been done on adsorption of benzene (Bz) on Pt(111). Such system is not only an useful benchmark for basis set but it also provides an insight in the interaction with the substrate of the molecular precursor elements.

The adsorption of benzene on metal surfaces has been widely studied experimentally and theoretically for its interest in corrosion mechanism, lubrication and in catalysis. Recently particular attention has been devoted to understanding such systems for molecular electronics, biomedical and pollution reasons, because the benzene, with its aromatic ring, is frequently assumed as a model system for larger aromatic systems. Electronically, its π electron participates directly to the chemisorption with a partial contribution from σ, and therefore represents and optimal base system to test reliability of methodology and, in particular, of local orbital basis sets. In the following part reliability of our LDA approach through benchmark of Bz adsorption on Pt(111) is shown; structurally through comparison of stable, unstable and metastable adsorption behaviors and energetically through energy differences that are maintained between LDA and GGA, as much as between plane waves and LCAO methods. Relative energy between three and four layers also validates the three layer approach to energetic description of large aromatic molecule adsorption on platinum.

Benzene adsorption is considered here on different number of layers in both localized orbital and plane waves methods, comparing the values obtained for energetic and structural parameters a reasonable convergence is obtained.

2.7.2.1 Description of the adsorption geometries

Six high-symmetry adsorption sites for benzene on Pt(111) have been studied, of them, five are stable/metastable. They are here classified according to the position of the center of mass (bridge, top and hcp) and the azimuthal angle of the C-C bonds in the molecule (0, 30) with respect to the Pt rows. In the hcp orientation, only the 0 angle has been considered.

The minimum energy configuration, bri30, is also the only stable structure with a 30 azimuthal angle, while bri0 is metastable, for translations toward fcc0 and hcp0 configurations and for rotations toward bri30. All configurations have six bonds with substrate. Bonds are considered “double” and “single” respectively when two or one carbon atoms are bonded to same Pt atom. Exclusively one kind of bond exists in fcc0 and hcp0 (double) and in top0 (single), while both are present in bri30 and bri0 (two double and two single).

Ground State: bri30 Such configuration (fig. 2.3 left) is the ground state. C-Pt average bond lengths are the shortest among all configurations calculated. Two bonds are “double” and two are “single”.

Unstable: top30 and fcc30 These configurations, in which benzene is respectively on top and fcc site forming 30 angle with Platinum substrate rows, are not stable and evolve with no diffusion barrier to bri30 configuration (fig. 2.3).

Stable minima other than the ground state: top0, hcp0 and fcc0

Top0: This configuration (fig. 2.4 left) has the benzene on top site and again all C-C bonds form 0 angle with substrate crystallographic directions. All bonds with substrate are single.

Hcp0: In this configuration (fig. 2.4 centre) the benzene is on hcp site and all C-C bonds form 0 angle with substrate crystallographic directions, and all bonds are “double”.

Fcc0: In this configuration (fig. 2.4 right) the benzene is on fcc site and all C-C bonds form 0 angle with substrate crystallographic directions, and all bonds are “double”. Due to similarity with hcp0, no huge total energy difference is expected as much as in bond distances.

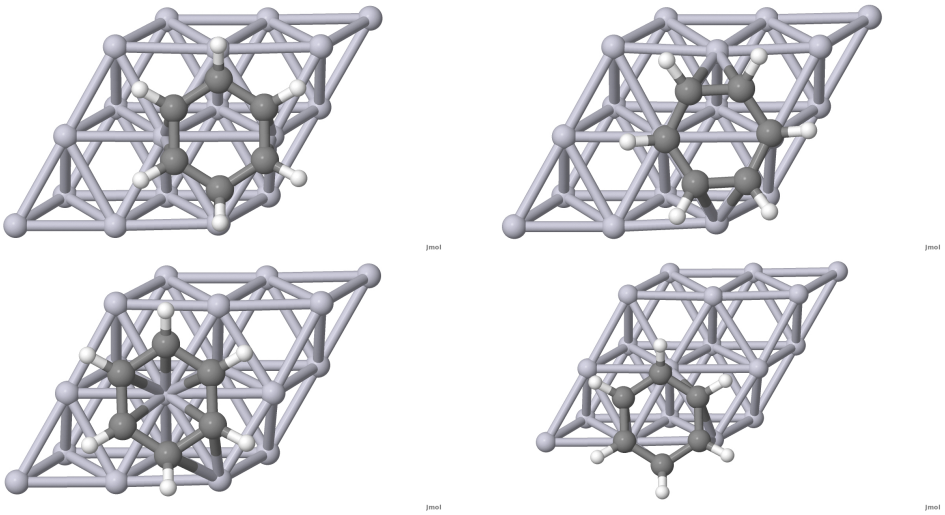

Figure 2.3: Ground State bri30 (up left) and metastable bri0 (up right), unstable top30 (down left) and fcc30 (low right)

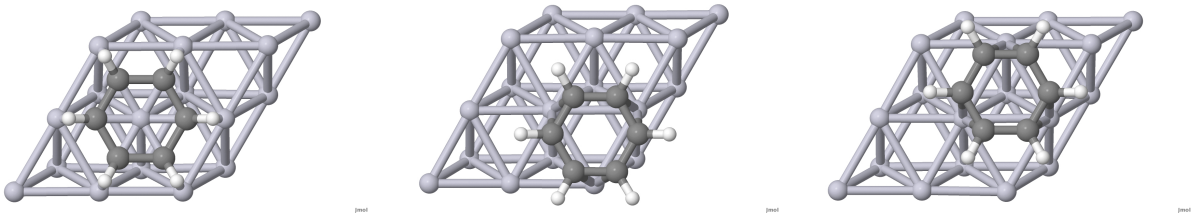

Figure 2.4: top0 (left), hcp0 (centre) and fcc0 (right)

Metastable geometry: bri0 In this configuration benzene is on bridge site but in a metastable position (fig. 2.3 right); characterized by two double and two single Pt-C bonds, under small rotation ($\geq 10^o$) or under small shift (≥ 0.15 Å 2.5), evolves into bri30 or into hcp0/fcc0.

Such behavior is then remarkably important once benzene like structures are part of larger and more complex system and, behaving as "anchor", can determine the molecule diffusivity.

Bond Distances In table 2.6 and 2.7 the C-Pt bond distances for both plane wave and localized orbital methods are shown In the first case both LDA and GGA calculation with known reference. For localized orbital calculations same values for a low (k-space grid 441) and high (Kgrid 551) convergence are obtained.

Bond lengths are also well maintained across the two codes for same functional, and, indeed are reported larger for GGA respect to LDA. Meanwhile the two bri0 single bonds are shorter than the two in bri30, the two pairs of double are much larger in bri0; therefore top0 represents the far less favorable orientation but its six single bonds are shorter than the double of the more favorable fcc0 (and hcp0). Adsorption and in general interaction of benzene aromatic ring on metallic platinum surface is then a complex matter in which distortion energetic is relevant.

2.7.2.2 VASP vs Openmx

The structural description of stable, metastable and unstable geometries among plane wave and localized orbital methods and between different functionals (LDA and GGA), is analogous; in addition also the energy differences between the various configuration are similarly maintained, as summarized in table 2.8 and 2.9.

Structurally bond distances show no appreciable difference between plane waves and LCAO methods. The calculations confirm that although absolute adsorption energies are quite different for the LDA and GGA approximations, both functionals do provide the same energy differences among the various relevant configurations.

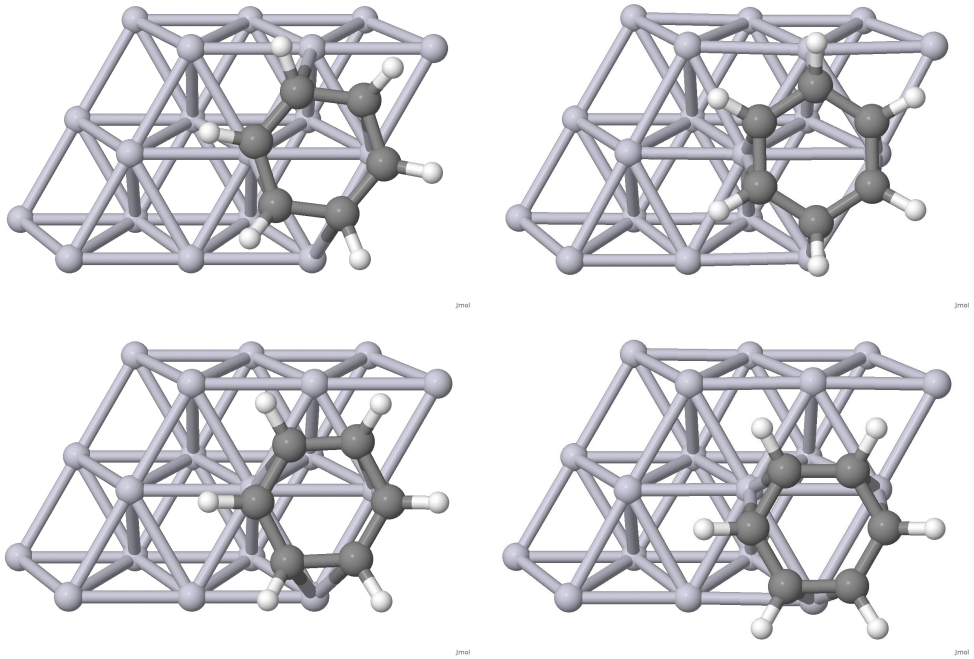

Figure 2.5: Metastable bri30. Initial rotation of 10º (top left) evolves toward bri30 (top right). Initial shift (low left) evolves to fcc0 (low right)

	VASP$^{MP551}_{\sigma=0.25}$		
(Å)	LDA	GGA	Reference[74]
bri30	2.13; 2.14; 2.16, 2.17; 2.16, 2.17;	2.18; 2.18; 2.21,2.22; 2.21,2.22	2.18; 2.18; 2.22, 2.22; (2 pairs)
top0	2.16 (6 bonds)	2.22 (6 bonds)	
bri0	2.08; 2.08; 2.28, 2.28; 2.28, 2.29	2.13; 2.13; 2.38, 2.38; 2.34,2.35;	2.15; 2.15 2.51
hcp0	2.17, 2.17 (3 pairs)	2.20,2.22; 2.22,2.22; 2.22,2.22	2.22, 2.22; (3 pairs)
fcc0	2.17, 2.17 (3 pairs)	2.22, 2.22 (3 pairs)	

Table 2.6: Carbon Platinum bond distances.

	Openmx		
(Å)	LDA$^{MP441}_{\sigma=0.01}$	LDA$^{MP551}_{\sigma=0.01}$	LDA$^{MP551}_{\sigma=0.25}$
bri30	2.13; 2.19; 2.18,2.23;2.17,2.23	2.14; 2.16; 2.19,2.22; 2.20,2.22	2.13; 2.15; 2.17,2.21; 2.17,2.21
top0	2.16 (6 bonds)	2.18 (6 bonds)	2.21 (3 bonds); 2.22 (3 bonds)
bri0	2.1; 2.1; 2.27,2.37; 2.29,2.36	2.1; 2.1 2.29,2.41; 2.28,2.37	2.12; 2.12 2.35,2.48; 2.34,2.42
hcp0	2.19,2.20; 2.19,2.21; 2.20,2.20	2.21,2.23; 2.22, 2.23; 2.22,2.23	2.21,2.23; 2.22, 2.23; 2.22,2.23
fcc0		2.20,2.20; 2.20,2.21; 2.20,2.21	2.21,2.22; 2.21,2.22; 2.21,2.22

Table 2.7: Carbon Platinum bond distances.

E_{ads} (eV)		VASP$^{MP551}_{\sigma=0.25}$			Openmx
initial	final	LDA	GGA	GGA[74]	LDA$^{MP551}_{\sigma=0.25}$
bri30		-2.67	-0.97	-0.90	-3.96
hcp30	bri30	-2.67	-0.97		-3.96
top30	bri30	-2.67	-0.97		-3.96
top0		-1.69	+0.25		-3.10
bri0		-2.01	-0.38	-0.30	-3.35
hcp0		-2.39	-0.75	-0.67	-3.57
fcc0		-2.30	-0.69	-0.61	-3.49
bri30-3L		-3.26	-1.51		
bri0-3L		x	-0.91		
hcp0-3L		-2.84	x		

Table 2.8: Adsorption energy values, for plane wave simulations (LDA and GGA) and LCAO methods (LDA with 441 and 551 k points grid)

$\triangle E_{ads}$ (eV)		Vasp$^{MP551}_{\sigma=0.25}$			Openmx
initial	final	LDA	GGA	GGA[74]	LDA$^{MP551}_{\sigma=0.25}$
bri30		0.00	0.00	x	+0.00
hcp30	bri30	0.00	0.00		+0.00
top30	bri30	0.00	0.00	x	+0.00
top0		+0.98	+1.22	x	+0.86
bri0		+0.66	+0.59	+0.60	+0.61
hcp0		+0.28	+0.22	+0.23	+0.39
fcc0		+0.37	+0.28	+0.29	+0.47
bri30-3L		0.00	0.00	x	
bri0-3L		x	0.60	x	
hcp0-3L		0.42	x	x	

Table 2.9: Adsorption energy difference respect to the ground state (bri30)

4 Layers$^{MP551}_{\sigma=0.25}$	Distortion Energy				
(eV)	$\triangle E_{ads}$	$\triangle E_{mol}$	$\triangle E_{slab}$	$\triangle(E_{mol}+E_{slab})$	$\triangle(E_{ads}+E_{dist_{tot}})$
bri30					
top0	+0.86	+1.93	+0.56	+2.48	-0.38
bri0	+0.61	-0.25	+0.21	-0.04	-0.65
hcp0	+0.39	-0.60	0.00	-0.61	-1.00
fcc0	+0.47	-0.63	0.00	-0.63	-1.10

Table 2.10: Adsorption and dis torsion energy difference in four layers slab.

	$Homo - Lumo_{molecule}$	Homo0=Homo-1	Lumo0=Lumo+1
bri30	4.26	no	no
top0	3.95	yes	yes
bri0	4.27	no	no
hcp0	4.80	yes	yes
fcc0	4.81	yes	yes

Table 2.11: LCAO: HOMO-LUMO gap and eventual degeneration (yes) of Homo0/Homo-1 and Lumo0/Lumo+1

	$Homo - Lumo_{molecule}$	Homo0=Homo-1	Lumo0=Lumo+1
bri30	4.02	no	no
top0	3.69	yes	yes
bri0	3.95	no	no
hcp0	4.54	yes	yes
fcc0	4.54	yes	yes

Table 2.12: Plane Waves: HOMO-LUMO gap and eventual degeneration of Homo0/Homo-1 and Lumo0/Lumo+1

Electronic Structure In tables 2.11 and 2.12 is shown the agreement in electronic structure description around Fermi level of adsorbing benzene in different configuration. Agreement between LCAO and Plane waves approaches is good and shows that Homo0 and Homo-1 as much as LUMO0 and LUMO+1 degenerate only in configurations where same kind of C-Pt bond is present, either all "single" or all "double". The band structure is also analogue between the two methodologies. Electronically results are also similar, HOMO-LUMO gaps are 5.18 eV and 5.19 eV respectively. For both methods, HOMO0 and HOMO-1 as HOMO-2 and HOMO-3 are respectively degenerated and with 0.01 eV energy difference. LUMOs description via LCAO method is progressively decreasing as expected.

2.7.2.3 Convergence with number of layers

Previously it has been show that energy differences and electronic properties are maintained between functional considered (LDA vs GGA) and between methods (plane waves vs local orbitals). The next step has been to show how similarities are maintained between adsorption on three and four layers, with same number of unconstrained layers during geometrical relaxation. This particular simplification is a strict requirements for adsorption of large polycyclic aromatic hydrocarbons on Pt(111), like the ones considered along this thesis. Therefore is extremely important to verify reliability of structural and energetic description on three layers; meanwhile is generically accepted that four layers are the minimum number which absolute energetic values are acceptable, relative energies can be maintained.

Surface relaxation differences between plane wave and LCAO approach are similar and upwards and downwards atomic shift is maintained in the two approaches. In bri30 case, the largest vertical relaxation differences are $5.0 * 10^{-2}$ and $5.2 * 10^{-2}$ Å all about one magnitude smaller. This same study shows that while absolute adsorption energies are also quite sensitive to the number of layers in the metal slab, energy differences among the different adsorption configurations are converged (with an error less than 5%) on a three-layer slab.

2.7.3 Graphene and Graphene on Pt(111)

The adsorption of graphene on Pt(111)$\sqrt{3} \times \sqrt{3}$ with 7 layers, of which two have been kept unconstrained during geometrical relaxation (fig. 2.6 left), has been considered to evaluate the not-hydrogenated carbon structure height on Pt(111) surface.

The graphene is much higher than benzene, as expected, and the height values are in good agreement between

4 Layers$^{MP551}_{\sigma=0.25}$					3 Layers				
(eV)	E_{ads}	E_{d_m}	E_{d_s}	E_{d_t}	$E_{ads}+E_{dt}$	E_{ads}	E_{d_m}	E_{d_s}	E_{d_t}
bri30	-3.96	+1.50	+0.21	+1.72	+5.68	-3.54	+1.81	+0.93	+2.74
top0	-3.10	+3.43	+0.77	+4.20	+7.30	-2.92	+3.95	+1.54	+5.49
bri0	-3.35	+1.25	+0.42	+1.68	+5.03				
hcp0	-3.57	+0.90	+0.21	+1.11	+4.68	-3.12	+1.13	+0.9	+2.03
fcc0	-3.49	+0.87	+0.21	+1.09	+4.58				

Table 2.13: Left: adsorption and distortion energies in four layers slab, K points grid 551, $\sigma = 0.25$. Right : adsorption and distortion energies for bri30, top0 and hcp0 configurations on 3 layers slab, as indication in systems with only single, double or both kind of bonds.

3/4 layers (eV) (eV)	E_{ads}	E_{d_m}	E_{d_s}	E_{d_t}	$E_{ads}+E_{dt}$	(eV) Ratio	E_{ads} 4 layers	E_{ads} 3 layers	$E_{ads}+E_{dist}$ 4 layers	$E_{ads}+E_{dist}$ 3 layers
bri30	0.91	1.09	4.17	1.45	1.08	bri30/top0	1.23	1.21	0.76	0.75
top0	0.92	1.06	2.04	1.23	1.10	bri30/hcp0	1.07	1.13	1.19	1.22
hcp0	0.86	1.1	4.29	1.64	1.06					

Table 2.14: Left: Energy ratio between 3 and 4 layers values. Right: Adsorption and distortion energy ratio between configuration bri30 and configurations top0 and hcp0, in 3 and 4 layers. E_{d_m} is the molecule distortion energy $E_{dist_{mol}}$; E_{d_s} is the slab distortion energy $E_{dist_{slab}}$; E_{d_t} is the total distortion energy $E_{dist_{totall}} = E_{dist_{mol}} + E_{dist_{slab}}$;

plane wave and localized orbital methods. Graphene sheet C-C bonds are therefore the same for two DFT approaches: 1.38 Å and similar values are obtained in adsorption condition. Good agreement between the two methods is also obtained for electronic structure (fig. 2.6).

2.7.4 Conclusions

The basis set chosen is able to reproduce structural and electronic characteristics of a wide range of organic molecules in different configurations, hydrogenation, doping and in the interaction with the platinum substrate. The study of benzene adsorption on Pt(111) with localized orbital and plane waves methods, shows that meanwhile total energy may be overestimated by Openmx, the differences are maintained between configurations, and such values are almost constant between plane waves and localized orbitals and between GGA and LDA functionals.

The relative energies between adsorption configurations on 3 and 4 layers are also constant and therefore, for large scale calculations, three layers slab is considered.

(eV)	$E_{ads}4l$	$E_{ads}3l$	$< z >_{mol}$ $4l$	$< z >_{mol}$ $3l$
bri30	-3.90	-3.54	2.12	2.08
top0	-3.18	-2.92	1.89	1.93
hcp0	-3.63	-3.12	2.14	2.09

Table 2.15: Adsorption Energy in 4 and 3 layers and relative height on surface.

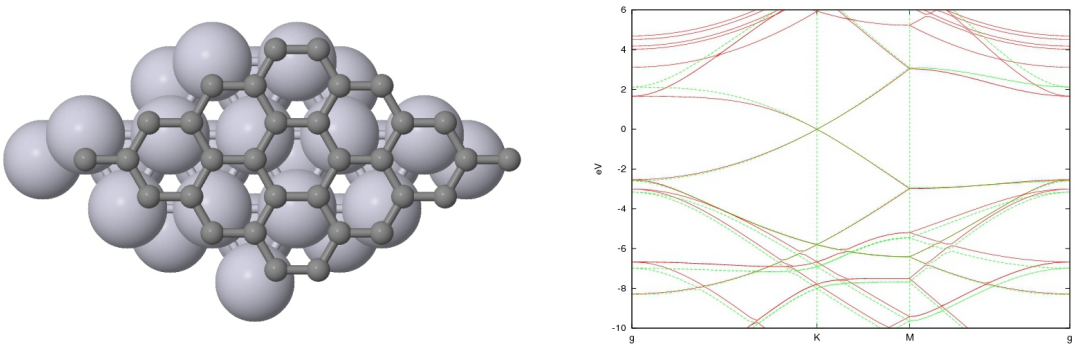

Figure 2.6: Left: Adsorption of graphene on Pt(111)$\sqrt{3}x\sqrt{3}x7$ slab. Cell has been multiplied in both x and y direction (perpendicular to view direction) to easy the visualization. Right: Band structure of graphene sheet: Vasp (red) and Openmx (green).

Chapter 3

Adsorption and related enantiomeric selectivity of $C_{60}H_{30}/Pt(111)$

The DFT characterization of the adsorption of fullerene molecular precursors $C_{60}H_{30}$ on Pt(111) surface, is one of the preceding steps required to understand the key issues that bring to the formation of isomerically pure samples of C_{60} after the cyclodehydrogenation process that occurs during annealing. In the following chapter, such matter is extensively discussed, and particular attention is firstly given to the experimental results (section 3.1), to the characterization of the molecule in the gas phase (section 3.2), to the choice of LDA as exchange correlation functional (section 3.3), to the adsorption of the molecule on Pt(111) (section 3.4), to the agreement with experimental results (section 3.5) and finally, it is discussed how metallorganic interaction energetics can be schematized in terms of C-Pt interactions (section 3.6) and the most important results summarized (section 3.7).

3.1 Motivation and Experimental Results

The wide class of polycyclic aromatic hydrocarbons (PAHs) have been intensively studied along the years in various fields[31, 32, 75, 76, 77, 78, 79, 80, 81, 82, 83, 84], from cosmology to biology, from simple to extremely complex molecules. They have been found in the interstellar medium, comets and meteorites, and are regarded as a possible basis for the earliest forms of life on Earth. For applications, their electronic affinity and optical properties have been intensively studied; in oil industry they are of interest because some are strictly linked to incomplete combustion of carbon-containing fuels, while others are carcinogens.

The PAH studied here, and depicted in fig. 3.3, is the molecular precursor from which the efficient surface catalysed cyclodehydrogenation forms fullerene after annealing at 750 K[85]. Therefore its full characterization is then important, in the gas phase, and not only as reference, as in the interaction with metallic substrates.

STM experiments at room temperature. identify two different molecular shapes (fig. 3.1), which depend on their orientation upon deposition and that are labeled R/L. In the shape a brightening central part can be distinguished, while different lobes disposition allows discrimination between L/R adsorbing structures. They are equally distributed (50% L, 50% R) and no cluster of L/R has been observed (fig. 3.2). All R/L molecules show a well defined positive/negative angle respect to the [1-10] crystallographic direction. Considering molecule and surface (111) symmetries, respectively 120º and 60º, a constant angular difference between L and R shapes is observed.

The molecule adsorption on Pt(111) at room temperature is then characterized by enantiomeric selectivity upon adsorption[86]; in particular the deposition leads to surface induced chirality caused by the different landing side, as revealed by in-situ RT scanning tunneling microscopy (STM): the surface becomes enantioselective "recognizing" the landing side of an individual molecule, discriminating on its chirality. To understand such behavior, its eventual importance for the adsorption and then for the cyclodehydrogenation, is necessary to analyze in details the metallorganic

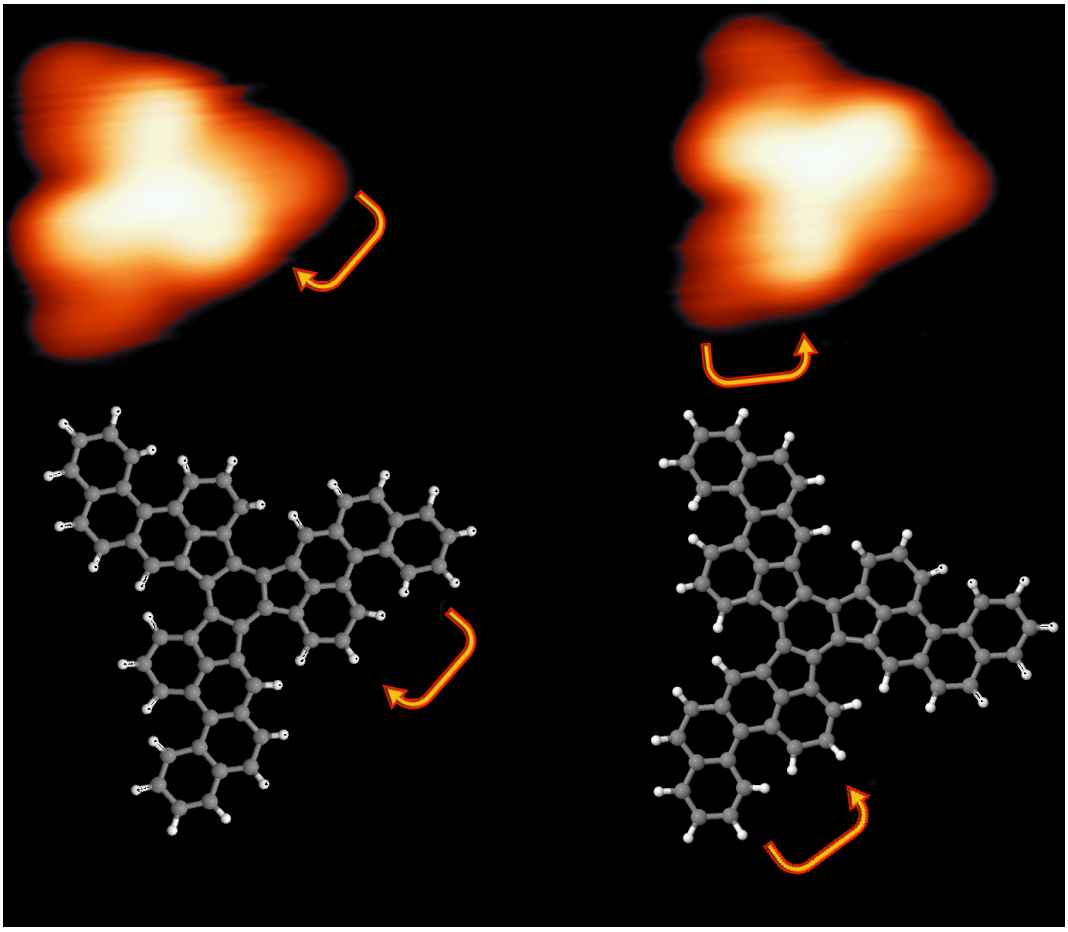

Figure 3.1: STM image of left/right hand landing $C_{60}H_{30}$ on Pt(111) and topological identification of distinctive elements.

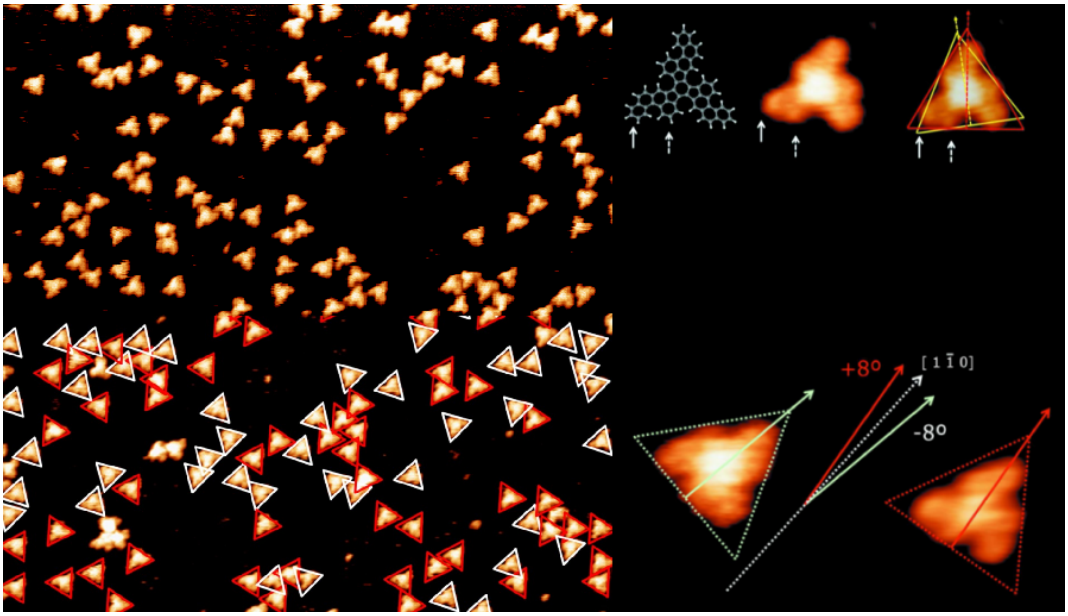

Figure 3.2: STM image of left/right hand landing $C_{60}H_{30}$ on Pt(111) at RT and their identification and angular characterization.

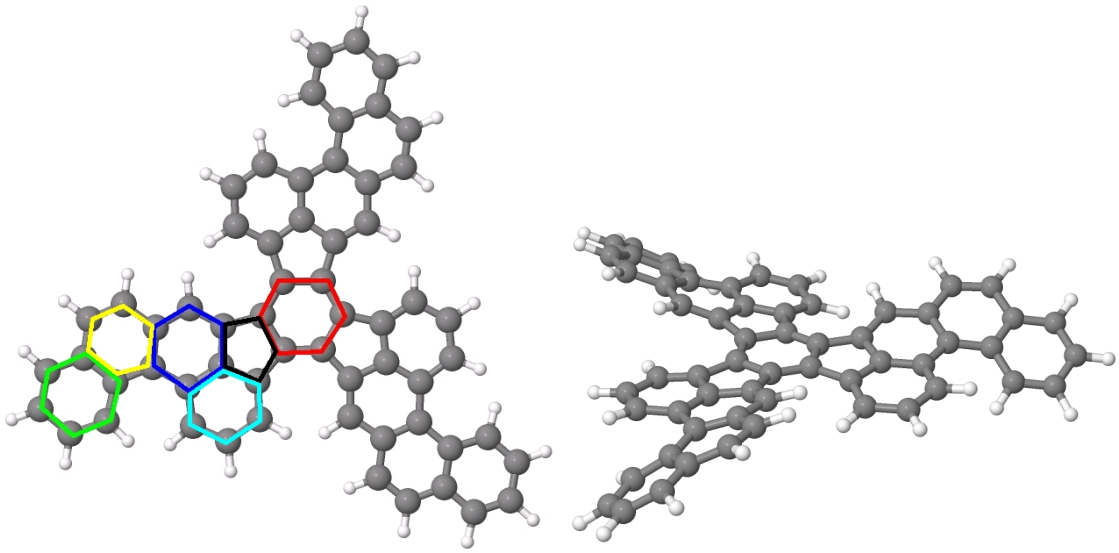

Figure 3.3: Polyarene $C_{60}H_{30}$ elements: central (red), pentagon (black), *iia* internal in axis (blue), *iooa* internal out of axis (cyan), *eia* external in axis (yellow) and *eooa* external out of axis(green).

interaction behind such process. Meanwhile such behavior could not be related to the cyclodehydrogenation process of the PAHs, it is essential to understand the adsorption mechanism, for fundamental knowledge of chirality mechanism and for the industrial applications in bio medicine, drugs targeting and delivering.

This work provides, through an exhaustive study of the phase space, focusing on highly symmetric adsorption sites, their translations and rotations, the unique definition of one configuration as ground state (and its multiplicity), and explains its enantiomeric adsorption in terms of its moieties components, which anchor the external parts.

Such components are, both structurally and electronically, similar to benzene, and the highly selective connection between landing sites can be rationalized in terms of adsorption energetics.

3.2 Polyarene: free molecule

Like other PAHs, the polyarene $C_{60}H_{30}$[44] considered in this work consists in fused aromatic rings and is characterized by a central hexagon and three identical wings, distant 120º. Each wing is connected to central hexagon by a pentagon (red in fig. 3.3). In each wing we identify "in axis" hexagons (internal -*iia*- and external -*eia*-, respectively blue and yellow in fig. 3.3) to which two others hexagons are bonded and labeled as "out of axis" (internal -*iooa*- and external -*eooa*-, respectively cyan and green in fig. 3.3). In each wing two atoms of *iooa* hexagon with two atoms of adjacent wing *iia* hexagon and two atoms of central hexagon, form the "internal open ring" -*ior*-, while "external open ring" -*eor*- refers to the unclosed part between external and internal hexagons. In the molecule four different kind of carbon atoms can be identified: graphene bulk (coordinated with other 3 carbon - central part of the molecule), armchair (external in axis C-H pairs), corner (C-H pairs in external out of axis hexagons) and zigzag (C-H pair in the internal in axis hexagon).

In the gas phase, the molecule is markedly twisted, with each of the three wings adopt an helical shape. As consequence of the steric congestion of their bay positions forces, the outer aromatic ring (*eooa*) of each wing to flip up with respect to the plane of the central ring. The twisted conformation can be described by the distance the most external carbon atom is placed above the mentioned plane (0.89 Å) and by the twisting angle of each molecule branch (30.5º). In particular, these results are the same, considering localized orbitals (Openmx[67, 68, 69]) and plane waves (VASP[60, 61]) approaches.

3.3 Approach to study the adsorption of large aromatic hydrocarbons on platinum surfaces: Openmx with LDA XC-functional

When adsorption on Pt(111) surface is considered, a plane waves approach is not possible for the large unit cell required to accommodate the molecule and for the complexity of the phase space because the adsorption depends on position and orientation of the ad-molecule. A localized orbital method is then considered through Openmx[67, 68, 69].

The software is a norm-conserving Troullier-Martins pseudopotentials[87] code, which functions are expanded by a linear combination of multiple pseudo - atomic orbitals (LCPAO) with a kinetic energy cutoff for the real-space grid technique. that is needed to perform calculations with the extremely large unit cell (involving almost 400 atoms)

As mentioned in chapter 2, the exchange functional chosen in this work is LDA. Meanwhile not the best functional (e.g. total energy are overestimated), in system which structural molecule - substrate matching is extremely important, LDA reproduces a substrate lattice constant (3.928 Å) more similar to experimental values (3.92 Å[73, 88]) than GGA (3.985 Å); furthermore the energy differences between the configurations are also maintained along GGA and LDA, and with 3 and 4 layers, when smaller $C_6H_6/Pt(111)$ is considered (chapter 2). GGA approach with localized orbital is not considered, as it requires a computationally demanding basis set for platinum, that includes also f orbitals.

The atomic orbitals considered for carbon hydrogen and platinum atoms are chosen, and eventually optimized, as explained in chapter 2.

Supercell approach is adopted, considering periodic boundary conditions on the three Cartesian axis for 10×10 Pt(111) surfaces unit cell. One single molecule was set on only one side of the slab, which consisted of three atomic layers, and geometrical relaxation permitted for the molecules for the first two slab layers along all Cartesian directions. The unit cells size considered, makes neighbors interaction negligible along the infinite array of slab on x,y plan; on the direction perpendicular to the surface, appropriate vacuum size (twice the slab thickness) has been set to minimize interaction and dipole effects, which can be considered negligible on adsorbed benzene. Total energy calculation of the isolated molecule (gas phase) has been performed with the Γ point, while the Brillouin space has been sample with a 221 mesh for adsorption calculations. Electronic and ionic convergence are set respectively 10^{-6} Hartree ($2.7 * 10^{-5}$ eV) and $2x10^{-4}$ Hartree/Bohr (10^{-2} eV/Å).

3.4 Adsorption of the Polyarene on Pt(111): structure

3.4.1 Looking for the ground state

The wide phase space of possible adsorption configurations have been explored through initially flat geometries, characterized by different position of the central hexagon, and considering the competition between the outer hexagons in the wings, that share the same orientation, and the central hexagon, that is rotated by 30 degrees.

Among the various geometries considered, stable and unstable configurations are obtained. In particular the configuration labeled 2bri30fcc0-top0 relaxes geometrically towards 3bri30-bri0 (fig. 3.4), which has the lowest energy (-14.03 eV) respect other minima obtained (table 3.1).

The ground state (3bri30-bri0) geometrically relaxes inducing a curvature (fig. 3.5) that depends on kind of carbon atom considered. The hydrogenated external parts (corner C), minimize the distance with substrate (2.12 $\AA$) and therefore bond through p_z with tilted C-H bonds, behavior proper of benzene on same substrate (chapter 2). Central parts, in which carbon atoms bond only with other carbon atoms, increase their height on surface (2.53 $\AA$), like graphene. These two different behaviors induce the observed curvature reported in column II, III and IV in tables 3.1 and 3.2.

The geometrical orientations of molecule hexagons, table 3.1 and 3.2, show that the favorable adsorption configuration for the external hexagons in the wings control the energetics.

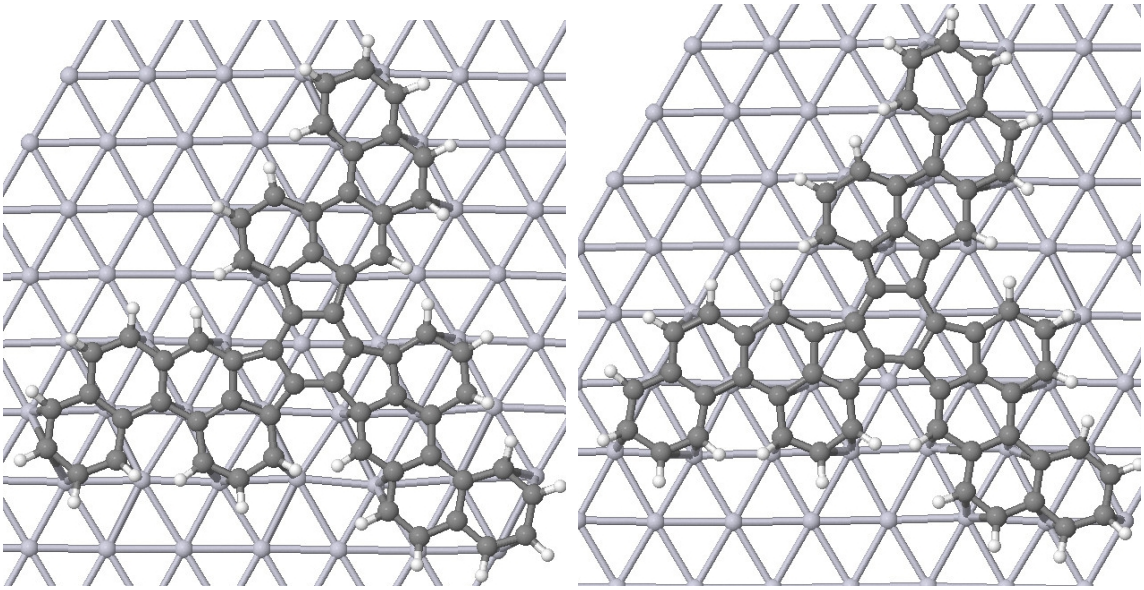

Figure 3.4: Initial configuration 2bri30fcc0-top0 and final configuration 3bri30-bri0 to which it converges. Only one substrate layer is shown to ease the visualization.

	E_{ads} (eV)	$< z >_{C_{hex}}$ (Å)	$< z >_{Ext_{out}}$ (Å)	$\triangle z$ (Å)	Ext_{out} W_1	W_2	W_3	Ext_{in} W_1	W_2	W_2
3bri30-bri0	+0.0	2.53	2.12	0.41	bri30	b30	b30	b30	b30	b30
chiral	+0.03	2.43	2.12	0.31	b30	b30	b30	b30	b30	b30
+72*	+1.97	2.63	2.17	0.46	$\sim b0$	$\sim b0$	$\sim b0$	b30	b30	$\sim b0$
3hcp0-hcp30	+1.61	2.38	2.14	0.24	h0	h0	h0	$\sim b30$	$\sim t0$	b30
3top0-top30	+4.79	2.73	2.08	0.75	t0	t0	t0	f0/t0	t0	f0
2bri0fcc0-top30	+2.25	2.72	2.09	0.53	b0	f0	b0	b0	f0	b30

Table 3.1: Adsorption energy difference respect to ground state, height of central and external out of axis hexagons and their difference. Final adsorption configurations for external out of axis (Ext_{out}) and in axis (Ext_{in}) hexagons per wing (W_1, W_2, W_3). Initial configurations are considered from rotation of bri0 position. Configuration 72* is a direct rotation of most favorable adsorption configuration. Notation used: b30=bri30, b0=bri0, f30=fcc30, f0=fcc0, t0=top0, h0=hcp0

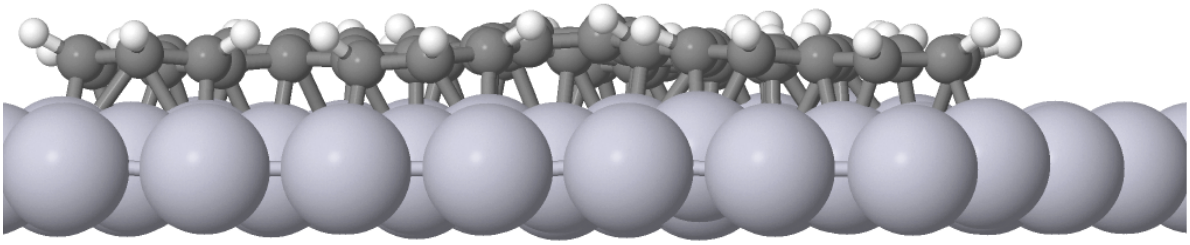

Figure 3.5: 3bri30-bri0: side view. Only one substrate layer is shown to ease the visualization.

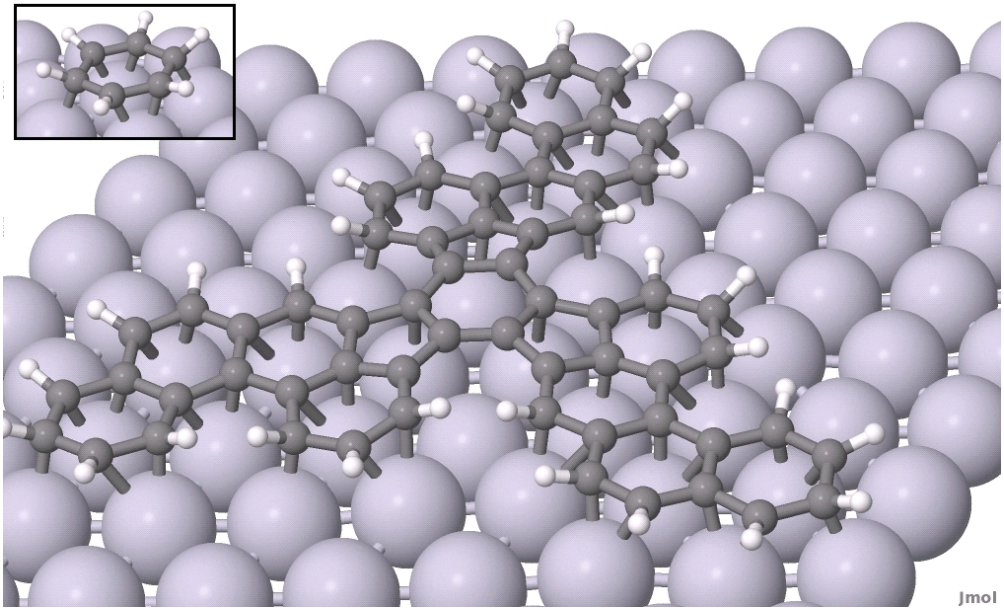

Figure 3.6: Ground state 3bri30-bri0. Insert shows benzene bri30 adsorption. Only one substrate layer is shown to ease the visualization.

Adsorption energies are maximized by bri30 optimal orientation (ground state and chiral) and decrease with the benzene adsorption assumed by external out axis hexagons. Less relevant is the contribution of the internal out of axis hexagons.

The chemisorbed external parts dominate adsorption energies, while difference on molecular height ($\triangle z = < z >_{C_{hex}} - < z >_{Ext_{out}}$) suggests that height of central hexagon may not be important (3bri30-bri0 and its chiral total energies differ by a negligible 0.03 eV, while $\triangle z$ by a relevant 0.15 Å).

Tables 3.1 shows that adsorption is dominated by adsorption orientation of external out of axis hexagon, in a benzene like behavior.

These results show that the molecule tries to maximize the number of favorable adsorption positions for all of its individual benzene-like rings. The former dominate, leading to the ground state configuration labeled then 3bri30-bri0, where the 3 outer hexagons are in the bri30 position, while the central hexagon is on a bri0 position (fig. 3.6).

To maximize the number of C-Pt bonds for bri30 like adsorption position, the molecule wing axis needs to be along the [1-10] direction.

The distances between analogous carbon atoms (O, X in fig. 3.7) is slightly inferior to Pt-Pt substrate distance (2.73Å) and the hexagons can adsorb "locked" between two adjacent [1-10] directions in the ground state configuration, fig. 3.11. Again, such symmetric orientation is simultaneously possible in the three wings, due to the 120º wing angular distance that matches with the multiplicity of angular distances of crystallographic directions of substrate (111) geometry, 60º.

Additional confirmation that the polyarene may be considered as an ensemble of benzene moieties, is that the two in axis hexagons resemble naphthalene-like rings, which, for the ground state, adsorb in the naphthalene most favorable di-bri30 position, following notation used for orientation of aromatic ring orientation on the substrate as from Ref. [89]. In naphthalene two di-bri30 orientation are possible, different by orientation of the crystallographic directions with respect to molecule bond, labeled $\alpha di-bri30$ for 0º angle and $\beta di-bri30$ for 30º (fig. 3.8); due to the strain induced by other hexagons, only $\alpha di-bri30$ orientation is observed in the ground state configuration contemporary in all the wings.

Ground state and its chiral image adsorb identically, bond lengths are substantially similar and their total energy difference is 0.03 eV.

Their angular distance with [1-10] is the same (18º) but opposite in sign; then they are mutually distant 36º.

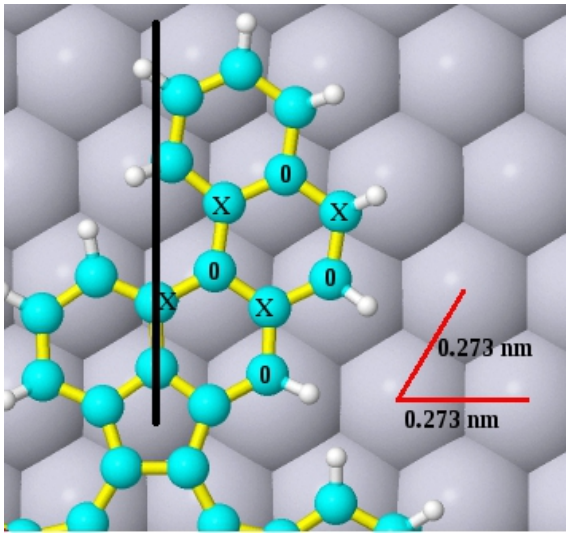

Figure 3.7: $C_{60}H_{30}$ wing adsorption. Internal hexagon common side should have to be parallel with two side of external out of axis hexagon. In axis hexagons atoms are alternatively in top (0) or hollow (X) positions.

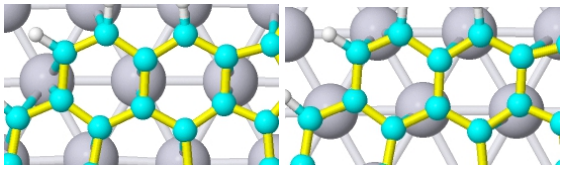

Figure 3.8: The di-bri30 naphthalene adsorption orientations for in axis hexagons: αdi-bri30 (left) and βdi-bri30 (right)

This result shows that upon deposition, the ground state angular distance is uniquely defined in agreement with the experiment, but not with the absolute value experiments report.

3.4.2 Understanding the preferential orientation

The next steps focus on understanding the existence of only one preferred orientation and on the disagreement between theory - experiment on the angle. First, to verify the possible existence of another ground state, a systematic study of the rotation of the already obtained minimum energy configuration (3bri30-bri0) is carried.

The systematic exploration of the rotations from the ground state orientation starts from an highly symmetric position to which the 3bri30-bri0 is shifted to (0º in table 3.2). This new configuration is negligibly different from original as all elements have identical orientation respect to the substrate but the central hexagon is in perfectly symmetric bri0 position. Nonetheless, upon relaxation, it converges to the original minimum (fig. 3.10 left). Considering the symmetries, 120º the molecule and 60º the substrate, initial rotation angles are considered from -10º up to 110º, spaced by 10º. Around the ground state, also $\pm$5º rotations have been considered. Results, fig. 3.9 and table 3.2, show that no other ground state is found else than for the already obtained.

In fig. 3.9, the ground state is represented by the well defined minimum in energy curve, and by its 60º multiplicity according to the substrate 60º symmetry, forms a -18º angle with [1-10] crystallographic direction, and so 36º with the chiral counterpart. The higher mobility of the molecule observed on other metals, disappears on Pt(111) where proper “channels” for the benzene “insertion” exist as consequence of the geometry of the substrate. This structural matching between the molecule bri30 geometries and the [1-10] is important to decrease molecular diffusivity on the surface, as much as the electronic properties of substrate-molecule interaction. If low diffisivity was merely linked to the electronic affinity other deep minima would be observed. The importance of the substrate molecule matching validates the LDA approach adopted.

α_i	α_f	E_{ads} (eV)	$< z >_{C_{hex}}$ (Å)	$< z >_{Ext_{out}}$ (Å)	$\triangle z$ (Å)	Ext_{out} W_1	W_2	W_3	Ext_{in} W_1	W_2	W_3
-5	-4.8	+0.4	2.46	2.11	0.35	b30	b30	b30	f30	b30	b30
0	0^T	+0.0	2.53	2.12	0.41	b30	b30	b30	b30	b30	b30
+5	+3	+1.41	2.45	2.08	0.37	t0	b30	b30	f30	f30	b30
+10	+9.8	+3.56	2.39	2.13	0.26	$\rightarrow b0$	b30	$\rightarrow f0$	$\rightarrow b30$	b30	f30
+20	+17.4	+2.80	2.46	2.15	0.31	b0	b0	b0	$\sim f0$	f0	$\sim f0$
+30	+28	+3.35	2.47	2.11	0.36	$\sim b30$	$\sim b30$	$\sim b30$	f0	b0	t0/b0
+40	+40.3	+2.29	2.44	2.11	0.33	$\sim b30$	f0	$\sim b30$	b0	b0	b0
+50	$+56.3^{TR}$	+2.47	2.44	2.13	0.31	b30	$\sim b30$	$\sim b0$	b30	b30	t0
+55	$+59.4^{RT}$	+0.00	2.46	2.10	0.36	b30	b30	b30	b30	b30	b30
+60	+59.6	+0.27	2.46	2.12	0.34	$\sim f0$	b30	b30	b30	b30	b30
+70	+68.2	+3.54	2.70	2.28	0.42	$\sim f0$	$\sim f0$	t0	b30	b30	b30
+72	+71.0	+3.13	2.37	2.15	0.22	b0	t0	h0	h30	t0	h30

Table 3.2: Initial and final angle for each geometrical relaxation. Adsorptin energy difference respect to the ground state, height of central and external out of axis hexagons and their difference. Final adsorption configurations for external out of axis (Ext_{out}) and in axis (Ext_{in}) hexagons per wing (W_1, W_2, W_3). Initial configurations considered are rotation from highly symmetric position bri0 for central hexagon, which spontaneously relaxes into ground state. Superscript R and T indicate rotation and translation. Notation used: b30=bri30, b0=bri0, f30=fcc30, f0=fcc0, t0=top0, h0=hcp0

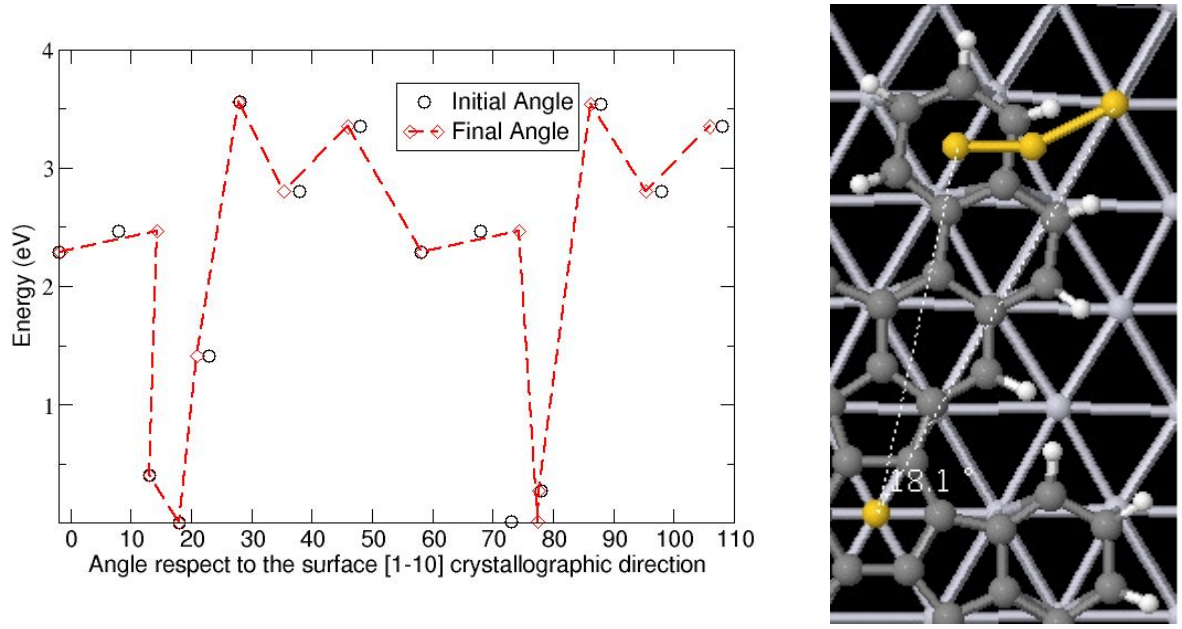

Figure 3.9: Left: Energy curve for enantiomeric adsorption of polyarene ground state 3bri30-bri0 rotation on Pt(111), angles are considered respect to the crystallographic direction. Right: geometrical definition of the angle.

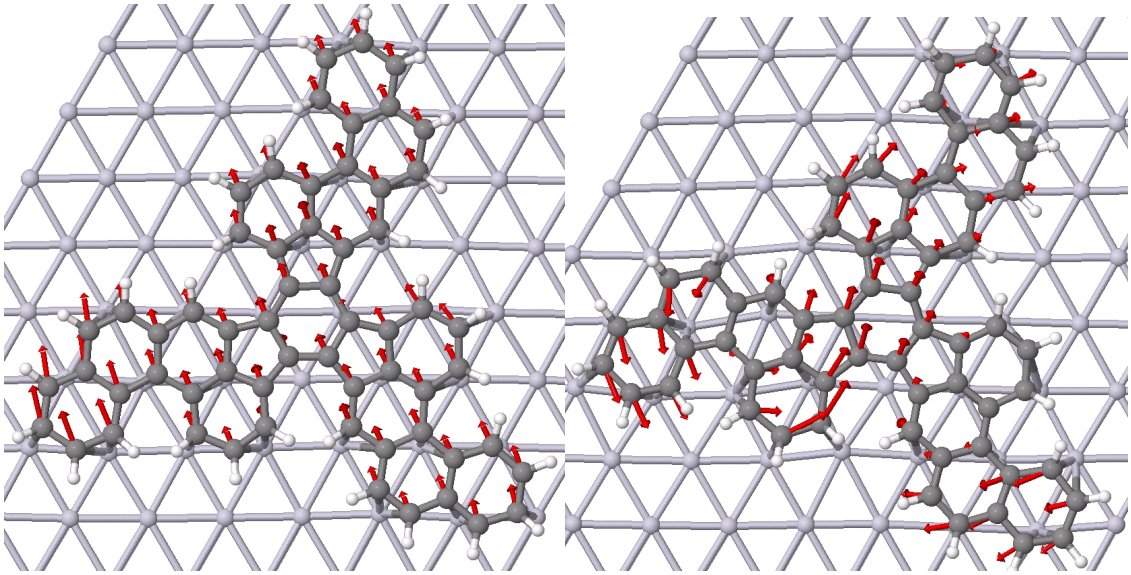

Figure 3.10: Two configurations for 0º (final) and 10º rotations. Red arrows (significantly enhanced) point towards respective initial configuration. Only one substrate layer is shown to ease the visualization.

In general, most configurations tend to adjust their angle with small variations and their position with small shift, while others only via rotation or translations, some more than others. The relaxation process is anyway particularly complicated and it is showin in fig. fig. 3.9, through the aid of arrows that point toward the initial configurations. It can occur through simple translations (fig. 3.9 left) or through complex movements generated by unstable adsorption orientations for single hexagonal rings (top0 for almost all elements of one wing in fig. 3.9 right)

The asymmetry of the curve (fig. 3.9) shows the complexity of relaxation process, and the low diffusion barriers between all minima else than the ground state. Depending on which rotation/translation is firstly exploited by the molecule relaxation, similar angle configurations may end differently: $\alpha_i = 50º$ ends at $\alpha_f = 56.3º$, while $\alpha_i = 55º$ configuration ends with $\alpha_f = 59.4º$. In the first case rotation follows the translation, while the opposite occurs in the second case.

Considering clockwise direction as positive, for initial angle $\alpha_i < 40º$ (ground state 0º/60º), relaxation is anticlockwise and $\triangle\alpha < 5º$; on the opposite for $\alpha_i \geq 50º$, rotation is clockwise and $\triangle\alpha > 5º$, while for $\alpha_i = 40º$ no effective rotation is observed. Energy profile in fig. 3.9 also suggest a more favorable clockwise rotation.

Such behavior is strictly related with adsorption toward the ground state. For rotations which initial angle is $\alpha_i > -10º$ the rotation is driven by the naphthalene-like structure composed by the in axis hexagons that tend to "fall" into the [1-10] channels; else the angular shifts are only of minor amount because are driven toward the ground state by the *eooa* hexagons, which higher flexibility and reactivity with substrate are unable to drag all the wings.

The low energy differences among the rotations of ground state (low diffusion barriers) and the deep energy well in which the obtained ground state lies into and the high diffusion barriers, confirm that, like for experiments, the global minimum (ground state) is uniquely determined.

Adsorption of 3bri30-bri0 occurs so that the four hexagons per wing lock inside three [1-10] parallel crystallographic directions (fig.3.11) and its chiral (-3bri30-bri0) counterpart owns identical orientation with opposite direction. Such behavior among the two different landing sides is expected for simple geometrical reasons: for the two molecules, in each wing, the internal hexagons (*iia* and *iooa*) share same orientation respect to the bisectrix of two [1-10] directions, so the external hexagons (*eia* and *eooa*) in one molecule are the specular images of the homologous hexagons in the other molecule. Therefore the *eia* hexagons form identical angle with [1-10] and *eooa* hexagons form identical angle with opposite direction for the symmetry of hexagon built on two adjacent hexagon bonds (60º). The angle observed between molecules and the crystallographic direction is then equal in modulus and opposite in sign for the L/R adsorbed molecules. For geometrical reasons, if the molecule is considered flat, the angle formed with the

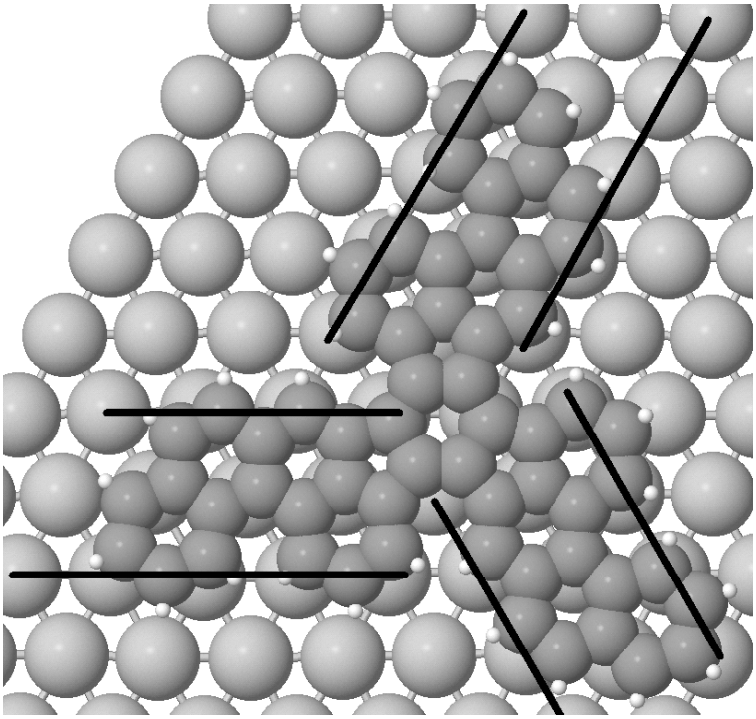

Figure 3.11: 120º symmetry of polyarene wings in ground state configurations, where are "locked" into [1-10] crystallographic directions. Only one substrate layer is shown to ease the visualization.

crystallographic direction (15º) is still similar to value obtained upon relaxation (18º).

Similar landscapes for adsorption energy and the variation respect to molecular height of the ground state are shown in fig. 3.12, where the configuration at 30º has also been artificially force to pass what it seemed a barrier.

3.5 Making contact with the experiments

STM experiments at RT, reveal an outstanding homogeneous shape for all scanned molecules, which adsorb enantioselectively, and which orientation depends on deposition. Such similarity among various molecules sampled, is another evidence that each configuration and its 60º multiplicity share analogous adsorption sites geometries. Analogously, the theoretical approach to adsorption of the fullerene molecular precursor show an uniquely side dependent orientation respect to crystallographic directions. Never the less, theory and experiments apparently come to a disagreement on angular distance between the two L/R molecules.

3.5.1 STM simulations with the Tersoff-Hamann approximation

The simple superposition of the STM image and the structure of the molecule suggests that STM is not showing part of the molecule, the reason can be a combination of structural and electronic effects so that *eooa* hexagons are not visible, explaining that STM angle respect to [1-10] directions is not taken considering the same points it was supposed to, and which are used in the theoretical evaluation of the angle.

In the previous section the ground state is uniquely determined by DFT calculations and, meanwhile total energy values may differ with other functionals, energy differences strongly identify one and only ground state orientation; as no other minima energetically similar to the ground state are obtained, the possibility that geometrical and electronic effects "hide" the *eooa* hexagons is a reasonable explanation of the disagreement on angular distances. Geometrical analysis of adsorption configuration already revealed that bonding parts of the molecule, *eooa* hexagons, are 0.41 Å lower than central part, so the electronic analysis of the density of states, as much as of the molecular orbitals can provide a further insight on eventual undetectability of external parts of the wings.

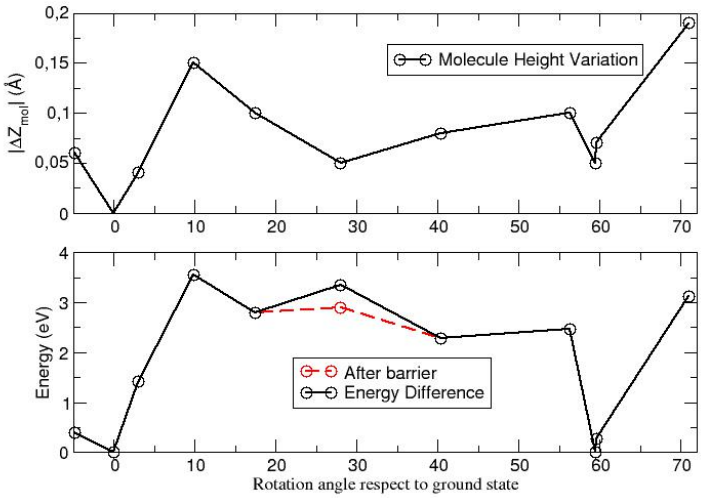

Figure 3.12: Up: Molecule height difference (module) respect to ground state value. Down: Energy profile for rotation of ground state.

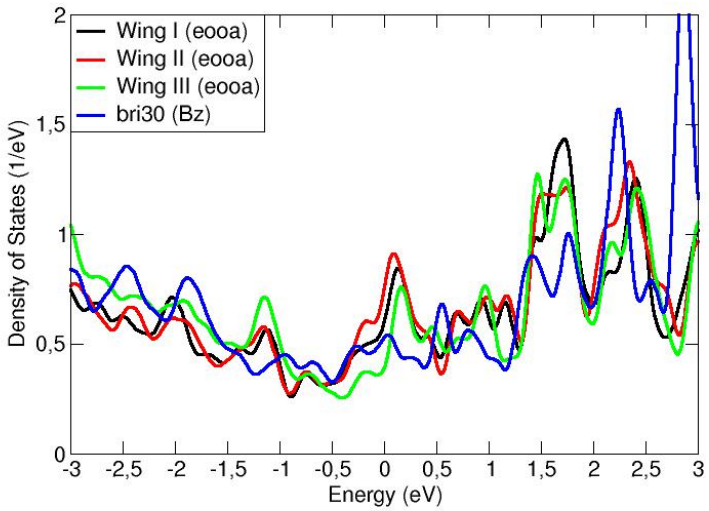

Figure 3.14: PDOS analysis for polyarene external wings and bri30 benzene adsorption.

The sum of DOS projected on the p_z orbitals for the central ring, one iia and one eooa hexagons are shown in fig. 3.13. The comparison with the sum of the total DOS projected on those atoms clearly shows that the states around the Fermi level are essentially of p_z character. The DOS is dominated in the [-1,1] eV energy range by the central ring, while the contribution of the outer rings, more strongly bonded and closer to the surface away from the center, is significantly depleted. The benzene like behavior of *eooa* hexagons is also shown in fig. 3.14, where density of states is comparable with benzene adsorption on same surface for a wide range of energies.

In addition, the broad density of state in the energy range considered [-1, 1] does not vary significantly in good agreement with experimental STM images which are similar for filled and empty states.

The Tersoff-Hamann[90] approximation is a procedure that allows to associate the calculate molecular orbitals to

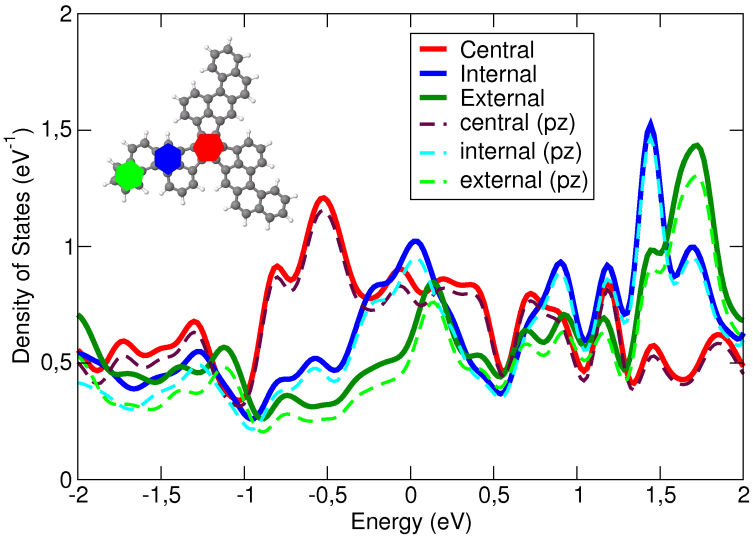

Figure 3.13: DOS (straight line) and PDOS (line dot) for ± 2 eV around Fermi level for central hexagon (red), internal in axis (blue) and external out of axis (green).

STM images. In this method the tunneling current $I(R)$ is proportional to the local density of states, as from[91]:

$$I(R) \propto \sum_{E_n > E_F - eV_{bias}}^{E_n < E_F} |\psi(R,E_n)|^2 =: n(R,V_{bias}) \tag{3.1}$$

where E_n the eigenstates, E_F if the Fermi level, V_{bias} is the bias voltage and n the electron density. On metal surfaces, to an isosurface of 1×10^{-4} Å^{-3} corresponds a current of 1 nA.

In many situations, the model provides a reliable qualitative picture of the surface topography. Meanwhile lacking on eventual effects depending by the devices tip, is a good approximation of general behavior that can be expected, being tip independent, and saving computational time. The approximation is used on the calculated local density of states $\rho(r,E)$ integrated in the energy range $(E_F - 1, E_F)$ is shown in fig. 3.15 (left) and corresponding to the isosurface of a constant value of the LDOS of 4×10^{-4}Å^{-3}, shows a corrugation height close to the experimental values (0.7 Å).

3.5.2 Matching Theory and Experiment in the angle formed between the molecules and the surface crystallographic directions.

The ground state configuration for adsorption shows marked differences in height with respect to the surface for the various rings in the molecule: the carbon atoms on the central hexagon have relaxed outwards and are on average 0.41 Å higher than the atoms on the outer hexagons (average height: 2.12 Å). At the same time, the simple Tersoff-Hamann approximation reported, shows an experiments compatible corrugation height, while LDOS is larger in the central part and in the C rings close to the pentagons of the molecule, than in the peripheral C-rings.

Therefore the geometrical and electronic explanations of the clear maxima around the central hexagon and the pentagons, and of the missing outermost rings in each of the wings in the STM image, are obtained combining the mentioned height differences and the weight of the density of states (DOS) associated to the π orbitals in the relevant energy range around the Fermi level.

In fig. 3.15 (right) the combination of circles and triangles obtained by the theory are superimposed to experimental STM image, which reveals enhanced intensity in the molecular region corresponding to the centre of the molecule, but reduced for the outer rings (*eooa*). Therefore the difference between the real molecular structure and STM shape has to be taken into account to consider the angular distances respect to the [1-10] crystallographic direction. Constructing an experimental corrected triangle (orange in fig. 3.15 right) and considering the calculated ground state, the possible thermal drift and the experimental errors, the angular difference between molecules adsorbed is defined as 34 ± 6º, in

good agreement with the theoretical result.

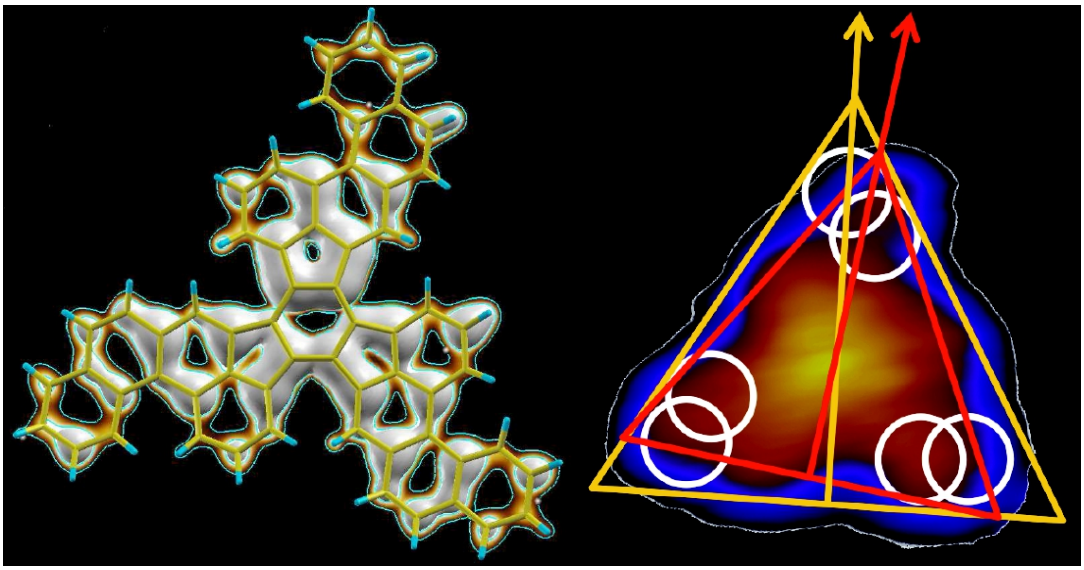

Figure 3.15: Left: Tersoff-Hamann approximation based on the calculated local density of states $\rho(r,E)$ integrated in the energy range (E_F-1,E_F). Right: Experimental STM image does not show the outermost hexagonal-carbon rings of the molecule (white circles), and consequently a correction factor of 9º has to be added to the experimentally determined value.

3.6 A Simple Model to describe the adsorption of large PAHs on Pt(111)

It has been proof that, structurally, the polyarene is enantiomerically anchored by its external out of axis hexagons in a benzene like behavior. The density of states analysis had shown that *eooa* hexagons resemble also electronically a benzene in bri30 adsorption (fig. 3.14). On such assumptions, the aim is to create a simple model for the interaction of the large PAHs, and in particular of the fullerene molecular precursor, as ensemble of benzene like moieties.

3.6.1 Building the model: Benzene Adsorption on Pt(111)

The adsorption energy E_{ads} can be written as the sum of two energetic terms, the bonding E_b and the distortion E_{dist} ones, as follow:

$$E_{ads} = E_b + E_{dist} \tag{3.2}$$

and where E_b is the sum, over all bonds.

$$E_b = \sum_{bonds} E_{bond,morse} \tag{3.3}$$

Such term can be approximated with a simple Morse potential, and defined as follow

$$E_M = D_e[(1-e^{\alpha(r_e-r)})^2 - 1] \tag{3.4}$$

where α the parameter that control the width of the well, r is the bond length, r_e is the equilibrium distance and D_e is a prefactor representing the depth of the potential well when $r = r_e$.

As expected, the Morse potential does not correctly reproduce the simple C-Pt interaction for large distances from equilibrium, but it is a good approximation in the small bond length variations considered in this work.

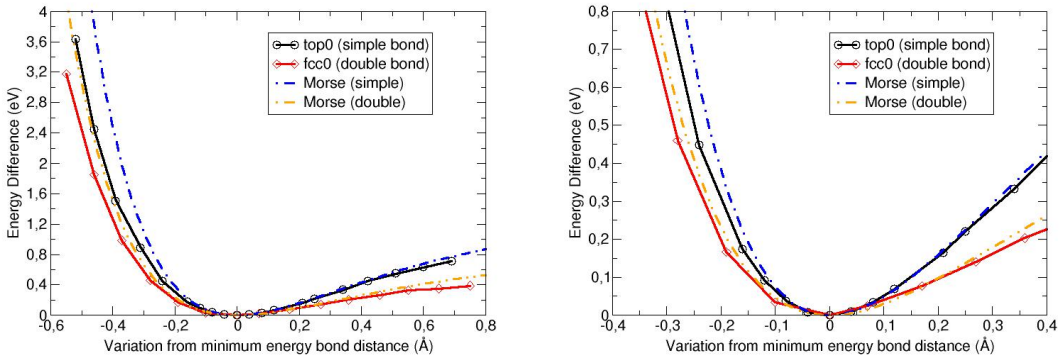

Figure 3.16: Variations from equilibrium bond distance between simple and double bonds, obtained respectively from top0 and fcc0

	E_M (eV)	$E_{ads}+E_{dist}$ (eV)	Single (Å)	Double (Å)
bri30	5.61	5.62	20º	19º
bri0	5.31	5.15	0º	28º
top0	7.56	7.55	35º	-
fcc0	4.61	4.55	-	17º
hcp0	4.62	4.68	-	17º

Table 3.3: Column I: benzene adsorption configurations. Columns II and III: Morse potential model reliability for benzene adsorption. E_Σ is the sum of adsorption and distortion energy while E_M is the value obtained modeling C-Pt interaction with Morse potential. Column IV and V: angle considered between the perpendicular to the surface and the bond between Pt and C, single or double; values are calculated as difference between 90º and angle formed between the bond and the [1-10] crystallographic directions.

Need of two Morse potentials Next step has been to consider the energetic profile for two adsorption orientations of benzene (Bz), characterized each by either only double or single bonds, respectively when two or one carbon atoms are bonded to same Pt atom. The energy variation of each kind of bond respect to tehir respective equilibrium distance is in fig. 3.16. The profiles are obtained through rigid height variation of minimum energy adsorption geometry in each case. No unique Morse potential can describe the two different interactions between substrate and aromatic ring, then an additional refinement is required considering one potential per kind of bond.

Nevertheless, systems may have both single and double bonds (bri30, bri0). To describe such systems, is important to understand the energy profile difference between single bonds in top0 and bri30 and between double bonds in fcc0 and bri30.

To do so the angles formed between the direction perpendicular to the surface and the bond (single/double) should approximately similar. Table 3.3 shows that it must not be the case as the angles for all considered benzene configurations are shown.

Single bond For the single bonds, the energetic variations from equilibrium distance in top0 system (6 single bonds) and in bri30 (2 single and 4 double bonds) can be compared. In both systems, single bonds are approximately normal to the surface. In mixed system bri30, the energy of single bond is obtained with the approximation provided by equation 3.5 for the energy of the single bond.

$$E_{s_{bri30}}(d) = [E_{bri30}(d) - 2(E_{fcc0}(d))/3]/2 \tag{3.5}$$

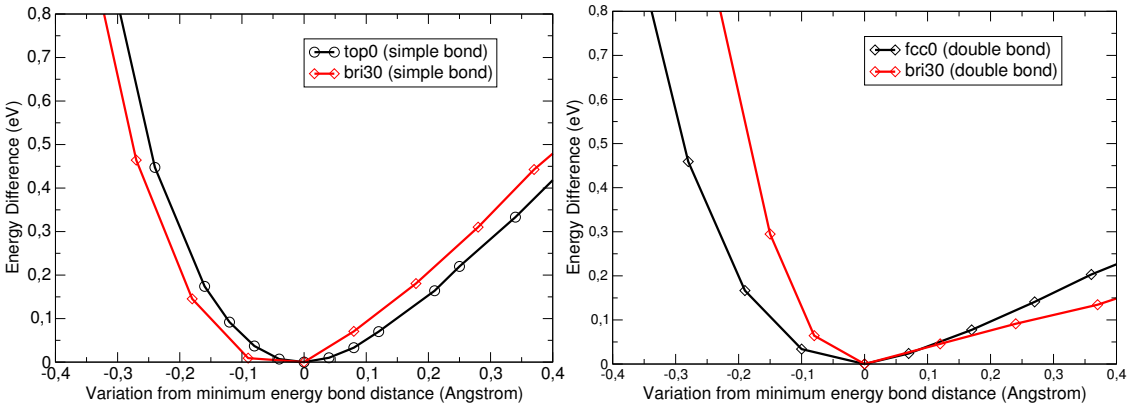

Figure 3.17: Left: Variations from equilibrium bond distance for single bond in top0 and in bri30 (calculated with 3.5) . Right: Variations from equilibrium bond distance for double bond energy profile obtained in fcc0 and in bri30 (calculated with 3.6).

in which $E_{bri30}(d)$ and $E_{fcc0}(d)$ are the adsorption energies at certain distance d in bri30 and fcc0 configurations. $E_{s_{bri30}}(d)$ is obtained as half the value (bri30 has two single bonds) of the difference between $E_{bri30}(d)$ and two pairs of double bonds, calculated in fcc0 system (three pairs of double bonds) through $2(E_{fcc0}(d))/3$. In fig. 3.17 the two configurations (top0 and bri30) own similar single bond energy profiles, therefore bri30 single bond can be approximated with top0 single bond parameters. The differences increase with distance from equilibrium, fig. 3.17, due to the approximation in d, but the similar behaviors confirm that considered approximation in equation 3.5 (fcc0 double bond angle (17°)≈ bri30 double bond angle (19°)) as viable.

Double bond In analogous way, it is considered the energy difference from equilibrium bond length for double bonds in bri30 and fcc30. Considering single bond formed between Bz and the substrate as analogous, in orientation, to single bond for top0 configurations, the energy for double bond in bri30 ($E_{d_{bri30}}(d)$) can be obtained from equation 3.6

$$E_{d_{bri30}}(d) = [E_{bri30}(d) - (E_{top0}(d))/3]/4 \tag{3.6}$$

in which $E_{bri30}(d)$ and $E_{top0}(d)$ are respectively the total energy of bri30 and top0 configurations. The value of each the four double bonds in bri30 $E_{d_{bri30}}(d)$ is obtained as a one fourth of the difference between the bri30 total energy and two single bond energies obtained for similar distances d in top0 ($E_{top0}(d)/3$). Bri30 double bond energy profile is increasingly different for distances shorter than equilibrium, from the profile obtained for fcc0, fig. 3.17; apart from the approximations in definition of d, the angular difference between single bond in top0 (35°) and in bri30 (20°) used in equation 3.6 is important and becomes more relevant when angle increases (molecule is nearer to the surface).

3.6.2 Model Details and Results

The model is set so that single bonds energies are determined by Morse parameters (equation 3.4) which describe accurately the energetics of top0 ($D_e = 1.267$ eV and $r_e = 2.15$ Å); while double bonds by parameters that describe accurately the fcc0 energetics ($D_e = 0.77$ eV and $r_e = 2.19$ Å). The parameter $\alpha = 2.15$, is obtained by the potential well width from biatomic molecule C-Pt energy fit.

The energetics of the considered configurations are reproduced with good accuracy and reported in table 3.3 only stable and metastable positions are shown.

It has been also considered the bri30 energetic profile for rigid vertical shifts from minimum energy. The graphics in fig. 3.18 shows that Morse potential can be used as appropriate approximation if not significant strain is induced.

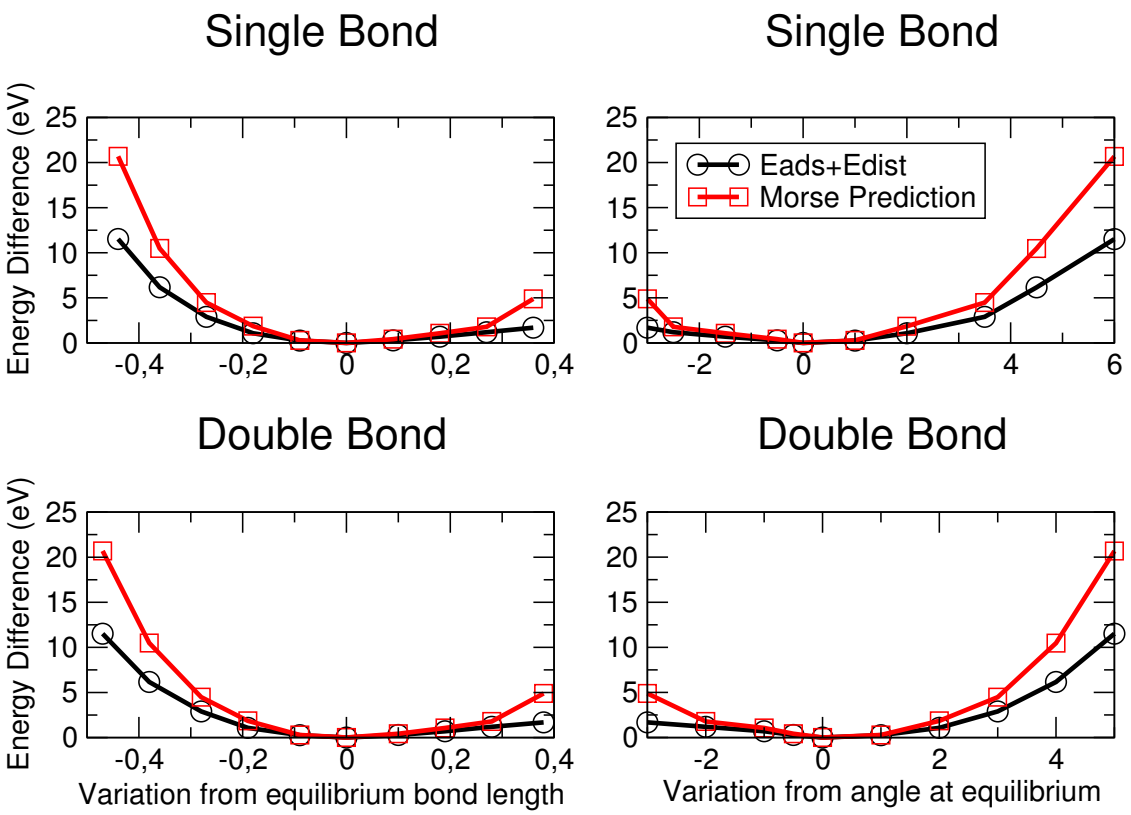

Figure 3.18: Agreement between E_Σ and E_M in bri30 adsorption configuration. Top left: energy difference from minimum energy for single bond variation from equilibrium bond length. Top right: energy difference from minimum energy for single bond variation as function of angle (shorter bonds imply positive angular variations). Down left: energy difference from minimum energy for double bond variation from equilibrium bond length. Down right: energy difference from minimum energy for single bond variation as function of angle (shorter bonds imply positive angular variations).

When the bond length r is much shorter than equilibrium distance r_e, approximation fails because the description of single bonds is not angle dependent and for the same distance d, the bond energetic of top0 (from which Morse parameters are considered) occur at 35º while in bri30 at 20º and in bri0 at 0º. In particular for bri0 the difference between values obtained by DFT and Morse is the highest.

3.6.3 Application to Polyarene adsorption

Once the same model is applied to polyarene adsorption on Pt(111), the results reproduce the adsorption curve shape (3.19). As for benzene, the angle independent description of bonds is not sufficient, especially when "benzene" moiety plane is not parallel to the surface. Nonetheless, the ground state is properly obtained as much as comparable are the energy differences calculated via DFT and through the simple model (table 3.4 column II and VIII)

The model applied to polyarene confirms structural and electronic similarity between polyarene and benzene adsorption, and its adsorption can be analyzed with a simple benzene like model, that describes properly adsorption and distortion energies sum for benzene on Pt(111). Such model could be used for preliminary exploration of the phase space, saving computational time through good initial guess configuration.

3.7 Conclusions

The important enantiomeric adsorption of the fullerene precursor $C_{60}H_{30}$ on Pt(111), have been studied in details.

Polyarene diffusivity is low, due to anchoring adsorption of external hexagons hexagons, because the wings are

(eV)	ΔE_{ads}	$E_{dist-mol}$	$E_{dist-slab}$	$E_{dist}+E_{ads}$	E_M	$E_M - E_{dist}$	$\Delta(E_M - E_{dist})$
3bri30-bri0	0.00	9.75	10.69	35.48	36.78	16.34	0.00
10	+3.56	10.85	11.15	33.48	36.30	14.30	2.04
20	+2.80	11.22	11.10	34.54	37.15	14.83	1.51
30	+3.35	11.30	11.20	34.10	36.81	14.44	1.90
40	+2.29	11.40	11.33	35.48	37.12	14.39	1.95
50	+2.47	10.47	10.71	33.75	34.83	13.65	2.69
60	+0.27	10.80	9.31	20.11	36.47	16.36	-0.02
Chiral	+0.03	9.94	11.41	36.36	3737	16.02	+0.32

Table 3.4: Morse potential model applied to polyarene. E_Σ is the sum of adsorption and distortion energy while E_M is the value obtained modeling C-Pt interaction with Morse potential.

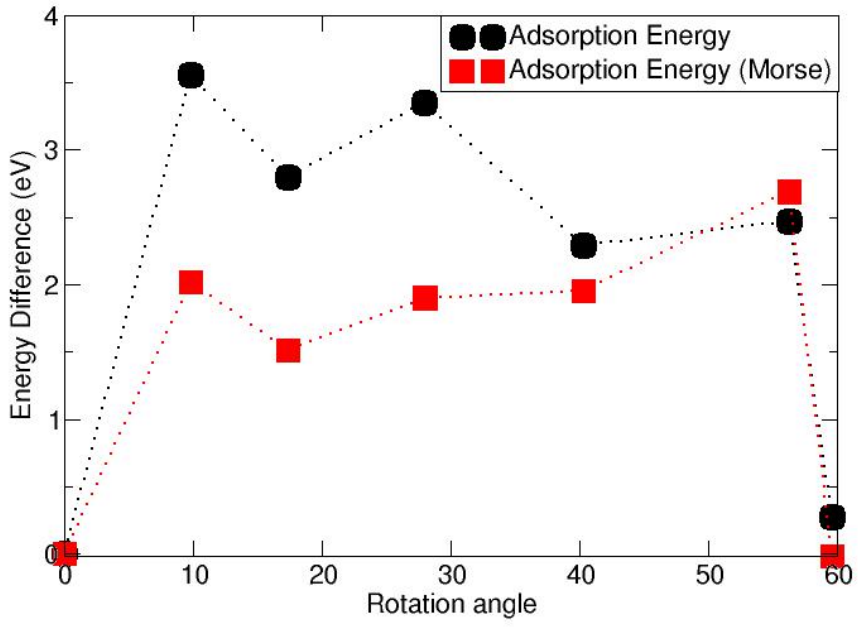

Figure 3.19: Adsorption energies difference, calculated via DFT (black circles ΔE_{ads}) and via Morse (red squares $\Delta(E_M - E_{dist})$).

"trapped" by [1-10] channels, while central hexagon has the flexibility to increase height on substrate like graphene and then to shift/rotate the molecule if in unstable/metastable position.

The high diffusivity obtained on other metallic surfaces (e.g. Au), due to lack of hexagons substrates matching, confirms that adsorption on Pt(111) occurs with a deep ground state when wings adsorb inside the [1-10] channels of the substrate. Low energy differences between local minima, aside from the ground state, confirm high diffusivity between configurations not yet in the ground state and possible thorugh a clockwise rotation. Adsorption of molecular precursor is mainly due to outer hexagons.

More hydrogenated and flexible, external hexagons behave like benzene, decreasing their height on the substrate, and the central hexagon (not hydrogenated) increasing it, resembling graphene behavior.

The enantioselectivity is a combination of appropriate structural arrangements and electronic interactions, results of π orbitals bonding (as for most aromatic molecules) between the substrate and the benzene like moieties, intended as component of our PAHs.

To conclude, the enantiomeric adsorption is a characteristic of polyarene on Pt(111) that could be similarly found for other PAHs and in particular for other heterofullerene precursors, in which doping is included in the internal part (which interaction with substrate is less relevant). This study could be used to develop new routes for surface induced enantiomeric selection in cases where no crystalline domains with long-range order are formed.

Results show that molecule substrate interaction and the system energetic can be reduced to benzene moieties ensemble, in which carbon platinum different interactions are properly taken in account. A simple model based on benzene adsorption on Pt(111) has been also developed and that describe properly the minimum energy configuration in extended PAHs adsorption, and that can be potentially extended to other PAHs, other surfaces and used as guide to save computational time in the costly simulations that involve large systems.

Structural and electronic similarities between platinum and palladium suggest this as a candidate for alternative substrate. The enantioselectivity and the low diffusivity occurs for both lattice and electronic reasons and can be expected on structurally and electronically similar substrate.

Chapter 4

Adsorption of the Triazafullerene molecular precursors

In this chapter the study of the electronic and structural properties upon adsorption of the triaza analogue $C_{57}H_{33}N_3$, aims to understand the influences on adsorption, diffusivity and enantioselectivity of the nitrogen substituents and of the hydrogenation required to stabilize the structure. Therefore is structured in the following sections: overview of on motivation and experimental results (section 4.1), characterization of the free molecule (section 4.2), the pyridine adsorption on Pt(111) as reference system for nitrogen doping in benzene rings (section 4.3), the adsorption of the heteropolyarene on Pt(111) (section 4.4) and the understanding of the STM images and differences respect to polyarene (section 4.5).

4.1 Motivation and Experimental Results

The adsorption process of the fullerene molecular precursor on Pt(111), discussed in chapter 3, occurs through anchoring of its external parts in benzene like behavior. The low diffusivity obtained in platinum at room temperature is an essential a priori condition for the subsequent cyclodehydrogenation and formation of fullerene. In addition, upon deposition, the molecule substrate interaction is enantioselective, maintaining a well defined angle between molecules adsorbing on one or other side. To consider the polyarene as a reference system for the synthesis of heterofullerenes, the following study involves a structurally similar molecule, doped, which experimentally originate a new heterofullerene.

Then the understanding of doping and hydrogenation effects in this specific polyarene analogous may open new routes for a safe selective synthesis of molecular precursors for ad-hoc heterofullerenes. The study of the triazafullerene precursor $C_{57}H_{33}N_3$ is also extremely important for the synthesis of the triazafullerene $C_{57}N_3$ itself; in fact, such molecule has never been obtained before as no synthesis methodologies were available for azafullerene $C_{n-x}N_x$ with odd number of substituents (n>1).

Structural similarities between the two PAHs, could a priori suggest that little differences are carried by the doped molecules upon adsorption. Experiments data concerning such matter have not been extensively analyzed, but seem to agree that diffusivity is equally low. Similarly enantioselectivity appears in analogous way to polyarene case and therefore suggesting that adsorption in still driven by external parts of the molecule, independently by doping and hydrogenation.

On the other side, STM images obtained for the heteropolyarene adsorption on Pt(111) reveal a deposition side independent variety of topographic shapes for same orientation, a behavior that was not encountered in polyarene. Adsorption occurs without formation of aggregates, fig. 4.1, revealing low diffusivity of the molecule, as for polyarene. Depending on landing side, the molecule can be identically discriminated as L/R and, preliminary analysis, reveal its

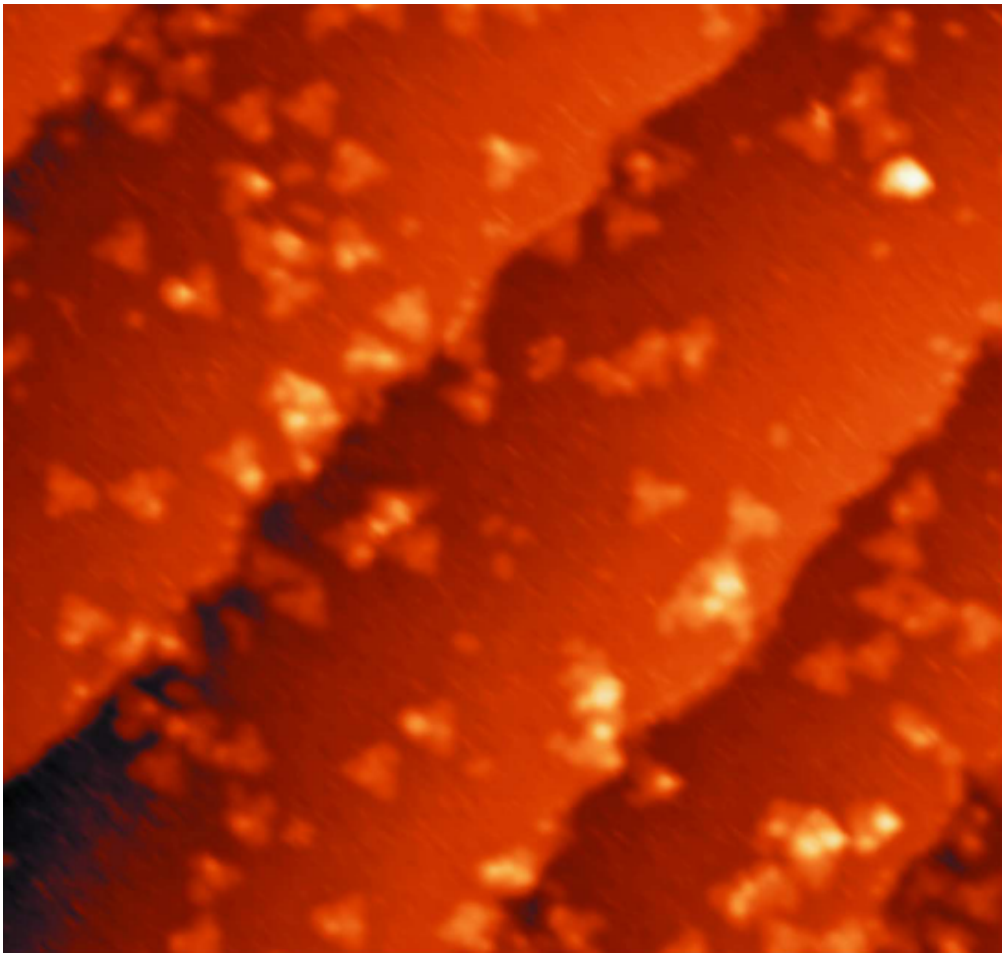

Figure 4.1: STM image of adsorbed heteropolyarene on Pt(111)

interaction with the substrate brings to enantiomeric discrimination. Such results seem in contrast with the mentioned three different patterns obtained for same orientation and landing side. As shown in fig. 4.2 such molecules are characterized by a brightening central part, pattern that is similar to polyarene shape, by two or only one brightening lobe.

These difference and similarities between polyarene and heteropolyarene adsorption on the same surface are extensively discussed in the chapter.

Respect to polyarene, the considered heteropolyarene seems to carry similarities in the adsorption, that is important for the cyclodehydrogenation, and differences in the STM patterns, therefore unrelated to cyclodehydrogenation; then it is significantly important to understand the influences of doping and hydrogenation. In general, the inclusion of nitrogen as dopant in carbon structures, is now seen not only essential for spintronics, but also as a much cheaper and much easier methodology for oxigen reduction, which find huge interest and applications in the next generation fuel cells, solar cell technologies etc.

4.2 Free molecule $C_{57}H_{33}N_3$

The molecule, which detailed synthesis is reported in [45], is composed by 93 atoms. In analogy with polyarene elements definition, the heteropolyarene is composed by a central hexagon to which three wings, distant 120º from each other, are attached by one pentagon, fig. 4.3; in each wing, apart from the pentagon, there are two internal and two external hexagons, which labeling can be further as in axis and out of axis. The three nitrogen atoms are substituents, one per wing, in analogous position and as the common atom between the internal in axis hexagon and the pentagon.

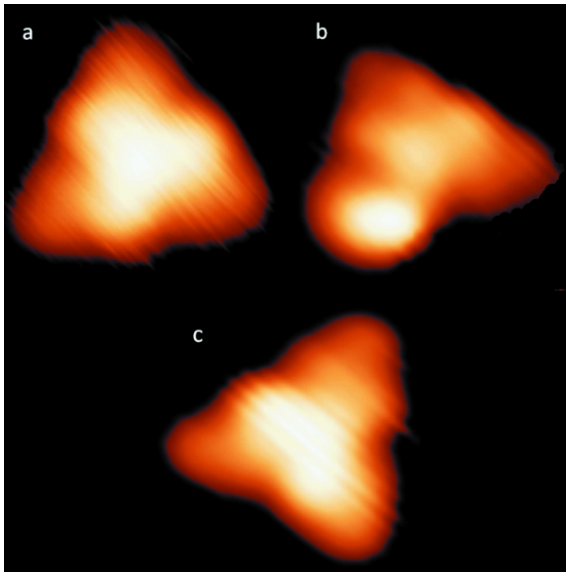

Figure 4.2: Different topographic shapes for adsorbed heteropolyarene

Therefore, for structural stability, the carbon atom first neighbor to nitrogen and belonging exclusively to the internal in axis hexagon, is double hydrogenated (fig. 4.3).

4.2.1 Doping and Hydrogenation effects: comparing polyarene and heteropolyarene

Upon geometrical relaxation in the gas phase, the two molecules consist in a flat central part (central hexagon and pentagons) to which *iia* and *iooa* are bonded. As shown in table 4.1, the aromaticity of the central hexagon is lost when doping is included first neighbor: nitrogen atoms are taking electrons from localized π like orbitals. The alternating single and double bonds with two characteristics bond lengths found in the central hexagon of polyarene are replaced by a single type of bond in heteropolyarene. When dehydrogenation of the CHH group is considered, C-N distances vary, but not the C-C in the central hexagon. Polyarene central hexagon bond lengths change from 1.38 and 1.43 to 1.42 and 1.43 Å (sp2-sp2 like to sp3-sp like). Flexibility is induced in the only *iooa* by its three hydrogen, while *iia* hexagon is only monohydrogenated (dihydrogenated for heteropolyarene) and therefore less flexible. The repulsive interaction between more internal *iooa* hydrogen and the one of *iia* (two for heteropolyarene) is the reason behind the steric geometry obtained for molecule relaxation in gas phase. Such interaction acts so that C-C distance in *ior* is maximized, respectively 3.38 and 3.16 Å for polyarene and hI (table 4.1). The other flexible parts of the wing is the *eooa*, 2/3 hydrogenated. The molecule height, measured from upward *eooa* to downward *iooa* atoms decreases of 0.20 Å when dopants are included. Such flattering is associated to nitrogen position which directly strengthen the wing axis and indirectly to the double hydrogenation of near C atom, that reduces the distances between *iia* and nearest wing *eia*. The *iooa* hydrogen atom is under symmetric repulsive action from the two hydrogen of *iia* carbon atom, and therefore its distance must be contemporary maximized. Nitrogen effect is, generally, to decrease this upwards/downwards flipping of the wings and to reduce the estimated ideal height.

4.2.2 Heteropolyarene: Nitrogen and Hydrogen atoms effects

To further the analysis of the block N-CH2 in the relaxation of PAHs, two more heteropolyarenes have been considered, hII and hIII. Cyclodehydrogenation of both of them would bring to formation of same triazafullerene. These two molecules have not been chemically synthesized. However, the comparison of their different behavior during dehydrogenation and cyclization provides useful information to understand the role of the substituents and the extra hydrogen in the process (fig. 4.4).

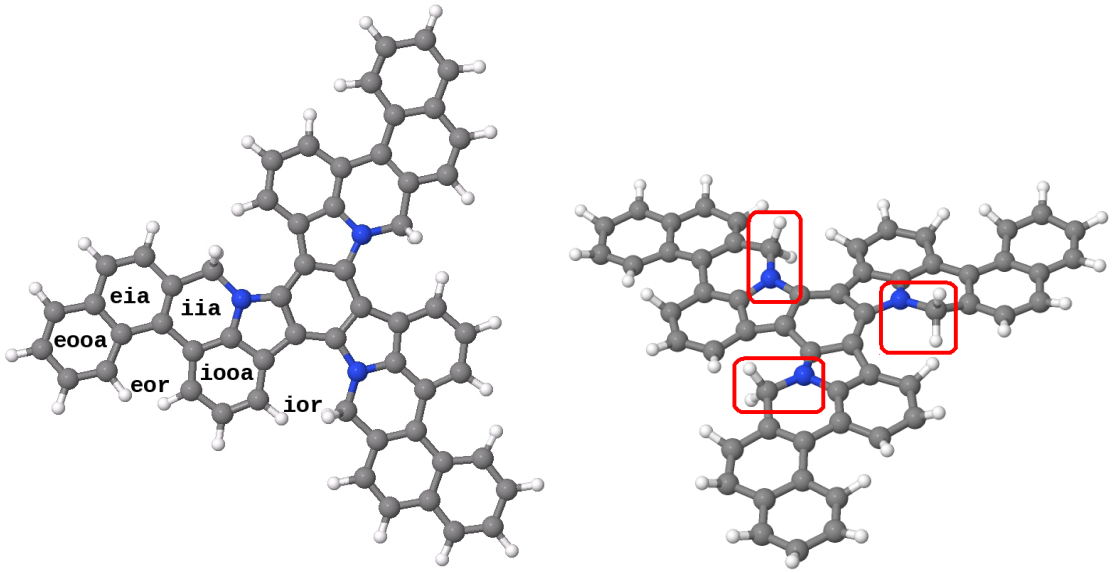

Figure 4.3: Left: Heteropolyarene components labels: internal in axis hexagon *iia*, internal out of axis hexagon *iooa*, external in axis hexagon *eia* and external out of axis hexagon *eooa*. Right: additional hydrogenation required to stabilize structures are in the red squares.

	distances (Å)				
	C-N	C-N	C-N	C-C	C-C
polyarene	1.37	141	1.48	1.38	1.43
heteropolyarene	1.46	1.39	1.4	1.42	1.43
mono-dehydro-heteropolyarene	1.38	1.40	1.42	1.42	1.42
tri-dehydro-heteropolyarene	1.39	1.40	1.42	1.42	1.44

Table 4.1: Distances for analogous bonds, occupied by nitrogen (carbon for polyarene) and neighbors carbons in heteropolyarene and polyarene, and in central hexagon, first C-C column is part of pentagon.

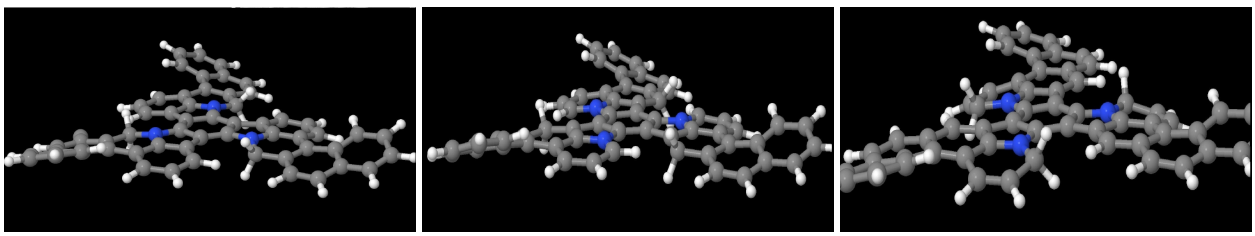

Figure 4.4: From left: heteropolyarenes hI, hII and hIII.

$C_{57}H_{33}N_3$	Distances (Å)		
	hI	hII	hIII
C-C (central)	1.41, 1.43	1.41, 1.42	1.41, 1.43
C-C (*ior*)	3.16	3.16	3.16
C-N	1.37, 1.38, 1.41	1.36, 1.38, 1.39	1.37, 1.37, 1.44
$\triangle z_{molecule}$	0.79	0.79	0.59
$\triangle z_{int-iooA}$	0.0	-0.06	-0.21
$\triangle E_{tot}$	0.00 eV	+1.17 eV	+0.83 eV

Table 4.2: Structural and energetic difference among the heteropolyarene with different substituents (hi and hII) and hydrogen (hII and hIII) positions.

Heteropolyarene hI and hII differ in the position of the N substituents, hII and hIII for additional hydrogen, and hI and hIII for both nitrogen and hydrogen positions. Energetically (table 4.2) the III is more similar to I, due to fact that cohesion energy is higher near the extra electron from nitrogen. The configuration I is, anyway, the most favorable among the heteropolyarenes considered. The total height of hII doesn't vary respect to hI (they differ by N positions), while hIII total height decrease of 0.20 Å respect to hII, from which it differs by hydrogen position. Between hI and hII no appreciable downward flip is observed for *iooa* hexagon (with and without nitrogen respectively), while in hIII a downward flip of 0.21 Å is observed (additional hydrogen near N in hIII). Hydrogenation, instead, induces a 0.20 Å flip, as observed in total height difference when supplementary hydrogen to moved from *iia* to *iooa* hexagons (from hII to hIII).

Nitrogen presence decreases *ior* C-C distance (3.16 Å) comparing with same distance in polyarene (3.38 Å), independently if nitrogen and hydrogen are located in *iia* or in *iooa*.

4.2.3 Density Of States: Polyarene and Heteropolyarene

In fig. 4.5, where the density of states of the polyarene and the heteropolyarene are compared, the gap appears analogous. Influence of dopant nitrogen is visible under -1.25 eV from Fermi level set to 0.0 eV for polyarene and HOMOs peaks equalized.

The density of states may help to analyze contribution given by dopant and by the (de)hydrogenation to the heteropolyarene. The spontaneous dehydrogenation to which heteropolyarene is subject in 3bri30-bri0, is here studied in its effect on electronic structure of the molecule itself.

The first step has been to consider the heteropolyarene $C_{57}H_{32}N_3$ in adsorption configuration 3bri30-bri0 without substrate. The Density of states analysis reveals levels change induced by distortion. The main contributions, at both Fermi level and under, come from pentagons (in which the nitrogen atoms are). In particular, at Fermi level, the dehydrogenated wing pentagon contribution is three times the others, while at energies lower than 1.10 eV, the density of states of the three wings are similar. Decomposing the contribution per elements in the dehydrogenated wing, as for polyarene, the external out of axis has the lowest contribution at the total DOS, while the internal in axis has the highest.

In fig. 4.6 (left) the nitrogen levels of the three wings of the isolated 3bri30-bri0 in the adsorption configuration (mono-dehydrogenated) is compared with eigenvalues associated to the free atom. The effects of the mono dehydrogenation, shown in fig. 4.6, are to create a peak associated to the strong p_z character orbitals of nitrogen in the dehydrogenated wing. Other nitrogen associated levels are more similar to free heteropolyarene nitrogen levels, and only slightly effected.

The electronic structure of a tri-dehydrogenated heteropolyarene show that, as expected more levels appears at Fermi energy. The PDOS per each molecule elements and per atom shows that the contribution at Fermi energy is

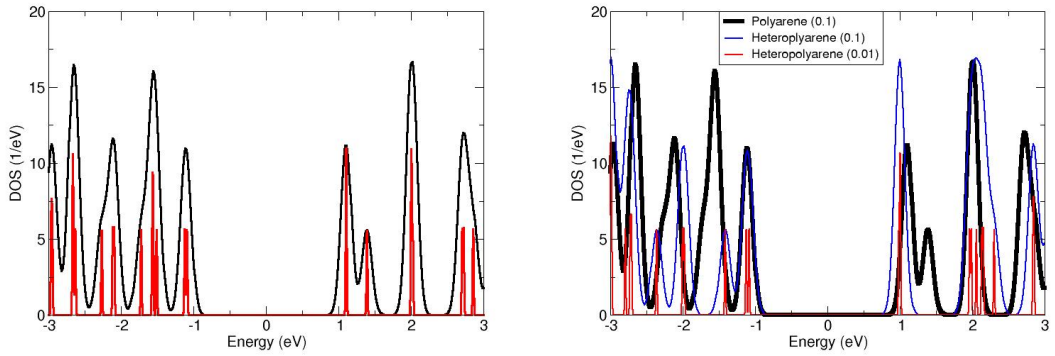

Figure 4.5: Left: Density of states of polyarene with two different smearing 0.1 (black) and 0.01 (red). Right: Density of States of heteropolyarene with two different smearing 0.1 (blue) and 0.01 (red) compared with density of states of polyarene (black)

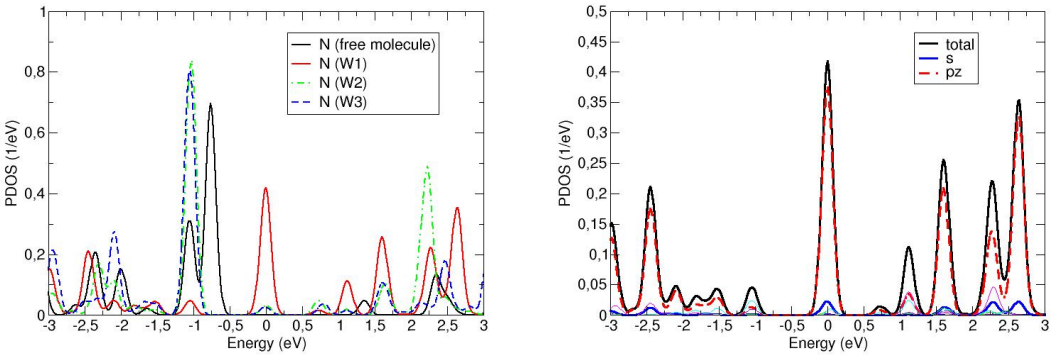

Figure 4.6: Left: comparison of the Partial Density of States of nitrogen atoms in the three wings of the mono-dehydrogenated heteropolyarene (adsorption configuration) in the gas phase with the nitrogen levels for the heteropolyarene. Right: decomposed contribution to density of nitrogen in the dehydrogenate wing.

observed in all components with intensity decreasing with the distance from dehydrogenated elements.

4.3 Pyridine/Pt(111): structural and electronic effects of nitrogen on benzenic ring

The study of nitro benzene homologous, the pyridine, on Pt(111) may help to understand eventual differences, structural and electronic, induced by nitrogen effects in the aromatic rings upon adsorption on Pt(111).

Orientations analogous to the benzene configurations have been considered, but due to different possible position of nitrogen for same orientation, discrimination on N-Pt bond has to be made. Results for stable configuration (fig. 4.7), are shown in table 4.3, where for same orientation, *s* and *d* indicate when substrate platinum atom is bonded only with nitrogen and when it is also bonded with a carbon atom.

The most favorable orientation is, as for benzene, the bri30, in particular the $bri30_s$ which N-Pt distance and bond angle is analogous to $top0$ but which is far more distorted; instead the $bri30_d$ distance is 10% larger than $bri30_s$, angle is similar, but distortion energy is almost 30% higher. Energetic comparison with benzene homologous is in table 4.4, which shows that nitrogen induces a strain except for single bonding. The electronic analysis of nitrogen bond with platinum is radically different, in which the single and the double resemble respectively the biatomic N-Pt interaction

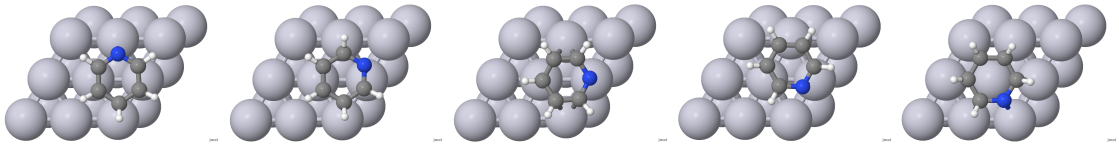

Figure 4.7: From left the stable pyridine adsorption orientations $bri30_s$, $bri30_d$, $bri0_s$, $fcc0$ and $top0$. Only two substrate layers are shown to ease the visualization.

	bri30		bri0		fcc0	top0
	s	d	s	d*	d	s
E_{ads}	-4.14 (0.00)	-3.80 (+0.34)	-3.35 (+0.79)	/	-3.45 (+0.69)	-3.71 (+0.43)
$E_{dist_{mol}}$	1.31 (0.00)	+1.74 (+0.43)	+1.45 (+0.14))	/	+0.95 (-0.36)	+3.54 (+2.23)
$E_{dist_{slab}}$	0.18 (0.00)	+0.19 (+0.01)	+0.52 (+0.34)	/	+0.17 (-0.01)	+0.95 (+0.77)
E_{dist}	+1.49 (0.00)	+1.93 (+0.43)	+1.97 (+0.48)	/	+1.12 (-0.37)	+4.49 (+3.00)
N-Pt	2.09	2.24	2.05	/	2.19	2.06
α	35.3	33.2	15.1	/	28.6	38.9

Table 4.3: Adsorption and distortion energies (eV), bond lenght (Å) and the angle (º) formed by N-Pt with perpendicular to the substrate for pyridine adsorption on Pt(111). Each configuration, when possible, has been considered with two different kind of N-Pt bond: s when one Pt atom is bond only with the nitrogen and d when it is also bonded to a carbon. $bri0_d$ configuration is unstable, and rotate toward $bri30_d$.

and the isolated atoms. Significantly relevant at Fermi energy, the single bonds levels associated to nitrogen, are similar for $bri0_s$ and $bri30_s$ while differ in $top0$; in double bonding are similar between $bri30_d$ and $fcc0$. The analysis of nitrogen orbitals contribution in the single bond with platinum for $top0$ and $bri30_s$ configurations shows that in single bond only system, nitrogen levels are more spread.

4.4 Adsorption of $C_{57}H_{33}N_3$ on Pt(111)

In polyarene, the enantioselectivity is consequence of one marked ground state with high diffusion barriers, while the ones between the other minima can be passed at room temperature. The experimental findings, meanwhile not complete, suggest that such characteristic in the interaction between substrate and molecule is maintained in the doped and hydrogenated heteropolyarene and that adsorption is mainly due to external parts and independent on hydrogenation and dopant, at least because bri30 adsorption geometry for six atoms ring is the favorable configuration, in benzene as much as in pyridine.

(eV)	bri30		bri0	fcc0	top0
	s	d	s	d	s
$\triangle E_{ads}$	-0.18	+0.16	0.0	+0.04	-0.61
$\triangle E_{dist_{mol}}$	-0.19	+0.24	+0.20	+0.08	+0.11
$\triangle E_{dist_{slab}}$	-0.03	-0.02	+0.09	-0.04	+0.18
$\triangle E_{dist}$	-0.22	+0.22	+0.29	+0.04	+0.29

Table 4.4: Adsorption and distortion energies differences between pyridine and benzene for analogous geometries.

	H	$\triangle E_{tot}$	$\triangle z_{w1}$	$\triangle z_{w2}$	$\triangle z_{w3}$	$\triangle z_{centre}$	$\triangle z$	$z_{C_{w1}}$	$z_{C_{w2}}$	$z_{C_{w3}}$
		(eV)	(Å)	(Å)	(Å)	(Å)	(Å)	(Å)	(Å)	(Å)
3bri30-bri0 (GS)	1	0.00	2.11	2.15	2.09	2.49	0.37	2.18	2.82	2.83
3bri30-bri0+10º	0	+2.99	2.11	2.19	2.20	2.52	0.35	2.74	2.80	2.73
3bri0-fcc30	0	+1.16	2.22	2.17	2.19	2.74	0.55	3.00	2.73	3.00
2bri30fcc30-top0	0	+2.14	2.13	2.15	2.18	2.73	0.57	2.74	2.74	2.73
Tri-deh I	3	-1.33	2.08	2.16	2.11	2.58	0.47	2.19	3.06	2.29
Tri-deh II	3	-1.35	2.10	2.15	2.09	2.38	0.26	2.17	2.29	2.04
3bri0-fcc30 H	1	+0.73	2.20	2.16	2.20	2.71	0.52	2.85	2.16	2.96

Table 4.5: Adsorption parameter for heteropolyarene in the ground state and other configurations. H indicated the number of dehydrogenated atoms. Ground state is mono-dehydrogenated. $\triangle E_{tot}$ is the total energy difference taken the configuration relaxed from the polyarene ground state as the reference (the molecule loses spontaneously one of the hydrogen atoms as discusses in the text) from ground state; $\triangle z_{w1,2,3/centre}$ the average height of the *eooa* hexagons in each wing and of the centre of the molecule; $\triangle z$ is the difference between the centre and the average of the heights of the *eooa* hexagons; $z_{C_{w1,2,3}}$ is the height of the di-hydrogenated carbon atom in each wing eventually mono-dehydrogenated.

4.4.1 Spontaneous dehydrogenation

To verify such assumptions, the simulation starting point considered has been the polyarene ground state. Its rotation and translations have been considered to explore the phase space. The adsorption notation for the heteropolyarene has been established accordingly with notation used for polyarene on same substrate; therefore the ground state is equally labeled 3bri30-bri0 where 3 indicates the multiplicity of the adsorption orientation of *eooa* hexagons, bri30 in this case, and then bri0 stands for the geometry of the central hexagon. The configuration is obtained via geometrical relaxation of the simple polyarene 3bri30-bri0 configuration, after substitution of the carbon atoms with nitrogen, addition of hydrogen in the appropriate positions, and when only CHH groups were unconstrained.

Upon adsorption the ground state is spontaneously mono-dehydrogenated, factor that depends on platinum interaction with downward hydrogen of the CHH group. To the dehydrogenation follows a new geometrical relaxation of the, now, $C_{57}H_{32}N_3$, which do not change adsorption of *eooa* hexagons, which average height on surface differs for less than 10^{-2} Å from correspondent polyarene ground state values. The dehydrogenate wing part decrease its height, while the other two rise, then the central hexagon height on surface decreases, on average, of -0.05 Å. Adsorption energy of 3bri30-bri0 is 13.97 eV, value comparable with polyarene ground state adsorption. Similarly the distortion energies are comparable with the one reported for polyarene, in particular E_{slab} differ of 0.01 eV, showing negligible effect of doping and (de)hydrogenation. Particular relevant are the heights of the carbon atoms in the CHH groups, which are even higher than central hexagon and to which C-H bond lengths $\sim$ 1.0 Å must be also added.

4.4.2 Further dehydrogenation

Two translation and one rotation of the ground state geometry have also been considered., but none dehydrogenate spontaneously.

Three additional configurations are shown in table 4.5, 3bri0-fcc30 H that is the geometrical relaxation of artificially dehydrogenated 3bri0-fcc30 configurations, where *eooa* hexagons are still unaffected by dehydrogenation and one wing decreases its height with respect to the substrate, and two di-dehydrogenated configuration of the mono-dehydrogenated ground state (Tri-deh I and Try-deh II). In the first case the 3bri30-bri0 has been simply di-dehydrogenated and geometrically relaxed, in the second the two wing have been lowered to an height similar to the 3bri30-bri0 spontaneously dehydrogenated one. These two configuration are energetically similar (0.02 eV), and indeed more favorable than 3bri30-bri0 configuration, but structurally different in the internal parts. During geometrical

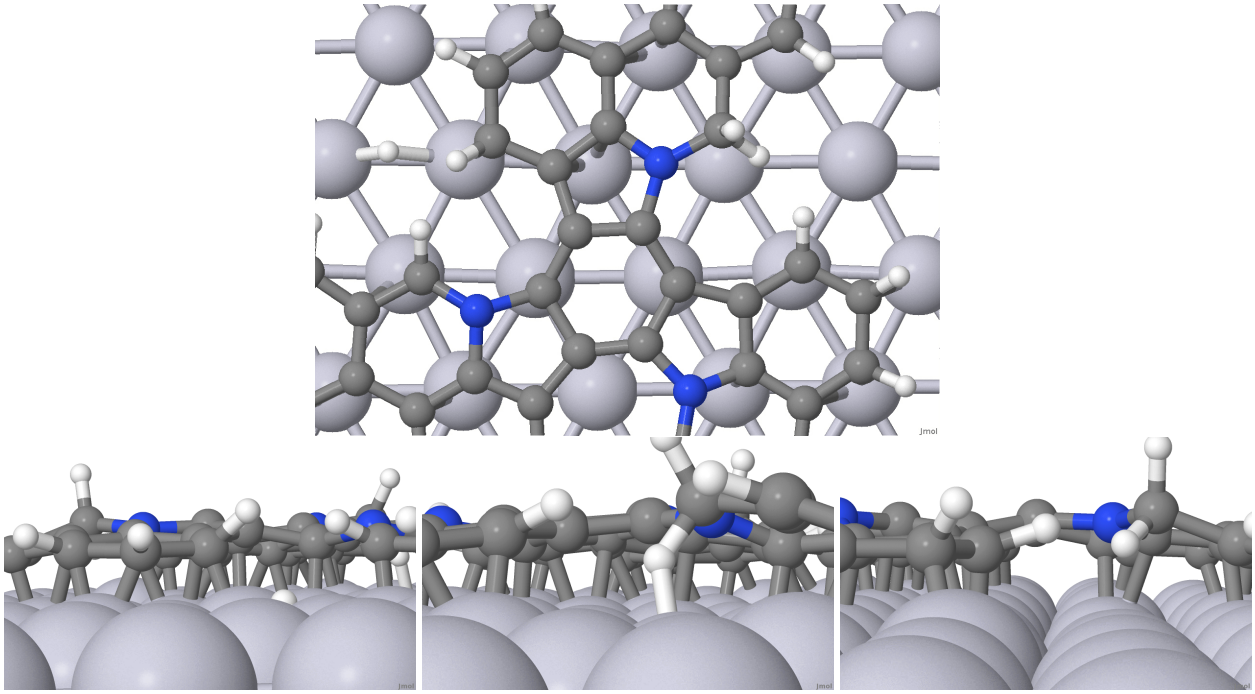

Figure 4.8: CHH group in 3bri30-bri0: wing 1 dehydrogenated (left), 2 (centre) and 3 (right). Only one substrate layer is shown to ease the visualization.

relaxation only one more wing of the tri-deh I lower its height on the surface, while the tri-deh II keeps the wing in a more polyarene-like heights. The configuration tri-deh I also owns a magnetization of $\mu B = -0.125$ not present in other configurations.

The difference between the average height on surface of the carbon atom of the "former" CHH groups among the try-deh I and tri-deh II is ~ 1.00 Å; therefore, in the flatter try-deh II configuration, the central hexagon height is 0.21 Å lower.

The *eooa* hexagons are unaffected by the dehydrogenation and the different height of central parts. The nitrogen doped parts of the molecules, near or far from the surface, do not affect the adsorption energy and therefore the fact that most favorable adsorption orientation of a six atoms ring doped with nitrogen (pyridine like) is bri30 as in benzene does not have any effect.

These results confirm the low diffusivity of the triazafullerene molecular precursors at room temperature, that adsorption mechanism is analogous to the one observed for polyarene and that the enantioselectivity found in polyarene adsorption on Pt(111) is obtained also for heteropolyarene. Structural flexibility observed in the internal part, in the variability of central hexagon height maintaining similar adsorption energy, suggests that adsorption of (hetero)fullerene molecular precursors is independent from doping and (de)hydrogenation in the internal parts, fact that could be an important asset in the synthesis of other heterofullerenes.

4.5 Understanding the variety of STM images

The enantioselectivity observed in the interaction between platinum and heteropolyarene is similar to the one with polyarene, but while, in polyarene (chapter 3), the STM images correspondent to central part of the molecules do not vary, for heteropolyarene for the same orientation, different images are obtained. Such results may seem in contrast with idea of similar behavior of the two molecules, but this is structurally true for the external parts that lead the adsorption orientation. As show in section 4.4, structurally the behavior of the two molecular precursors is radically different and, for presence of nitrogen and different dehydrogenation can also differ electronically for the same orientation.

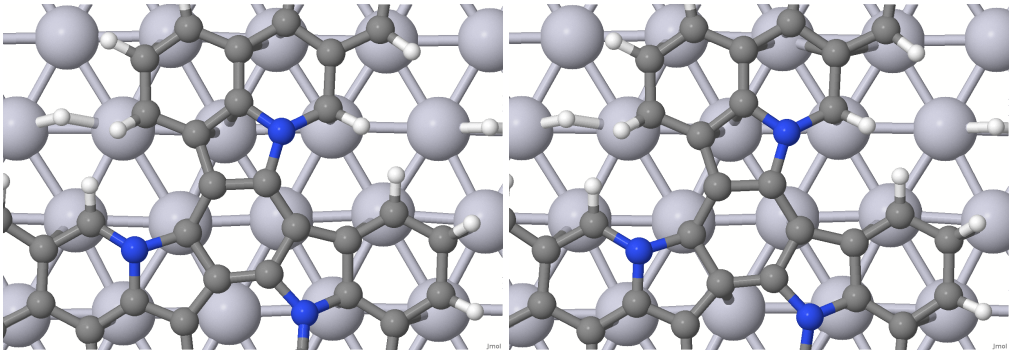

Figure 4.9: Upper view of the tri-deh II and tri-deh II dehydrogenated bond. Only one substrate layer is shown to ease the visualization.

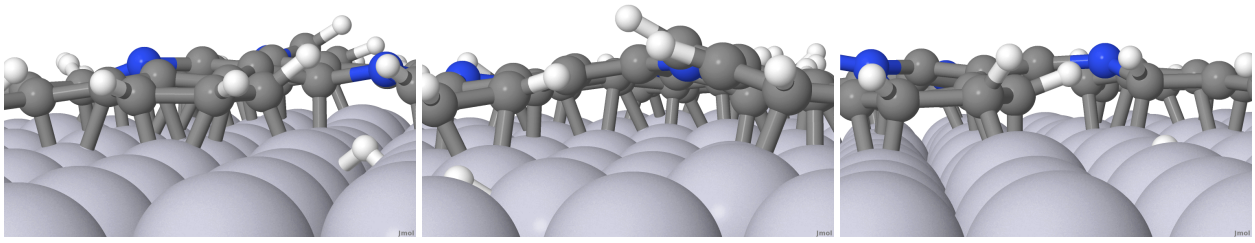

Figure 4.10: CHH group in tri-deh I : wing 1 (left), 2 (centre) and 3 (right). Only one substrate layer is shown to ease the visualization.

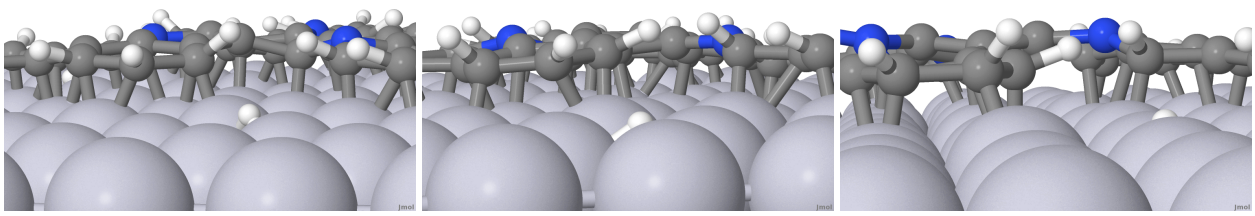

Figure 4.11: CHH group in tri-deh I : wing 1 (left), 2 (centre) and 3 (right). Only one substrate layer is shown to ease the visualization.

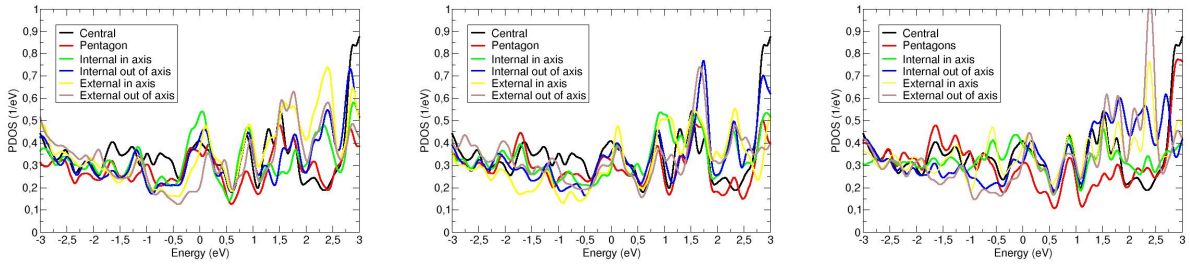

Figure 4.12: DOS of the each wing by contribution: wing 1, dehydrogenated (left), wing 2 (center) and wing 3 (right)

As shown in table 4.5, for same 3bri30-bri0 orientation mono e two tri-dehydrogenated molecules have been considered. These configurations, and in particular tri-deh I and tri-deh II that are energetically similar, have either one, two or three wings at the central hexagon height (as for polyarene) while the remaining one, if any, is much higher. It is then assumed that difference in the STM images is merely a geometrical consequence.

To verify the assumption, and that both hydrogenation and nitrogen do not affect electronically all the wing elements, a first analysis must consider the density of states, and then through the Tersof Hamann approximation, the simulation of experimental STM images with the molecular orbitals.

Density Of States Two important asset of this research must be verified through the density of states: 1) that in analogy with polyarene, the *eooa* contribution is much lower than internal parts, and 2) that no the dehydrogenated wing is different from the others.

In fig. 4.12 the density of states associated to the three wings is shown decomposed per elements: the *eooa* contribution is independent from dehydrogenation and the lowest among the other elements. Strong similarities are obtained between the two not dehydrogenated wings (wing 2 and wing 3), that they differ significantly from the dehydrogenated only in the *iia* hexagon contribution, which owns the dehydrogenated carbon. Adsorption is then both structurally and electronically independent from doping and (de)hydrogenation.

Never the less, the density of states associated to dehydrogenated hexagon is not significantly different from the one associated to hydrogenated part in other wings and compared other molecular part (central hexagon). For this last reason in particular, in tri-deh II configuration the expected STM image should be similar to polyarene ground state, because all the wings are also at similar heights and lower than the central hexagon.

Tersof Hamann Approximation The Local Density of States (LDOS) for the occupied and empty states in the energy ranges [-1.0, 0.0] and [0.0, 1.0] are shown in fig. 4.13. As for polyarene, no appreciable difference is observed between filled and empty states. The different patterns obtained experimentally reflect the different geometries, the two brilliant lobes are associated to 3bri30-bri0 (fig. 4.14), the one lobe to tri-deh I (fig. 4.15 left) and the only central brightening lobe that is similar to polyarene, to the tri-deh II (fig. 4.15 right), which wings are lower than central hexagons, like for polyarene, and that is the more likely to be observed on the surface.

4.6 Conclusions

To conclude, the heteropolyarene adsorption on Pt(111) is leaded by external hexagons, like the polyarene that, being undoped, can be then used as a reference system. Nitrogen doping, useful for many applications does not effect the adsorption process but may generate spontaneous dehydrogenation that causes the different shapes obtained by STM for same orientation. Considering different dehydrogenated molecules as the same molecule, the enantioselectivity of polyarene is also found for heteropolyarene.

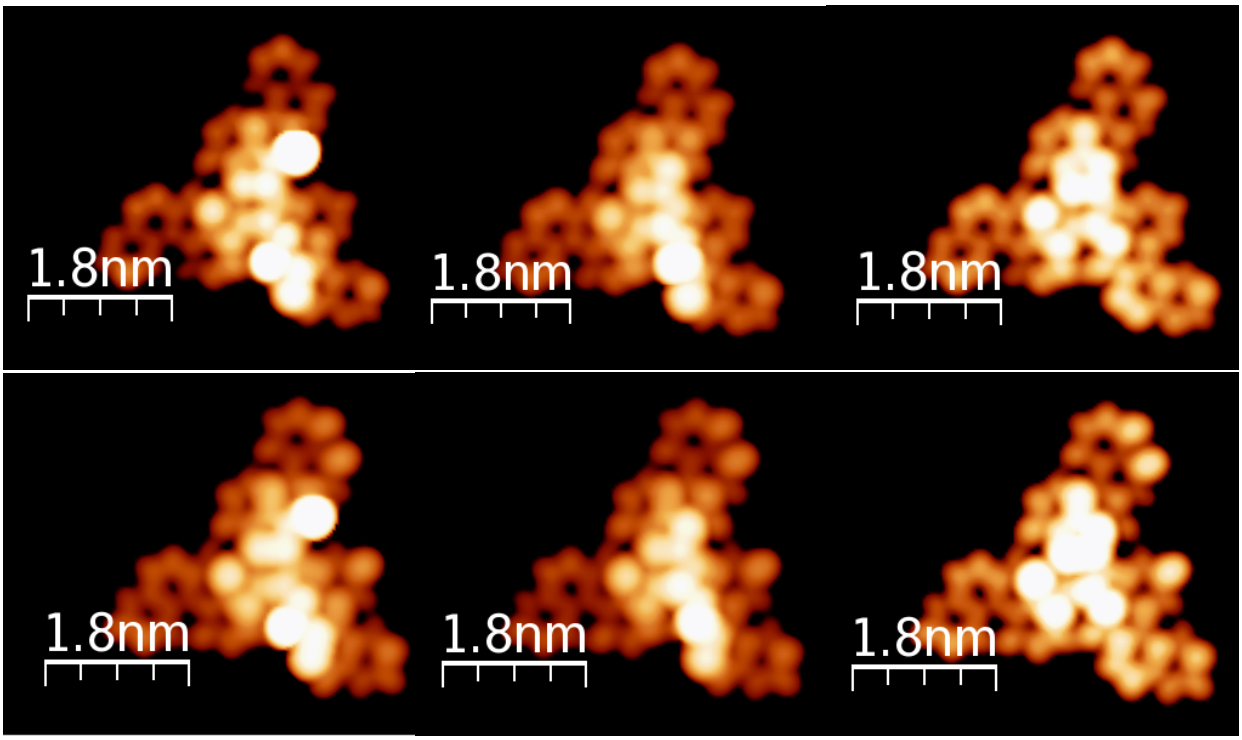

Figure 4.13: Up: LUMO. Down: HOMO. Theoretical STM images for Ground State (left), tri-deh I (centre) and tri-deh II (right). Molecular orbitals considered are between -1.0 and 0.0 eV for HOMOs. Isosurface 1×10^{-6}Å^{-3}.

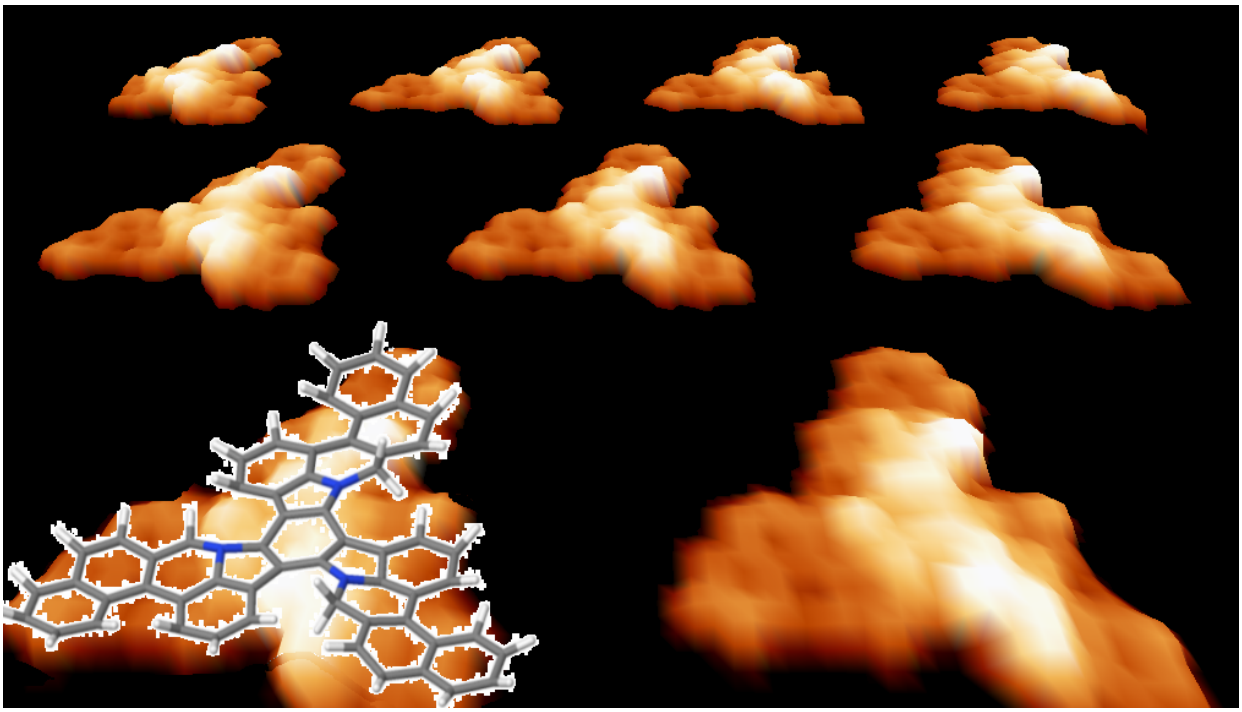

Figure 4.14: 3D theoretical STM image for the 3bri30-bri0 configuration. Filled states and isosurface 1×10^{-6}Å^{-3}.

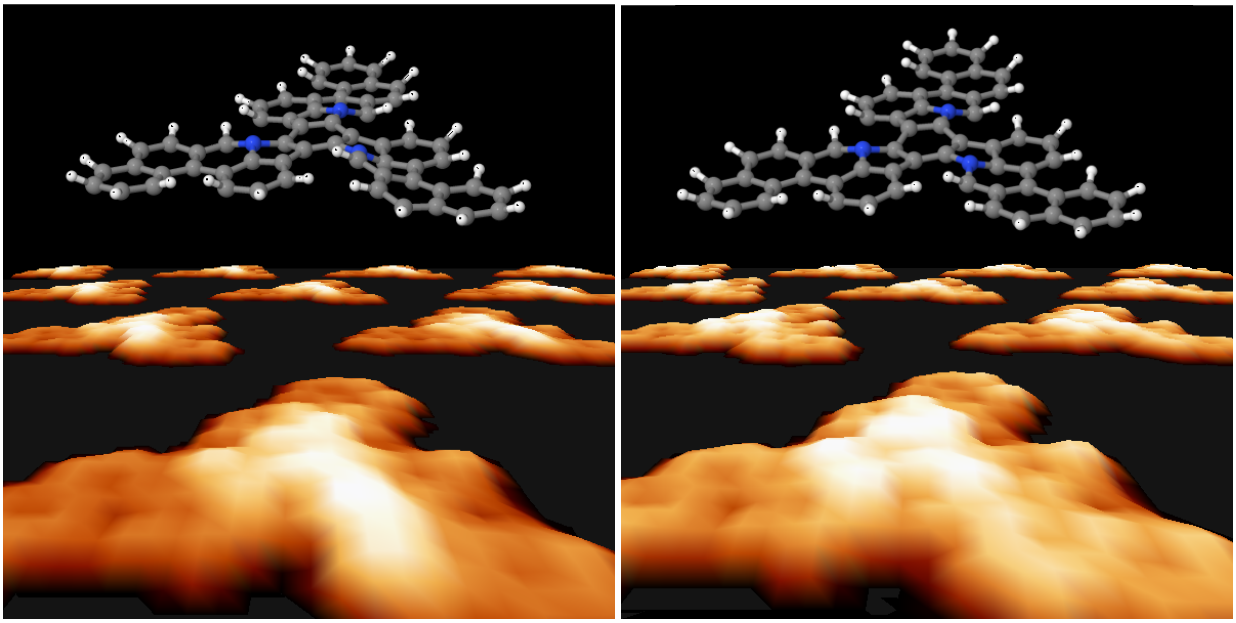

Figure 4.15: Theoretical STM image for the tri-deh I (left) and tri-deh II (right). Filled states and isosurface $1 \times 10^{-6}\text{Å}^{-3}$.

The results not only explain the difference in STM images between the two molecular precursors, but strengthen the idea that polyarene-like molecule adsorption is merely an external hexagons “duty” opening the way to new dopant in the internal part of the molecule.

Chapter 5

Fullerene adsorption on Pt(111): vacancies and dopant effects

In this chapter the study of the electronic and structural properties upon adsorption of the fullerene C_{60} and the N-doped heterofullerene $C_{57}N_3$ (triazafullerene) synthesized and characterized during this work for the first time. The aim is to understand the behavior of these molecules in different conditions associated to experimental results are increasing deposition and temperature.

The chapter is structured in the following sections: first an overview of on motivation and experimental results (section 5.1), then the fullerene adsorption on Pt(111) (chapter 5.2), the adsorption in case of substrate vacancy (chapter 5.3), its formation (chapter 5.4), of the triazafullerene (chapter 5.5) and, finally, the conclusions are resumed (chapter 5.6).

5.1 Motivation and Experimental Results

Recently particular relevance has been given to fullerene-platinum interaction for the high conductivity shown by the system $Pt - C_{60} - Pt$, with a clear dependence on molecule density[92]. The interaction between the fullerene and the platinum substrate, the molecule desorption and fragmentation temperature, reported higher than on other metals, are also studied as strictly related with application in microelectronics.

In addition, the new efficient synthesis procedure increased the interest surrounding the effective ability in obtaining nitrogen doped fullerene $C_{60-n}N_n$ with $n > 2$, which has never been synthesized before, and that may carry interesting structural rigidity properties as much as electronic and magnetic. The importance in the study of interaction between the $C_{57}N_3$ and metallic substrate comes from its possible application in solar cell technology, spintronics and many other fields.

Fullerene The STM images taken after annealing at 750 K, report the formation of round molecules with apparent height of 3.8 Å and a diameter of 15 Å. To validate the formation of fullerene from cyclodehydrogenation, such values have been compared with experimental data obtained for adsorption of fullerene on Pt(110) (respectively 4.0 Åand 13.5 Å) and Pd(110) (height 3.1 Å). Another comparison has been carried between the obtained "round" molecules with commercially available fullerenes adsorbed on the same surface under the same conditions, and no difference was observed. The fullerene adsorption has been then studied as function of deposition and temperature. In such sense, a recent experiment[54] proved that the fullerene platinum interaction involves formation of vacancy.

In fig. 5.1 are shown the different fullerene behaviors with the increase of temperature and deposition. The results show that at low coverage, the adsorbates are randomly orientated and no aggregates are formed, while with temperature increase, the fullerenes go to the step. When deposition rate is increased, island formation is observed with

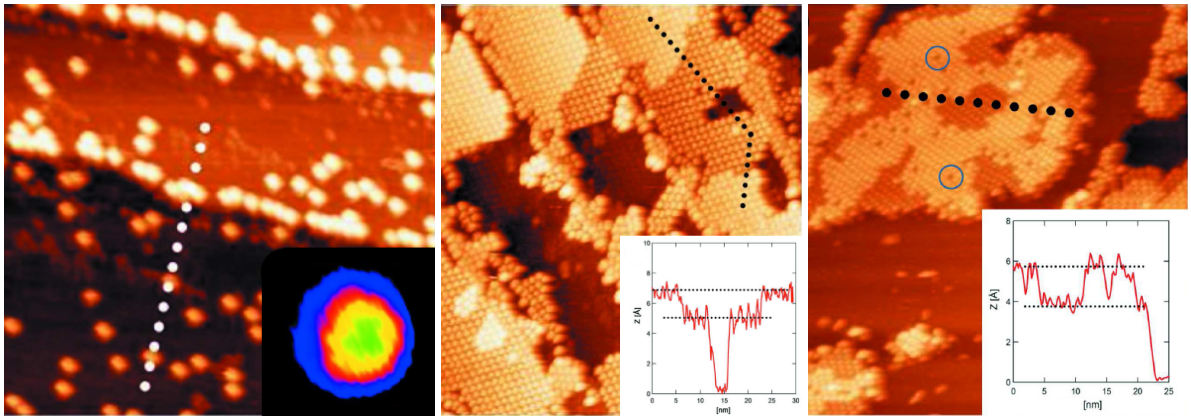

Figure 5.1: STM images for adsorption of fullerene with increasing coverage: random adsorption on the left at 875 K, on the central image second monolayer is forming on the first, and on right the decrease of adsorbate height with temperature at 575 K.

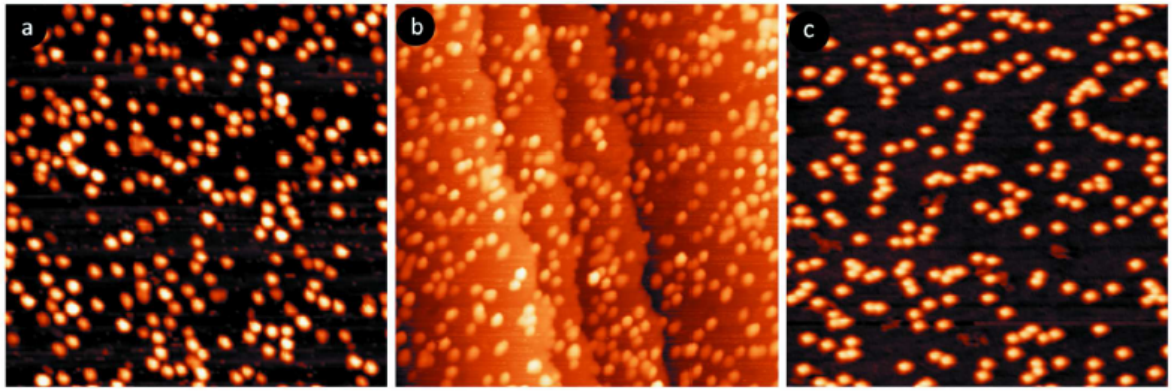

Figure 5.2: STM images of adsorption of fullerene and triazafullerene. Left (a): C_{60} obtained after cyclodehydrogenation of $C_{60}H_{30}$. Centre (b): $C_{57}N_3$ obtained after cyclodehydrogenation of $C_{57}H_{33}N_3$. Right (c): adsorption of commercial fullerenes in similar conditions.

30º orientation respect to the [1-10] crystallographic direction. At this stage the molecules of the formed islands are randomly oriented. When temperature increases, for low coverage no variation in the adsorption behavior is observed, while at high deposition, the molecules form $(\sqrt{13} \times \sqrt{13})R13.9º$ domains.

Triazafullerene On the other side, the adsorption of the triazafullerene resulting from the heteropolyarene cyclodehydrogenation cannot be compared with any azafullerene as the dimerization is the the common behavior for mono and diazafullerene.

The experiments show that triazafullerenes do not dimerize, possibly as consequence of high diffusion barriers induced by the strong covalent substrate-molecule interaction, which, at room temperature, seems to be larger than the interaction between fullerenes to form dimers.

The STM images (fig. 5.2) show no significant difference between the adsorption of fullerene and triazafullerene obtained after cyclodehydrogenation and of commercially available fullerenes adsorbed in the same conditions.

In particular, to understand the triazafullerene adsorption orientation, XPS spectra experiments have been conducted with surface coverage of 0.8 monolayers of precursor, 0.04 for the nitrogen, with respect to the surface (fig. 5.3). The weak emission from the 1s core level of nitrogen suggest that the topographic features is unique, while the core-level line shapes analysis shows two peaks, at 400.6 eV and at 398.2 eV. The two peaks suggest two different environment in which nitrogen is involved; in particular, the first is associated to sp^2 hybridization of nitrogen with carbon in graphite, while the second is associated to PtN compounds in which nitrogen is chemisorbed.

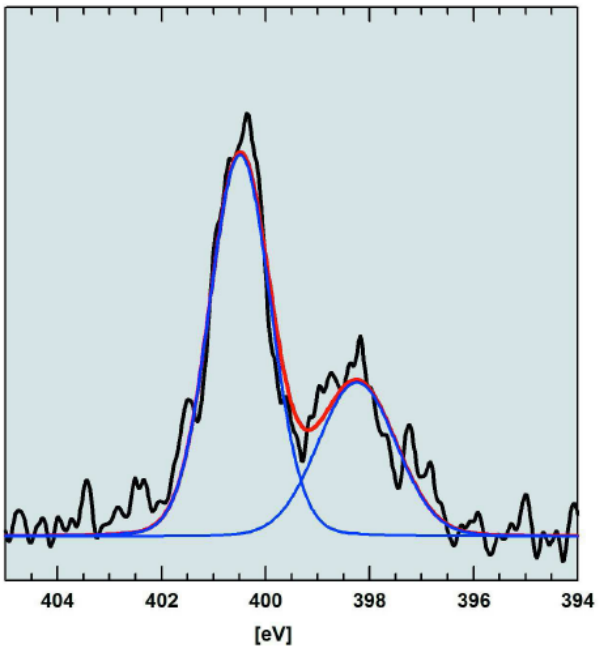

Figure 5.3: XPS peaks for adsorbed triazafullerene on Pt(111).

5.2 Fullerene Adsorption on Pt(111)

To study the adsorption of fullerene on Pt(111), two different unit cells are considered, the first in the limit of the isolated molecule (5×5), and the second for the reconstruction found by experiments ($\sqrt{13} \times \sqrt{13}$). In the smaller surface, the distance between the fullerenes is near to bonding distance and therefore fullerene are subject to mutual interaction.

5.2.1 Computational Methods and Geometries

The vacuum consisted in about 24 Å, while the surface and the molecule adsorbed are almost 12 Å. The molecule is adsorbed on only one side of the slab, and one layer was constrained during geometrical relaxation. The Brillouin space has been sampled with 441 and 881 grids.

The supercell approach with a three-layer Pt slab, meanwhile reported not to be sufficient to give a precise value of adsorption energetics, is an acceptable limitation because the aim is to discuss relative stability of many different configurations. One or more additional layers would have made simulations extremely demanding, limiting drastically the number of explorable configurations. Furthermore, as this work wants to contribute to understand the complexity of cyclodehydrogenation of fullerenes molecular precursors, the same theoretical approach (LDA) is considered in the other part of this work, is here maintained.

The explorable phase space is indeed very complex, depending on many possible different orientation and configurations. To restrict their number, only those that maximize the number of bonds are considered. On each surface, two different adsorption orientations are considered discriminating on lowest interacting part with the substrate: with dimer between two hexagons, labeled *dimer* or (6:6), and with hexagon, labeled *hexagonal* or (6).

Hexagonal geometries are additionally labeled following notation used for benzene orientation on Pt(111) (chapter 2), and the dimer geometries are analogously labeled indicating the adsorption geometries of the two hexagons which share the dimer; such elements are not flat (naphthalene) and therefore apparent similar configuration may differ in the bonded parts, to which the labels refer.

The orientation chosen are characterized by highest possible number of bonds between the molecule and the surface prior any relaxation. For hexagonal geometries all orientations possible are considered among the two surfaces,

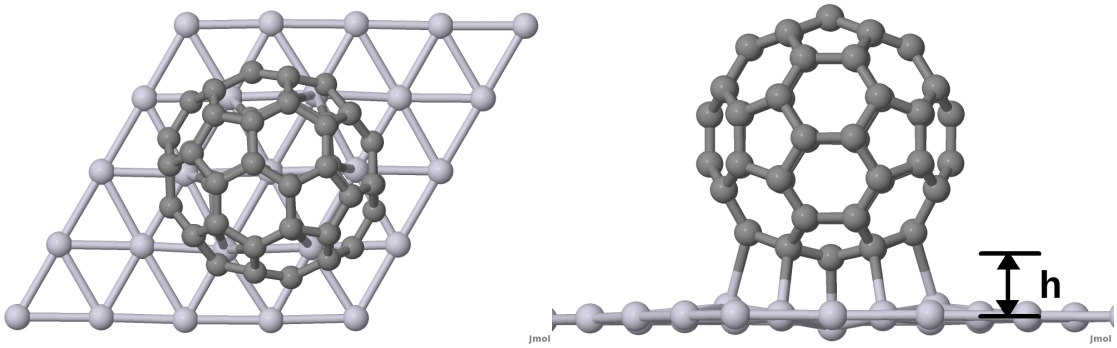

Figure 5.4: C_{60} on Pt(111)-(5×5): $\alpha di-bri30$ top and side views. Only one substrate layer is shown to ease the visualization

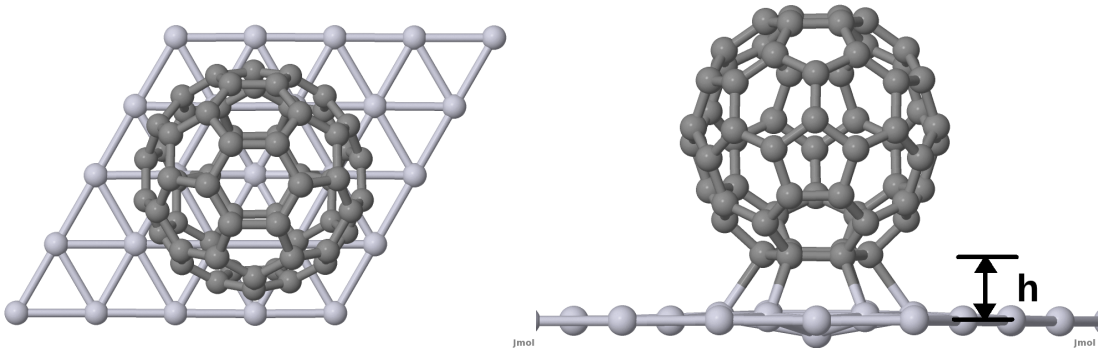

Figure 5.5: C_{60} on Pt(111)-(5×5): $top0$ top and side view. Only one substrate layer is shown to ease the visualization

with 0º and 30º respect to [1-10] crystallographic direction. For dimer geometries the orientation considered follow naphthalene orientation on Pt(111)[89] and benzene itself.

The adsorption energy E_{ads}, calculated as difference between the total energy of adsorbed fullerene and the sum of slab and of the isolated fullerene, can be decomposed as sum of two interaction energy terms $E_{sub-mol}$ and $E_{mol-mol}$, which indicate respectively the substrate-molecule and mutual fullerene interactions. The value of $E_{mol-mol}$ is obtained through geometrical relaxation of the fullerene in the unit cell and orientation obtained in each converged adsorption configuration, and therefore represents the mutual interaction generated by the fullerenes. The distortion energy E_{dist} is the configuration energy induced by the distortion of the element due to the interaction; it is calculated as $E_{dist_{mol/slab}} = E_{free_{mol/slab}} - E_{mol/slab}$, the difference between the total energies of molecule/slab in the ideal configuration $E_{free_{mol/slab}}$ and in the interacting geometry $E_{mol/slab}$; for the smaller unit cell the $E_{free_{mol}}$ is calculated in the unit cell itself.

The height of the fullerene on the substrate (set to 0) is shown in fig. 5.4 and 5.5 and given by the average height of the dimer/hexagon atoms depending on final adsorption orientation; the size of the molecule is the difference in height between the upper and lower parts of the molecule, calculated as average of their component, six/two depending on adsorption orientation hexagon/dimer.

5.2.2 Limit of isolated molecule: 5×5 unit cell

The adsorption energies, shown in table 5.1, indicate a defined ground state labeled $\alpha di-bri30$ (fig. 5.4). Another initial configuration (top30) almost achieves the ground state configuration by geometrical relaxation (fig. 5.6 left), and their energy difference $\triangle E = 0.66$ eV is consequence of different height on surface (0.25 Å). Other minima do not show any preferential order between hexagonal or dimer orientation, which energies are similar. The second most favorable configuration, βdi-bri30, is similar to the ground state and energetically similar to most favorable hexagonal configurations $top0$, which has the highest distortion energy. Such behavior is similar to what found for benzene in

(5×5) *hexagonal*	E_{ads} (eV)	$\triangle E_{ads}$ (eV)	E_{dist} (eV)	$\triangle z$ (Å)	h (Å)	(5×5) *dimer*	E_{ads} (eV)	$\triangle E_{ads}$ (eV)	E_{dist} (eV)	$\triangle z$ (Å)	h (Å)
top0	-6.82	0.00	1.85	6.77	1.93	$\alpha di-bri30$	-7.37	0.00	1.30	6.86	1.75
(top30) $\sim \alpha di-bri30$	-6.71	+0.11	0.97	6.80	2.00	$\beta di-bri30$	-6.83	+0.54	1.38	6.86	1.66
bri30	-6.69	+0.13	0.86	6.67	2.07	fcc0-hcp0	-6.72	+0.65	0.51	6.90	1.66
fcc30	-6.28	+0.54	1.05	6.72	1.98	bri0-top0	-6.72	+0.65	2.22	6.94	1.63
hcp30	-6.18	+0.64	0.93	6.72	2.03	di-fcc0	-6.40	+0.97	0.64	6.91	1.67
hcp0	-6.01	+0.81	0.40	6.65	2.09	fcc30-bri30	-6.30	+1.07	0.77	6.88	1.77
bri0	-5.86	+0.96	0.80	6.68	2.07						

Table 5.1: C_{60} on Pt(111)-(5×5): E_{ads} adsorption energy, $\triangle E_{ads}$ energy difference respect to ground state, E_{dist} distortion energy ($E_{dist_{slab}} + E_{dist_{mol}}$), $\triangle z$ molecule size on zeta direction (free molecule distance between hexagons is 6.47 Å and 6.93 Å between dimers), h is the average height of the hexagon/dimer respect to surface set to zero; $\alpha di-bri30$ and $\beta di-bri30$ differ for the [1-10] crystallographic direction considered beneath the two hexagons. In parenthesis the initial configuration; final configuration $\sim \alpha di-bri30$ is similar to $\alpha di-bri30$

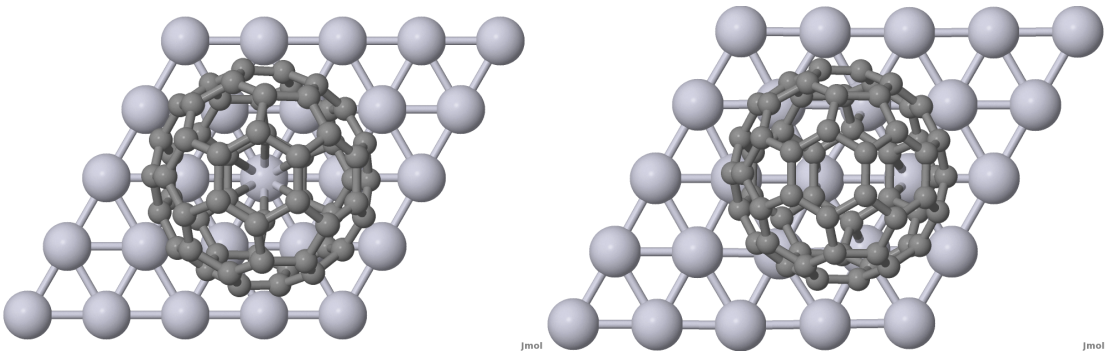

Figure 5.6: C_{60} on Pt(111)-(5×5): from top30 (left) to $\sim \alpha di-bri30$ (right). Only one substrate layer is shown to ease the visualization

top0; the substrate atom central to the bonding hexagon moves downward of 0.33 Å.

The molecule height on surface varies from 1.93 (top0, more elongated and higher distortion energy) to 2.09 Å (hcp0, less elongated and distorted). In particular, for the top0 configuration, the platinum surface is bonded with platinum through simple bond only, intending that one substrate atom is bonded only with one carbon atom, while in hcp0 (fig. 5.6 right) all bonds are double, meaning that three substrate atoms are bonded with two carbon atoms each.

One of the most interesting results in table 5.1 is that while hexagonal adsorbing fullerenes are ~ 0.30 Å longer than the free fullerene, the dimer adsorbing molecules are slightly shorter, but ~ 0.30 Å lower on surface than hexagonal homologous.

5.2.3 Reconstruction $\sqrt{13}\times\sqrt{13}$

In the small unit cell, as reported in table 5.2, the ground state is the $\alpha di-bri30$ configuration as in the 5×5 surface. In the limit of isolated adsorbate, the top30 configuration rotates almost toward the ground state, while in the smaller cell, the rotation is completed in the interacting part, while some difference still remain in the higher part respect to the ground state. Such similarity could make them indistinguishable at STM detection. The energy difference between these two configurations $\alpha di-bri30$ and $\alpha di-bri30$ from top30, in $5x5$ and $\sqrt{13}\times\sqrt{13}$, is respectively 0.57 and 0.43 eV (0.25 eV for E_{s-m}), while the height difference on substrate passes from 0.25 to 0.06 Å.

Similar behavior is obtained for two other configurations, which seem to shift to other minima, the fcc0 configuration towards bri30, while fcc30 shift its position. In top0 configuration, the substrate platinum atom, central respect

$(\sqrt{13}\times\sqrt{13})$ hexagonal	E_{ads}/E_{s-m} (eV)	$\triangle E_{ads}/\triangle E_{s-m}$ (eV)	E_{m-m} (eV)	E_{dist} (eV)	$\triangle z$ (Å)	h (Å)
(top30) $\alpha di-bri30$	-8.07/-6.61	0.00/0.00	-1.46	1.33	6.79	1.83
top0	-7.91/-6.49	0.16/0.12	-1.42	1.63	6.64	1.94
bri30	-7.76/-6.33	0.31/0.28	-1.43	0.80	6.56	2.07
$\sim fcc30$	-7.46/-6.03	0.61/0.58	-1.43	0.79	6.57	2.00
bri0	-6.85/-5.47	1.22/1.14	-1.38	0.72	6.56	2.09
(fcc0) $\sim bri30$	-6.79/-5.39	1.28/1.22	-1.40	0.80	6.58	2.08
$top0^*$	-7.88/-6.46	0.19/0.15	-1.42	1.32	6.59	1.82
$(\sqrt{13}\times\sqrt{13})$ *dimer*	E_{ads}/E_{s-m} (eV)	$\triangle E_{ads}/\triangle E_{s-m}$ (eV)	E_{m-m} (eV)	E_{dist} (eV)	$\triangle z$ (Å)	h (Å)
$\alpha di-bri30$	-8.50/-6.86	0.00/0.00	-1.64	1.51	6.86	1.77
bri0-top0	-8.05/-6.49	0.45/0.37	-1.56	1.75	6.88	1.61
di-fcc30	-7.63/-6.09	0.87/0.77	-1.54	0.79	6.91	1.74
di-bri0	-7.40/5.84	1.10/1.02	-1.56	1.46	6.85	1.70
di-fcc0	-6.26/-4.64	2.24/2.22	-1.62	0.58	6.94	1.99
fcc0-hcp0	-5.99/-4.41	2.51/2.25	-1.58	0.46	7.04	1.92

Table 5.2: C_{60} on Pt(111)-$(\sqrt{13}\times\sqrt{13})$: E_{ads} adsorption energy; $E_{s-m}=E_{sub-mol}$ substrate molecule interaction energy; $\triangle E_{ads}$ energy difference respect to ground state, $E_{m-m}$is the mutual fullerene interaction $E_{m-m}=E_{ads}-E_{s-m}=(E_{m-m}+E_{s-m})-E_{s-m}$; E_{dist} distortion energy ($E_{dist_{slab}}+E_{dist_{mol}}$); $\triangle z$ molecule size on zeta direction (free molecule distance between hexagons is 6.47 Å and 6.93 Å between dimers); h is the average height of the hexagon/dimer respect to surface set to zero; $\alpha di-bri30$ and $\beta di-bri30$ differ for the [1-10] crystallographic direction considered beneath the two hexagons. In parenthesis the initial configuration; final configuration $\alpha di-bri30$ from top30 is similar to $\alpha di-bri30$, when configurations are similar to other they are indicated with $\sim$

to bonding hexagon, moves downward of 0.34 Å. This particular result suggest that the huge strain to which top0 substrate is under is merely local because the substrate behaves identically in the two surfaces.

The top0 configuration is characterized by six symmetric bond C-Pt, low height on surface and huge strain which the surface undergoes. Considering the strain to which the molecule is subject a similar configuration is considered, simply slightly lower on surface. The idea is to verify is the strain induced by lower fullerene adsorption may be enough to lock the molecule in other minimum. This new configuration, labeled $top0^*$ is energetically similar to $top0$ but is 0.12 Å lower on the surface, its distortion energy is 0.31 eV lower and the substrate atom in the centre of the bonding hexagon moves downwards of 0.40 Å.

The bond lengths do not vary significantly between the two unit cells and therefore are reported exclusively for the smaller surface in table 5.3. Single and double bonds refer respectively when a substrate platinum atom is bonded only with one or with two carbon atoms. From this analysis, the ground state ($\alpha di-bri30$) has more and shorter C-Pt bonds than top0 configurations, which is lower on surface.

Energetically, in table 5.2, both E_{ads} and E_{s-m} are considered, the first includes both interactions between substrate and molecule (E_{s-m}) and between the molecules (E_{m-m}). Energies differences are maintained passing from E_{ads} to E_{s-m}, suggesting that E_{m-m} is uniform, larger for dimer adsorption than for hexagonal. This contribution is important as contribute significantly to rotations and shift of some configurations

The comparison between E_{ads} and E_{s-m} for the big and the small unit cell respectively for the same adsorption configuration, shows that the substrate molecule interaction decreases in the smaller surface. Such decrease is anyway

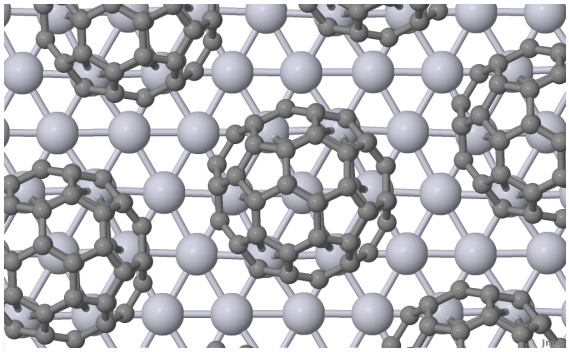

Figure 5.7: C_{60} on Pt(111)-($\sqrt{13}\times\sqrt{13}$): adsorption in the $\alpha dibri30$ configuration. Only one substrate layer is shown to ease the visualization

($\sqrt{13}\times\sqrt{13}$) hexagonal	$\triangle E_{ads}$ (eV)	$\triangle z$ (Å)	Single (Å)	Double (Å)
top0	+0.16	-0.05	2.17 (x6)	
bri0	+1.22	+0.26	2.07	2.23,2.24; 2.23,2.48; 2.11,2.55
fcc0 ($\sim bri30$)	+1.28	+0.31	2.07; 2.27	2.14,2.38; 2.15, 2.35
top30 ($\alpha di-bri30$)	0.00	0.00	2.11; 2.13; 2.26; 2.30	2.10, 2.12; 2.22, 2.25
bri30	+0.31	+0.10	2.12 (x2)	2.14,2.17; 2.17,2.19
$\sim fcc30$	+0.61	+0.19	2.08; 2.22	2.08,2.46; 2.1,2.49

Table 5.3: C_{60} on Pt(111)-($\sqrt{13}\times\sqrt{13}$): adsorption energy differences and fullerene height differences respect to the ground state; lengths for single and double bonds

	$\triangle E_{ads_{5x5}}$ (eV)	h (Å)	geometry	$\triangle E_{ads_{\sqrt{13}\times\sqrt{13}}}$ (eV)	h (Å)
$\alpha dibri30$	0.00	1.75	dimer	0.00	1.77
βdi-bri30	0.54	1.66	dimer		
top0	0.55	1.93	hexagonal	0.59/0.62	1.94
fcc0-hcp0	0.65	1.66	dimer	2.50	1.92
bri0-top0	0.65	1.63	dimer	0.45	1.61
$\sim \alpha dibri30$	0.66	2.00	hexagonal	0.43	1.83
bri30	0.68	2.07	hexagonal	0.74	2.07
di-fcc30			dimer	0.87	
di-fcc0	0.97	1.67	dimer	2.24	1.99
fcc30-bri30	1.07	1.77	dimer		
fcc30	1.09	1.98	hexagonal	1.04	2.00
hcp30	1.19	2.03	hexagonal		
hcp0	1.36	2.09	hexagonal		
bri0	1.51	2.07	hexagonal	1.05	2.09
fcc0			hexagonal	1.75	2.08

Table 5.4: Adsorption energies difference in the two surfaces from the ground state and adsorption energy difference

uniform along the configurations and the difference respect their respective ground state are mostly maintained, and so their order (table 5.4)

This analysis suggests that the molecule-substrate interaction among the two surface, is identical, that only with the increase of the deposition rate smaller unit cell may be considered as favorable respect to random adsorption, because adsorbates-substrate interaction is reduced by the one occurring between fullerenes.

5.2.4 Electronic Analysis

Ground state for STM Calculations in the smaller unit cell, have shown that two different configurations ($top30$ and $\alpha di-bri30$) generate similar ground state orientations ($\alpha di-bri30$), and that differ by strain and slightly by orientation of upper part of the admolecules. Ability by STM to distinguish between the two minima is here analyzed with a Tersoff Hamann approximation, that permits to approximate the STM images with molecular orbitals obtained as sum of HOMOs/LUMOs in the experimental energy range considered and through the choice of an appropriate isosurface. In fig. 5.8 the calculate STM patterns are shown, along with respective profile. To calculate, we considered all HOMOs between -1.0 and 0.0 eV and the 5×10^{-5} isosurfaces. The two molecules, differing in adsorption energy, cannot be differentiated one from another and therefore would appear identical at STM analysis.

5.3 Adsorption of C_{60} with surface vacancy

The next step considered adsorption of fullerene on Pt(111) with a surface vacancy. Such problem, as stated previously, is important to understand the metallorganic interaction in case of defects, and which motivations can be found in basic knowledge as much as in application of carbon structure in micro and nano molecular electronics. Experiments suggest that adsorption of fullerene, after formation of $\sqrt{13} \times \sqrt{13}$ domain (high coverage) and after increase of temperature, occurs in the same domain but through hexagonal orientation and lower on surface by 1.0 Å, in agreement with Ref.[54].

5.3.1 Geometries

Limiting the simulations to adsorption on the smaller unit cell ($\sqrt{13} \times \sqrt{13}$), the initial configurations considered are from both initial and final geometries obtained for hexagonal adsorption in the same surface and from the ground state $\alpha di-bri30$. For same geometry, different substrate vacancy positions have been eventually considered, to evaluate interactions of the defect.

Then labels follow the notation already used, and subscripts indicate which bond is broken by the formation of the vacancy (s= single, d=double, referring to multiplicity of bonds formed by the former Pt atom, fig. 5.9 left) and subscript c indicate the substrate atom located in the centre of bonding hexagons (fig. 5.9 right). In $bri30^{*}_{V}$ the vacancy is formed externally to substrate part interacting with the admolecule.

The adsorption energy E_{ads}, is calculated as difference between the total energy of adsorbed fullerene and the sum of slab with vacancy and of the isolated fullerene; the definition of other parameters, such as distortion energy, substrate molecule and molecule molecule energies follow same criteria in subsection 5.2.1, when, with slab is always intended the slab with vacancy.

5.3.2 Energetics and Structural difference

In table 5.5, the adsorption energies identify uniquely a ground state $top0_{V_C}$ in which vacancy is formed in the substrate atom located at the centre of bonding hexagons. The energy differences between the new ground state and the other configurations, are much higher than for adsorption on clean surface. This result is in good agreement with experimental findings that show a well defined hexagonal adsorption orientation on $\sqrt{13} \times \sqrt{13}$ surface at room temperature.

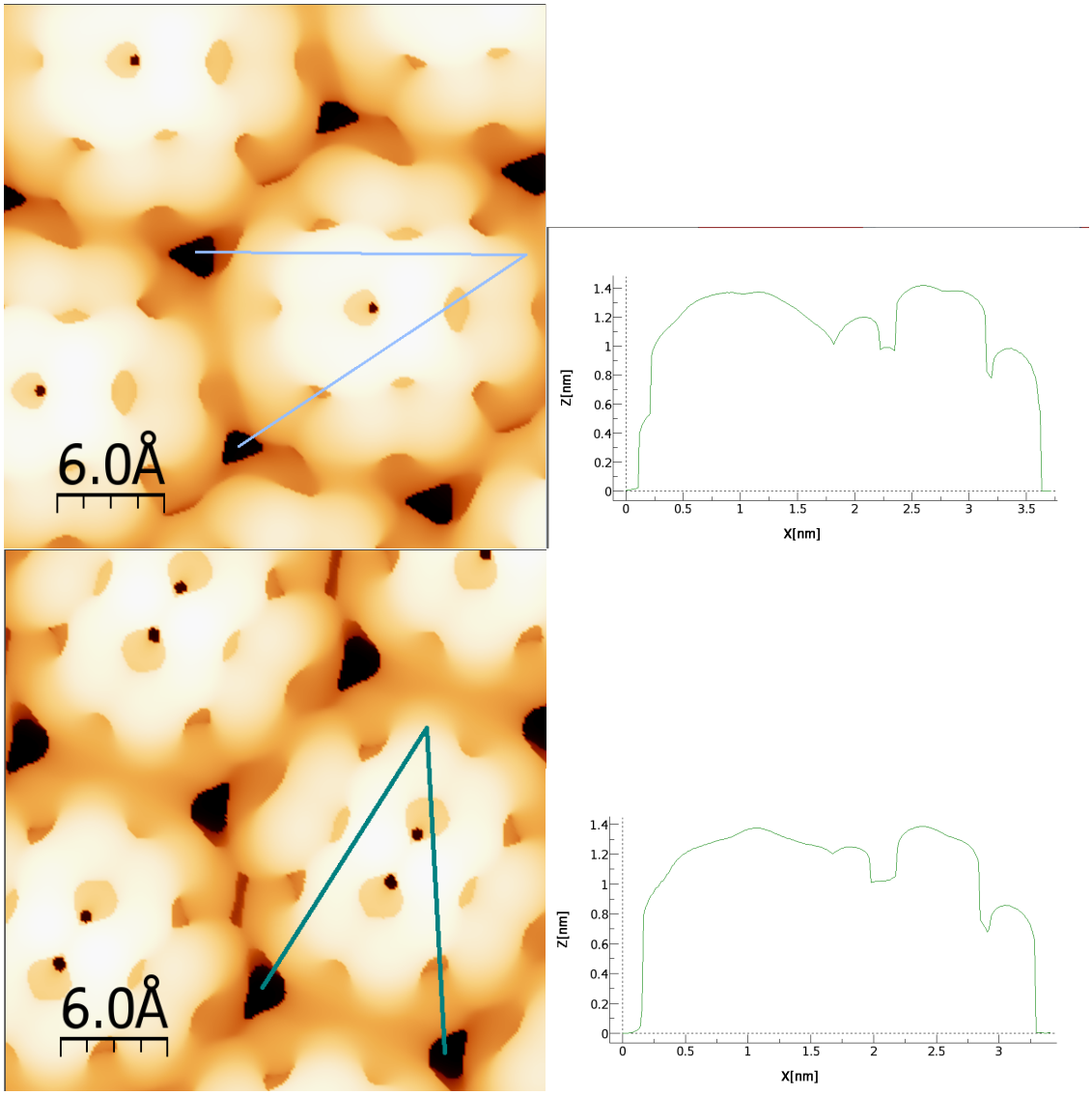

Figure 5.8: Calculated STM image (left) and profile (right) for ground state $\alpha di - bri30$, from $top30$ (up) and from $\alpha di - bri30$ (down) . Isosurface (5×10^{-5}) shown correspond to HOMOs between -1.0 and 0.0 eV.

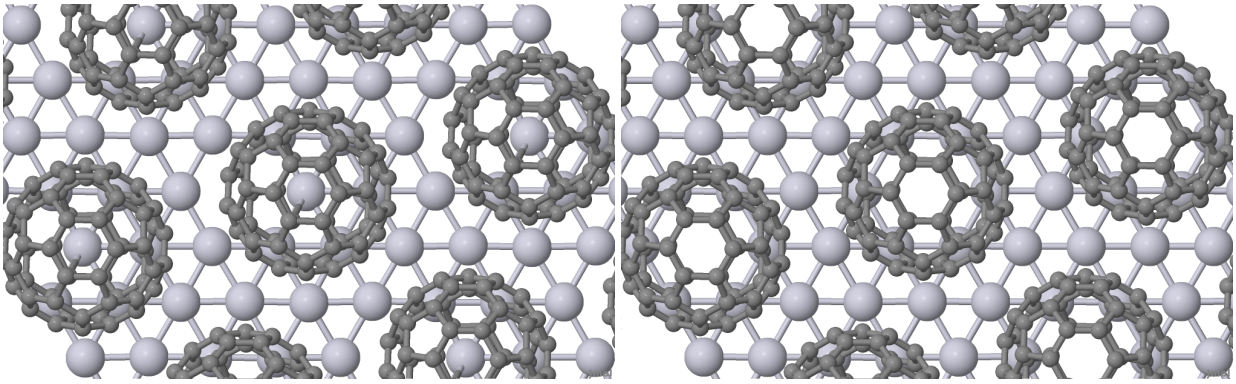

Figure 5.9: C_{60} on Pt(111)-($\sqrt{13} \times \sqrt{13}$) with surface vacancy: $top0_{V_S}$ (left) and $top0_{V_C}$ (right). Only one substrate layer is shown to ease the visualization

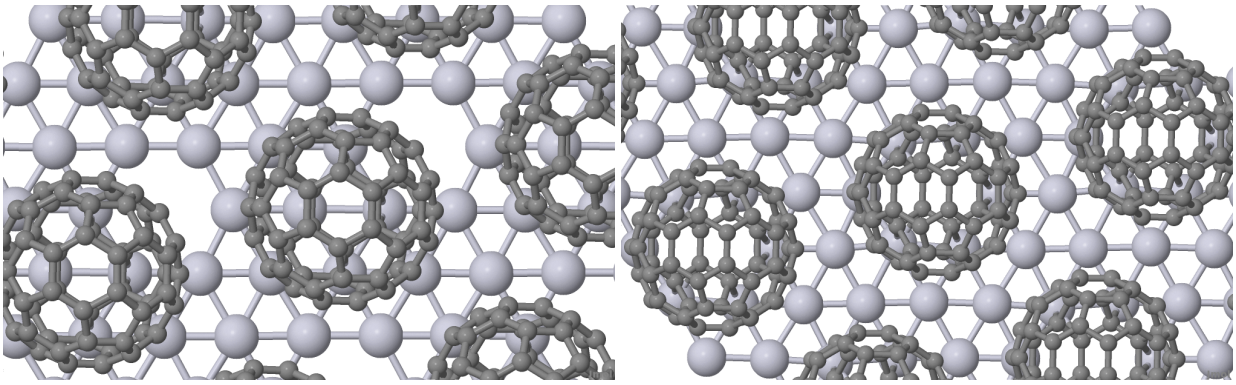

Figure 5.10: C_{60} on Pt(111)-($\sqrt{13} \times \sqrt{13}$) with surface vacancy: $bri30^*_V$(left) and $\alpha di - bri30_{V_d}$ (right). Only one substrate layer is shown to ease the visualization

The comparison with adsorption energy of analogous systems on clean surface, shows that any orientation which vacancy breaks a single bond is less favorable than without the vacancy by 0.40/0.50 eV.

Adsorption heights considered with their variation respect to their no vacancy analogous (when stable) show that molecules size $\triangle z$ do not vary significantly and, when present, correspond to a downward translation of the interacting part.

5.3.2.1 bri30 and $\alpha di - bri30$

When vacancy is created first near to fullerene substrate bonds (fig. 5.10 left, $bri30^*_V$), the height difference is negligible respect to adsorption of same configuration on clean surface; the configuration $bri30_{V_S}$ is energetically less favorable of almost 0.70 eV, which correspond, in part, to the single bond break. Migration of vacancy from $bri30^*_V$ to $bri30_{V_S}$ is then not favorable and fullerene is repulsive respect to vacancy migration.

The configuration $\alpha di - bri30_{V_d}$, that correspond to ground state for adsorption on clean surface, in which vacancy is formed in the position of the Pt atom double bonded with the dimer, is 1.43 eV less favorable than $top0_{V_C}$; its height on surface is lower than for $\alpha di - bri30$ but its upper part is higher, inducing a relevant strain. As for the adsorption on clean surface, from top30 orientation $\alpha di - bri30$ configuration is obtained (fig. 5.11), structurally similar to $\alpha di - bri30$ itself (fig. 5.10 right)

5.3.2.2 From top0

Single bond The break of a single bond and formation of a vacancy is not favorable when compared to adsorption in same orientation on clean surface and, again, an eventual migration of surface defect towards the central site ($top0_{V_C}$)

$(\sqrt{13}\times\sqrt{13})$ hexagonal	E_{ads}/E_{s-m} (eV)	$\triangle E_{ads}/E_{s-m}$ (eV)	E_{m-m} (eV)	E_{dist} (eV)	$\triangle z$ (Å)	h (Å)	H (Å)
$top0_{V_C}$	-9.93/-8.50 (-2.02)	0.00/0.00	-1.43 (-0.01)	1.44	6.66 (+0.02)	1.80 (-0.14)	8.46 (-0.12)
$top0^*_{V_C}$	-9.91/-8.40 (-2.03)	0.02/0.10	-1.51 (-0.09)	0.63	6.46 (-0.13)	1.42 (-0.40)	7.88 (-0.53)
$top0_{V_S}$	-7.45/-6.02 (+0.46)	2.48/2.48	-1.43 (-0.01)	1.33	6.61 (-0.03)	1.96 (+0.02)	8.57 (-0.01)
$\alpha di-bri30_{V_d}$	-8.83/-7.32 (-0.33)	1.10/1.18	-1.51 (-0.13)	0.89	6.98 (+0.12)	1.51 (-0.26)	8.49 (-0.14)
$top30_{V_C}$ $\alpha di-bri30^*_{V_d}$	-8.50/-7.04 (-0.43)	1.43/1.46	-1.46 (0.00)	0.91	6.94 (+0.15)	1.55 (-0.28)	8.49 (-0.13)
$bri30^*_V$	-7.93/-6.50 (-0.17)	2.00/2.00	-1.43 (0.00)	0.71	6.55 (-0.01)	2.00 (-0.07)	8.55 (-0.08)
$bri30_{V_S}$	-7.22/-5.79 (+0.54)	2.71/2.71	-1.43 (0.00)	0.51	6.51 (-0.05)	2.01 (-0.06)	8.52 (-0.11)
$fcc30_{V_d}$	-7.88/-6.45 (-0.42)	2.05/2.05	-1.43 (0.00)	0.73	6.55 (-0.02)	1.85 (-0.15)	8.40 (-0.17)
$bri0_{V_S}$	-7.18/-5.78 (+0.56)	2.75/2.72	-1.40 (-0.02)	0.70	6.59 (+0.03)	2.01 (-0.08)	8.60 (-0.05)
$bri0_{V_d}$	-6.73/-5.30 (+1.03)	3.20/3.20	-1.43 (-0.05)	0.46	6.53 (-0.03)	2.09 (0.00)	8.64 (-0.03)

Table 5.5: C_{60} on Pt(111)-$(\sqrt{13}\times\sqrt{13})$ with surface vacancy: E_{ads} adsorption energy; $E_{s-m}=E_{sub-mol}$ substrate molecule interaction energy; $\triangle E_{ads}$ energy difference respect to ground state, $E_{m-m}$is the mutual fullerene interaction $E_{m-m}=E_{ads}-E_{s-m}=(E_{m-m}+E_{s-m})-E_{s-m}$; E_{dist} distortion energy ($E_{dist_{slab}}+E_{dist_{mol}}$); $\triangle z$ molecule size on zeta direction (free molecule distance between hexagons is 6.47 Å and 6.93 Å between dimers); h is the average height of the hexagon/dimer respect to surface set to zero; H is the total height of the molecule. In parenthesis the the variation respect to the analogous system on clean surface. Subscripts indicate which bond is broken by the formation of the vacancy (s= single, d=double, referring to multiplicity of bonds formed by the former Pt atom) and subscript c indicate the substrate atom located in the centre of bonding hexagons. In $bri30^*_V$ the vacancy is formed externally to substrate part interacting with the admolecule.

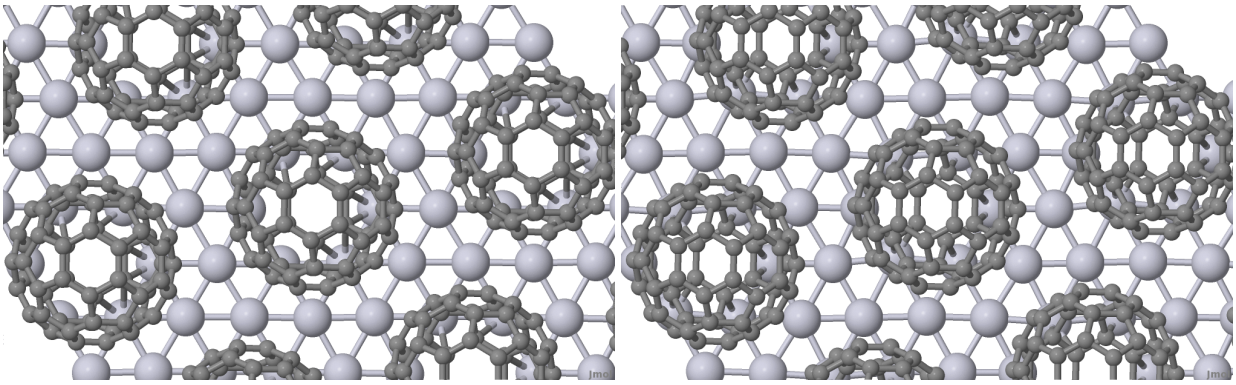

Figure 5.11: C_{60} on Pt(111)-$(\sqrt{13}\times\sqrt{13})$ with surface vacancy: geometrical relaxation from $top30_{V_C}$ (left) to $\alpha di-bri30^*_{V_d}$ (right). Only one substrate layer is shown to ease the visualization

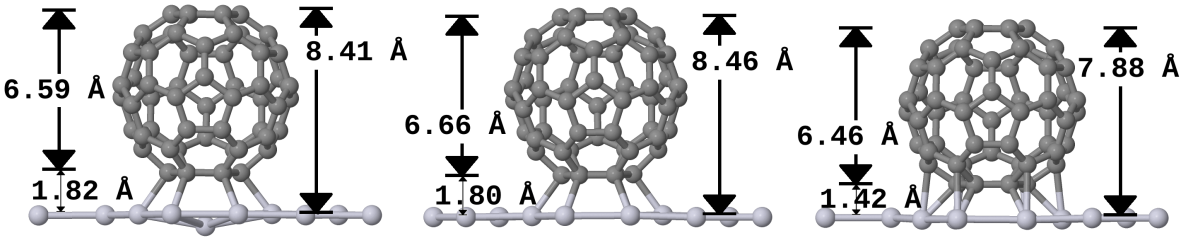

Figure 5.12: Adsorption in top0 orientation on $\sqrt{13}\times\sqrt{13}$: $top0^*$ (left), $top0_V$ (centre) and $top0_V^*$ (right). Height of interacting hexagon on surface is respectively 1.82, 1.80 and 1.42 Å. Height of $top0$ is 1.94 Å, not shown. Only one substrate layer is shown to ease the visualization

is precluded.

Central The formation of vacancy in the site of the substrate atom in the centre of bonding hexagon (fig 5.9 right) has been considered from the two different configurations obtained on the clean surface $top0$ and $top0^*$, and therefore labeled $top0_{V_C}$ and $top0_{V_C}^*$, which adsorption energy is similar. The converged configurations total height (H in table 5.5) difference is 0.58 Å, while $top0$ and $top0^*$ differ of 0.17 Å.

The distortion energy of $top0_{V_C}^*$ configuration is much lower than for the similar $top0_{V_C}$ (0.81 eV) and is mainly associated to fact that its $\triangle z$ is similar to the height of free fullerene. Between $top0_{V_C}$ and $top0_{V_C}^*$ exists an energy barrier, which at the moment, has not been calculated.

5.3.3 Electronic Analysis

In fig. 5.13, 5.14 and 5.15, the Tersoff Hamann approximation of the STM image through the molecular orbitals (HOMOs considered in a range between -1.0 and 0.0 eV and 2×10^{-6} isosurface) shows that the lowest profiles are associated to $top0^*$ and $top0_V^*$ configurations, which differ by almost 1 Å respect to $top0$ and $top0_V$; geometrically such difference is 0.17 Å between $top0^*$ and $top0$, and 0.58 Å between $top0_V^*$ and $top0_V$. The height difference in the STM profile is then to be associated with different interaction with the substrate. Further analysis with different exchange correlation approximations and DFT method may help to understand better the $top0$ adsorption orientation.

5.4 Vacancy Formation

Vacancy formation and diffusion are important parameters to understand the adsorption of fullerene on Pt(111); meanwhile an extensive study on migration barriers on different configurations should be necessary, is not the main object of the work and therefore, the following discussing is limited to its formation energy E_{f_V}.

On clean surface Two possible approaches to estimate such value have been considered, none considering formation of Frenkel pair (vacancy formation, adatom at the kink). In the first case E_{f_V} is obtained as from:

$$E_{f_{V1}} = E_V - (\frac{n-1}{n})E \tag{5.1}$$

Where E and E_V are respectively the total energy of the slab without and with the vacancy and n is the number of atoms of the clean slab. The calculated values in $\sqrt{13}\times\sqrt{13}$ surface are 1.40 and 1.81 eV in GGA and LDA for plane waves method, and 1.91 eV in LDA for localized orbital method. In the larger unit cell (5×5) the E_{f_V} obtained with localized orbital method in LDA is 1.92 eV. This approximation is more reliable when the surface atoms are not in significant amount respect to the others. For this reason values are overestimated.

In the second case, more accurate, E_{f_V} is given by the following equation

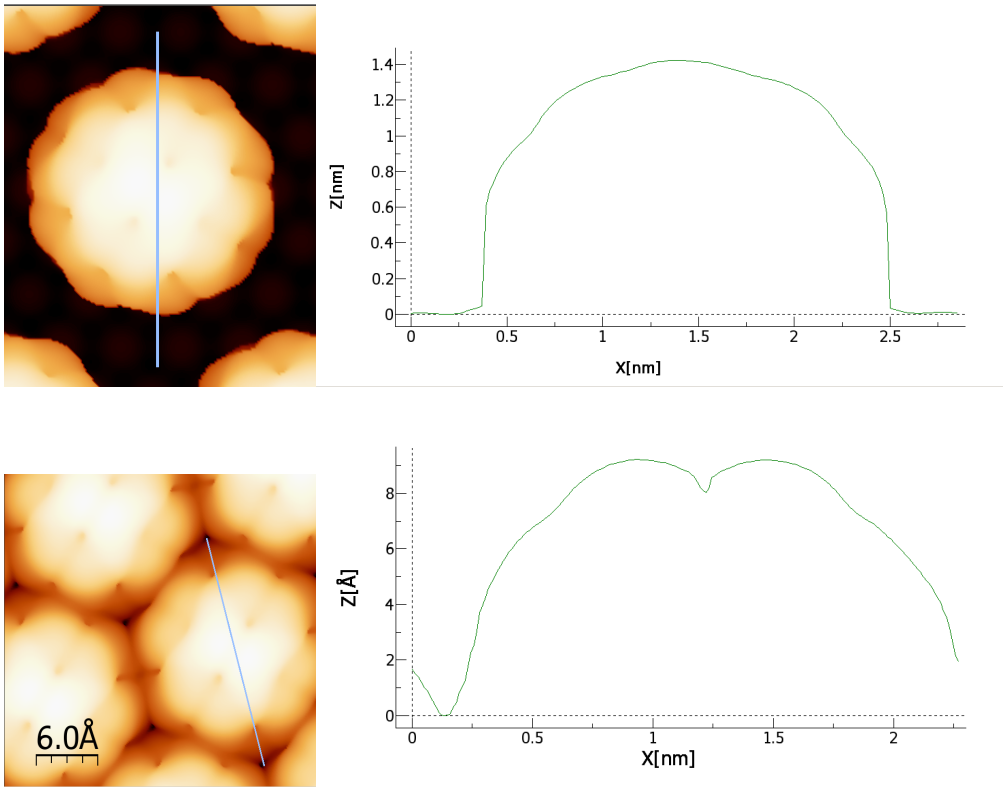

Figure 5.13: Tersof Hamann approximation of STM images and profiles for $\alpha di - bri30$ in 5×5 (up) and $\sqrt{13} \times \sqrt{13}$ (down). The isosurfaces (1×10^{-6}Å^{-3}) shown correspond to the filled states between -1.0 and 0.0 eV.

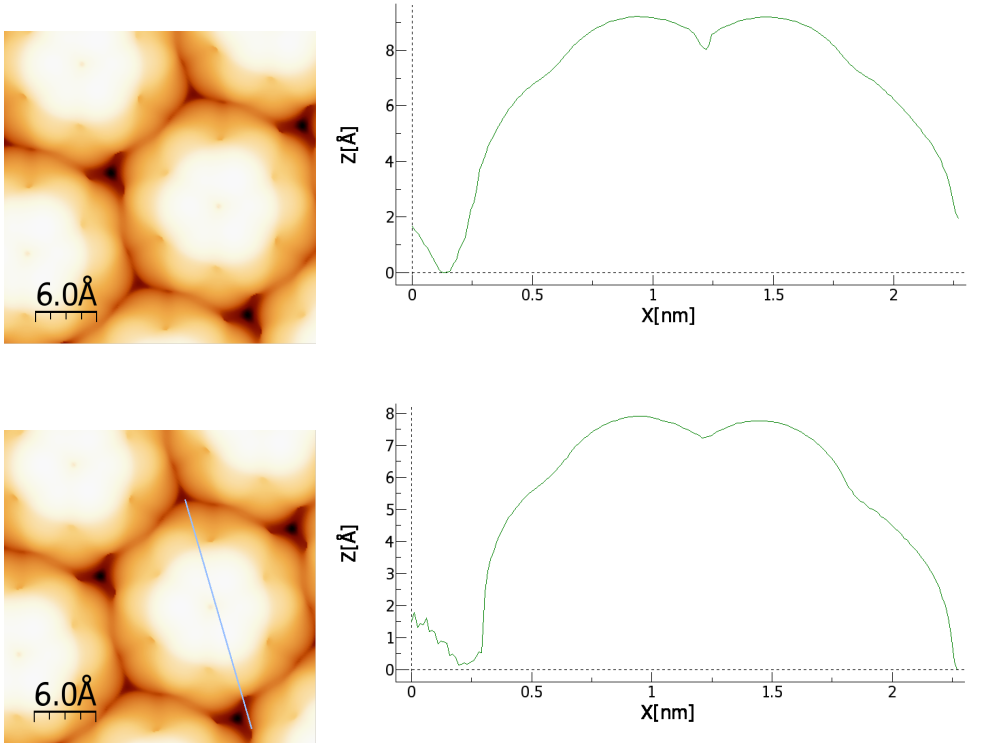

Figure 5.14: C_{60} on Pt(111)-($\sqrt{13} \times \sqrt{13}$): Tersof Hamann approximation of STM images and profiles for $top0$ (up) and $top0^*$ (down). The isosurfaces (1×10^{-6}Å^{-3}) shown correspond to the filled states between -1.0 and 0.0 eV.

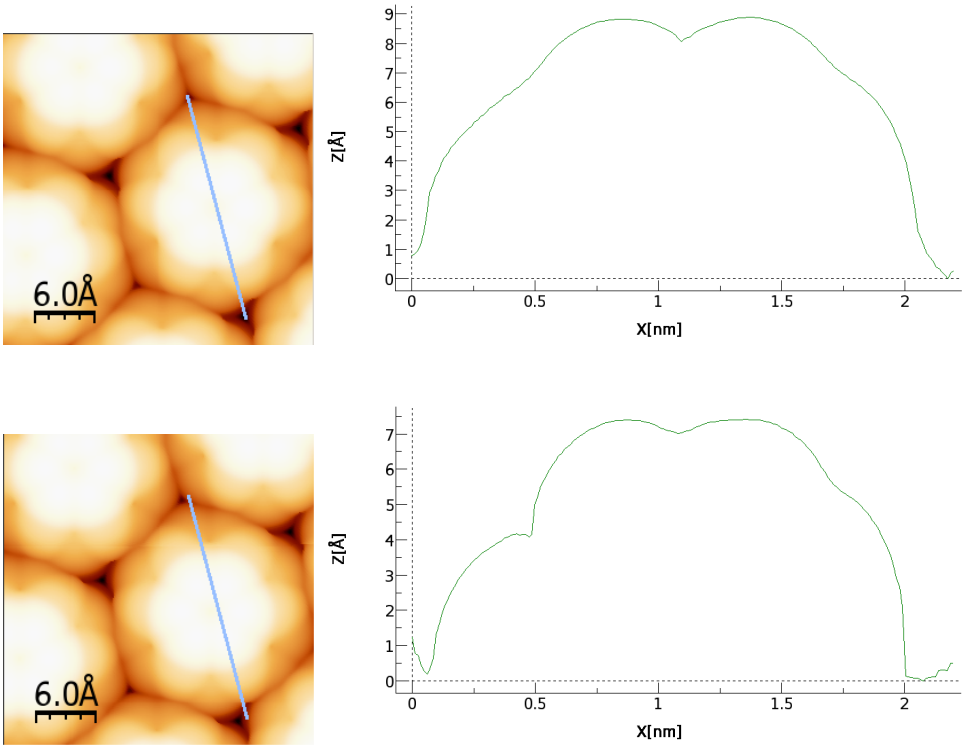

Figure 5.15: C_{60} on Pt(111)-($\sqrt{13}\times\sqrt{13}$): Tersof Hamann approximation of STM images and profile for $top0_V$ (up) and $top0_V^*$ (down). The isosurfaces (1×10^{-6}Å^{-3}) shown correspond to the filled states between -1.0 and 0.0 eV.

$$E_{f_{V2}} = (E_V + \mu_{Pt}) - E \tag{5.2}$$

as the difference between the sum of the total energy of the slab with vacancy E_V and the chemical potential μ_{Pt}, and the total energy of the clean slab E. In this formula it is assumed that the substrate atom move to the bulk, and therefore μ_{Pt} is $E_{bulk}+E_{at}$, where E_{bulk} and E_{at} are the bulk energy and the atomic energy reference for platinum (chapter 2). Negative values indicate that configuration with vacancy is energetically favorable.

The calculated value for $\sqrt{13}\times\sqrt{13}$ is -1.55 eV for LDA with Openmx, similar to reported value -1.49 eV[93], obtained for $\sqrt{3}\times\sqrt{3}$ surface on 7 and 9 layers with LDA localized orbital method implemented by the simulation code QUEST. The similar result obtained validates the approximation made with the choice of 3 layers thickness of the slab.

With Fullerene Similar approaches can be used for the adsorption of fullerene in the $\sqrt{13}\times\sqrt{13}$ surface.

Through equation 5.2, considering for E and E_V the total energies of adsorbates in the same configuration without and with the surface vacancy respectively, only two configurations are favorable when vacancy is formed: $top0_V$ and $top0_V^*$ (table 5.6). These configuration are characterized by decrease of distortion energy, generated by formation of vacancy in place of the substrate atom at the centre of the bonding hexagons. Such atom is indeed the lowest of the first layer moving downward for more than 0.30 Å. Vacancy formation in other sites is not favorable.

5.5 Adsorption of N-Doped fullerenes

The azafullerenes are fullerene in which the cage atoms have been substituted by nitrogen atoms and labeled $C_{60-X}N_X$. The many possible different choices for same number X of substituent dopants, may bring to formation of a wide

(eV)	$bri0_s$	$bri0_d$	$top0_{V_S}$	$top0_{V_C}$	$top0^*_{V_C}$	$bri30_s$	$bri0^*$	$\alpha di-bri30$	$fcc30_d$
E_{f_V}	+1.06	+1.51	+1.85	-0.62	-0.55	+1.93	+1.22	+0.63	+0.97
$E_{dist_{slab}}$			0.75	0.75	0.65	0.24			
$E_{dist_{slab_V}}$			0.64	0.20	0.35	0.27			

Table 5.6: Vacancy formation energy, assuming the atom to move to bulk, and distortion energy for configuration with and without vacancy. In $top0$ and $top0^*$ the substrate atom central to bonding hexagon move downwards of 0.34 and 0.40 Å respectively (0.33 Å for $top0$ orientation in 5×5 unit cell)

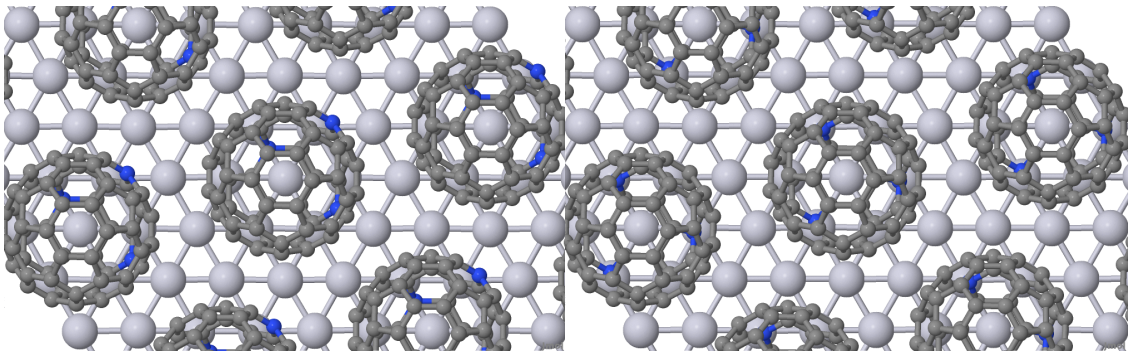

Figure 5.16: $C_{57}N_3$ on Pt(111)-($\sqrt{13}\times\sqrt{13}$): adsorption orientation $top0$, *uud* (left) and *ddd* (right). Only one substrate layer is shown to ease the visualization

range of molecule with different properties, either locally or equally distributed across the molecule. Meanwhile addressed as potentially interesting for application in spintronics and many other field, only the monoazafullerene has been synthesized and the diazafullerene is considered elusive. In addition, being the monoazafullerene an open shell molecule, it is mostly observed forming dimers.

In the following section, the adsorption of the triazafullerene $C_{57}N_3$ as obtained from cyclodehydrogenation of the heteropolyarene $C_{57}H_{33}N_3$ is discussed.

5.5.1 Triazafullerene adsorption on Pt(111)

Without a clear experimental overview on adsorption orientation and domain organization of the molecule, the adsorption of the triazafullerene is here considered in the $\sqrt{13}\times\sqrt{13}$ unit cell , with and without vacancy, considering orientation with either three downward orientated nitrogen (label *ddd*, fig. 5.16) or with only one (label *uud*, fig. 5.16). For the experimental reasons mentioned before, calculation with three upward nitrogen has been carried at lower precision and proof to be less favorable than the other configurations.

This approach, meanwhile limited in explored configurations, provides a description of effects of the nitrogen doping in the adsorption behavior. The cage orientation considered are $\alpha di-bri30$ and $top0$.

When vacancy in the substrate is considered, further discrimination has been done. The calculation has been limited to the two orientations with formation of vacancy in different position; the configurations $\alpha di-bri30_V$, considered from $\alpha di-bri30_{V_d}$, labeled N and d_b have vacancy respectively in the substrate position that was bonded respectively with nitrogen ($\alpha di-bri30_{V_S}$) and with the dimer (fig. 5.17).

Energetics

The results for energetic and structural parameters are shown in table 5.7. On clean surface, the energetic interaction seems more complicated than for adsorption of fullerene, as dimer adsorption is not significantly more favorable than hexagonal. On surface with vacancy the hexagonal adsorption is more favorable than through the dimer, but less than for fullerene. This behavior is related to adsorption of nitrogen atom, which induce rotation of the configuration to

$\sqrt{13}\times\sqrt{13}$	E_{ads}/E_{s-m} (eV)	$\triangle E_{ads}/\triangle E_{s-m}$ (eV)	E_{m-m} (eV)	E_{dist} (eV)	$\triangle z$ (Å)	h (Å)	H (Å)
$\alpha di-bri30$							
uud	-8.36/-6.68	0.18/0.62	1.68	1.63	6.83	1.73	8.56
ddd	-8.52/-6.97	0.02/0.33	1.55	1.60	6.87	1.72	8.59
C_{60}	-8.50/-6.86		1.64	1.51	6.86	1.77	8.63
$top0$							
uud	-8.17/-6.91	0.37/0.39	1.26	1.66	6.64	1.87	8.51
ddd	-8.54/-7.30	0.00/0.00	1.24	1.46	6.66	1.96	8.62
C_{60}	-7.91/-6.49		1.42	1.63	6.64	1.94	8.58
$\alpha di-bri30_{V_d}$							
N	-8.90/-7.18	1.88/2.36	1.72	1.42	6.87 (0.00)	1.70 (-0.02)	8.57 (-0.02)
d_b	-9.25/-7.74	1.53/1.80	1.51	1.45	6.86 (-0.01)	1.70 (-0.02)	8.56 (-0.03)
C_{60}	-8.83/-7.32		1.51	0.89	6.98 (+0.12)	1.51 (-0.26)	8.49 (-0.14)
$top0_{V_C}$							
uud	-10.47/-9.21	0.31/0.33	1.26	1.38	6.64 (0.00)	1.73 (-0.14)	8.37 (-0.14)
ddd	-10.78/-9.54	0.00/0.00	1.24	1.93	6.65 (-0.01)	1.74 (-0.22)	8.39 (-0.23)
C_{60}	-9.93/-8.50		1.47	1.44	6.66 (+0.02)	1.80 (-0.14)	8.46 (-0.12)

Table 5.7: $E_{s-m}=E_{sub-mol}$ and $E_{m-m}=E_{mol-mol}$, respectively substrate molecule and molecule molecule interaction energies. E_{ads}/E_{s-m} adsorption energies and molecule substrate energetic interaction, their energy differences, admolecules mutual interaction $E_{mol-mol}$ is the difference between E_{ads} and $E_{sub-mol}$, E_{dist} distortion energy, $\triangle z$ molecule height (fullerene free molecule distances: hexagon-hexagon 6.47 Å, dimer-dimer 6.93 Å, h average height of the interacting part (hexagon or dimer) on surface and H total height as average between highest and lowest parts. Their fullerene counterpart is indicated in table as C_{60}. For the system with vacancy ($top0_{V_C}$), in parenthesis, the comparison respect to same configuration without vacancy. The configurations $\alpha di-bri30_{V_d}$, labeled N and d_b have vacancy respectively in the substrate position bonded with nitrogen and with the dimer.

bond with the substrate.

The difference in adsorption and the substrate molecule interaction energies E_{ads} and E_{s-m} are similar for the hexagon adsorption orientation ($top0$), while change when dimer adsorption is considered ($\alpha di-bri30$). Independently by presence of vacancy, mutual triazafullerene interaction ($E_{mol-mol}=E_{ads}-E_{sub-mol}$) is 0.20 eV lower than for correspondent adsorption of fullerene.

Triazafullerene adsorption energy differences between same configuration ($top0$) with and without the vacancy, are 2.24 and 2.30 eV for ddd and uud configurations respectively, larger than for adsorption of fullerene (2.02 eV). This result suggest than vacancy formation could be, in general easier.

The triazafullerene mutual energy contribution E_{m-m} increases significantly (0.20) when the bond between substrate and nitrogen is lost. Such effect may be extremely important for the formation of dimers, as E_{s-m} decrease. Structurally the adsorption of triazafullerene is similar to the fullerene on the same surface.

5.6 Conclusions

Adsorption of fullerene on clean surface The ground state is identified for the $\alpha di-bri30$ configuration which maximize the number of bonds. Similar configuration can be obtained also from rotation of top30 configuration, in the limit of isolated adsorbate and in the small unit cell considered. In general, the energy differences are maintained

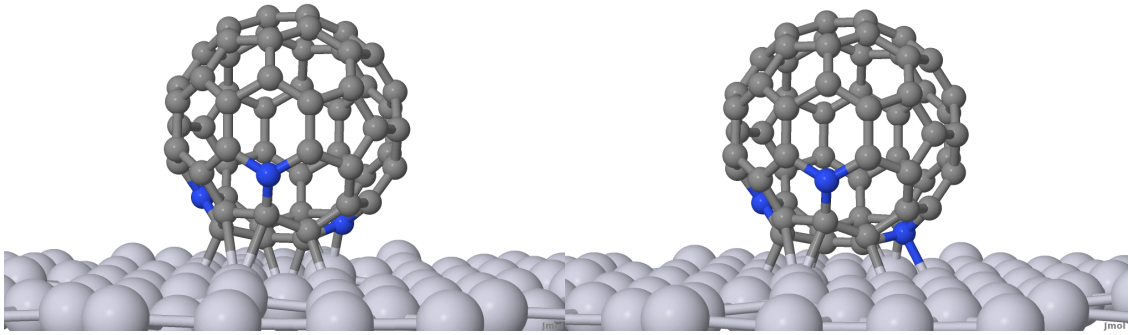

Figure 5.17: $C_{57}N_3$ on Pt(111)-($\sqrt{13}\times\sqrt{13}$): The configurations $\alpha di-bri30_{V_d}$: labeled N (left) and d_b (right) have vacancy respectively in the substrate position bonded with nitrogen and with the dimer. Only one substrate layer is shown to ease the visualization

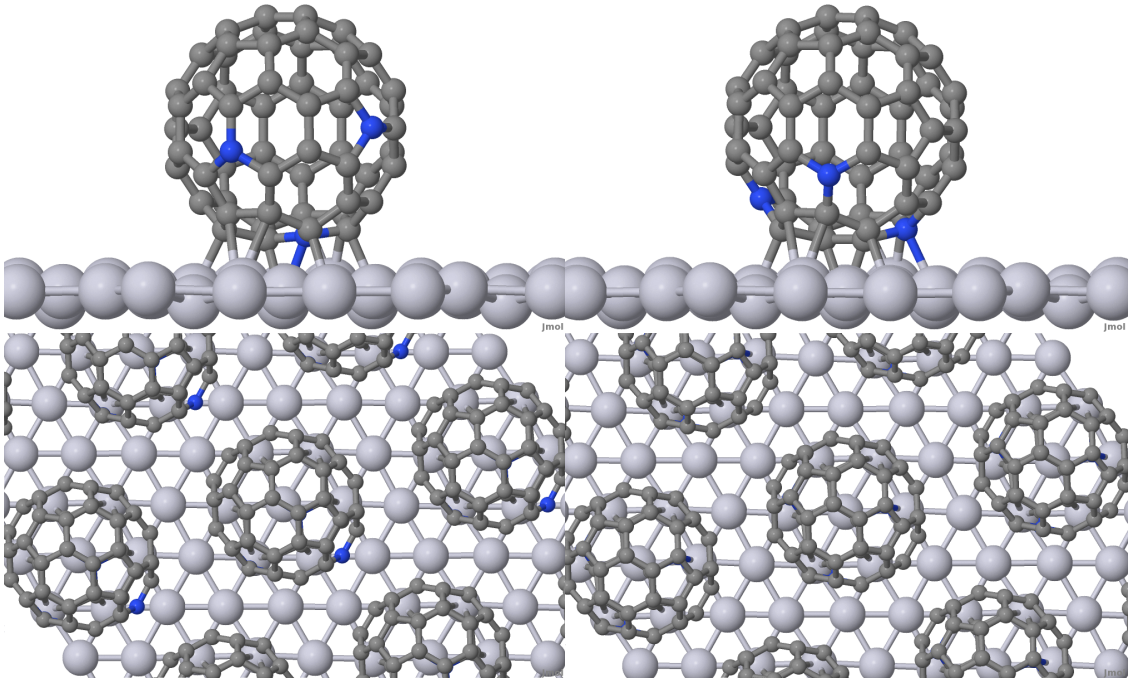

Figure 5.18: $C_{57}N_3$ on Pt(111)-($\sqrt{13}\times\sqrt{13}$): adsorption configuration $\alpha di-bri30$, *uud* (left) and *ddd* (right). Side view (up) and frontal (down). Only one substrate layer is shown to ease the visualization

	$E_{sub-mol_{5\times5}}$ (eV)	h (Å)	$E_{sub-mol_{\sqrt{13}\times\sqrt{13}}}$ (eV)	h (Å)	$E_{subV-mol_{\sqrt{13}\times\sqrt{13}}}$ (eV)	h (Å)
$top0/top0^*$	-6.82	1.94	-6.49; 6.4	1.94; 1.82	-8.50; 8.40	1.80; 1.42
$bri0$	-5.86	2.07	-5.47	2.09	-5.78; -5.30	2.01; 2.09
$bri30$	-6.69	2.07	-6.33	2.07	-5.79; -6.50	2.00; 2.01
$fcc30$	-6.28	1.98	-6.03	2.00	-6.45	1.85
$\alpha di-bri30$	-7.37	1.75	-6.86	1.77	-7.32	1.51

Table 5.8: Substrate-molecule energy in the surfaces 5×5, $\sqrt{13}\times\sqrt{13}$ and $\sqrt{13}\times\sqrt{13}$ with vacancy.

between configurations in the two different unit cells, where the fullerenes mutual interaction provides a relevant contribution to the adsorption energy. These findings are in good agreement with experiments, which show that, at low temperature, and in case of low coverage, the adsorption orientation is random, as consequence of high adsorption energy. With the increase of temperature and deposition rate, the formation of $\sqrt{13}\times\sqrt{13}$ islands is more probable, with the important contribution of the mutual interaction of the adsorbates. The decreased fullerene - substrate interaction with increasing density observed passing from 5×5 to $\sqrt{13}\times\sqrt{13}$ may also explain the reported lower conductivity between platinum tips by an increasing number of fullerenes[92]. Consequence of the mutual interaction between fullerenes, the fragmentation temperature could be higher and, perhaps, small cluster desorption energy could be lower than for single admolecule.

Adsorption of fullerene on surface with vacancy The obtained ground state orientation ($top0_{V_C}$ and $top0^*_{V_C}$) is in good agreement with experimental results, as it appears after formation of a vacancy and at lower height on surface. The vacancy migration towards fullerene in $top0$ to form $top0_{V_C}$ can also be discarded as implies migration barriers and breaking a single bond forming a $top0_{V_S}$ configuration which is energetically less favorable than adsorption $top0$. In table 5.8 the substrate molecule interaction energy is compared for some configurations, representative of low fullerene coverage (5×5), reconstruction at high densities ($\sqrt{13}\times\sqrt{13}$) and with formation of vacancy in the substrate after island formation ($\sqrt{13}\times\sqrt{13}$). In general random adsorption is favorable, but, once$\sqrt{13}\times\sqrt{13}$ domains and substrate vacancy are formed, the $top0_{V_C}/top0_{V_C}$ is the most favorable orientation.

Adsorption of triazafullerene on surface with and without vacancy The results show a preference for one of the nitrogen to move downwards and bond with the substrate, result that is in good agreement with experimental finding that show that one nitrogen is bonded with the substrate (XPS). Due to limitation of explored configurations and complexity of phase space, is not possible to identify any ground state.

Chapter 6

Cyclodehydrogenation

In the following chapter, the possible paths involved in the cyclodehydrogenation occurring during experimental annealing, are proposed. Such insight is to be considered mostly qualitative, for the nature of the process itself, and, once it is examined on the surface, for the drastic limitations required by simulations. The aim, is to clarify the possible paths in the both gas phase and on Pt(111), and, doing so, to understand the reasons behind the low efficiency in the first case and that are not occurring on surface. Such approach may help to understand possible extension of the methodology to other systems. The chapter is organized as follow: first the experimental results (section 6.1), to which follows the analysis on the complete dehydrogenation before any cyclization in the gas phase (section 6.2) and on surface (section 6.3) and then the analysis of cyclization and dehydrogenation as progressively alternated (section 6.3.3).

6.1 Motivation and Experimental Results

The dehydrogenation of carbon nanostructures to form other compounds which synthesis would be otherwise complicated, is an important new technique that has recently shown great potential and that is methodologically approached in different ways[30, 53, 94].

In the case studied in this thesis, the cyclodehydrogenation is thermally induced by surface reaction to exclude activation of much mechanism by electronic current from STM tip, as reported on adsorbed aromatic molecules[95], the dehydrogen signal in mass spectrometer is studied as function of temperature.

To avoid artefact consequences of dehydrogen desorption from experimental apparatus, the deuterated triaza analogue $C_{57}H_{27}D_6N_3$ has been synthesized (fig. 6.1) and its dehydrogenation and its deuteration studied.

In fig. 6.2, the black line correspond to signal before any molecule deposition, while the other two signals are associated to formation of biatomic molecules HD and D_2 (curve depleted by factor eight). These results indicate there is neither modification of the molecular shape, nor dehydrogenation below 400 K and that at 500 K the molecule can be already partially dehydrogenated, while at about 700 K a rapid desorption process takes place.

STM images show that from triangular shaped molecules, smaller but higher spherical one, are obtained after annealing (fig. 6.3), and which sizes are compatible with fullerene (chapter. 5 section 5.1)

When similar experiment is considered on Au(111), after annealing the formation of fullerene occurred with an efficiency similar to the value reported in the gas phase [30] (1%), showing that on such surface, the cyclodehydrogenation either occur after desorption (gas phase) and/or at the steps where the molecular precursors adsorb.

To study the overall process, to understand the differences in efficiency between gas phase (1%) and on surface ($\sim$ 100%), the cyclization in the two environments is treated separately with different theoretical methods and techniques, for different possible cyclization paths.

In the gas phase, geometrical relaxations, molecular dynamics (MD) and nudged elastic band (NEB) calculations are carried, respectively with plane waves method (Vasp), localized orbitals by Openmx and by Fireball. On the

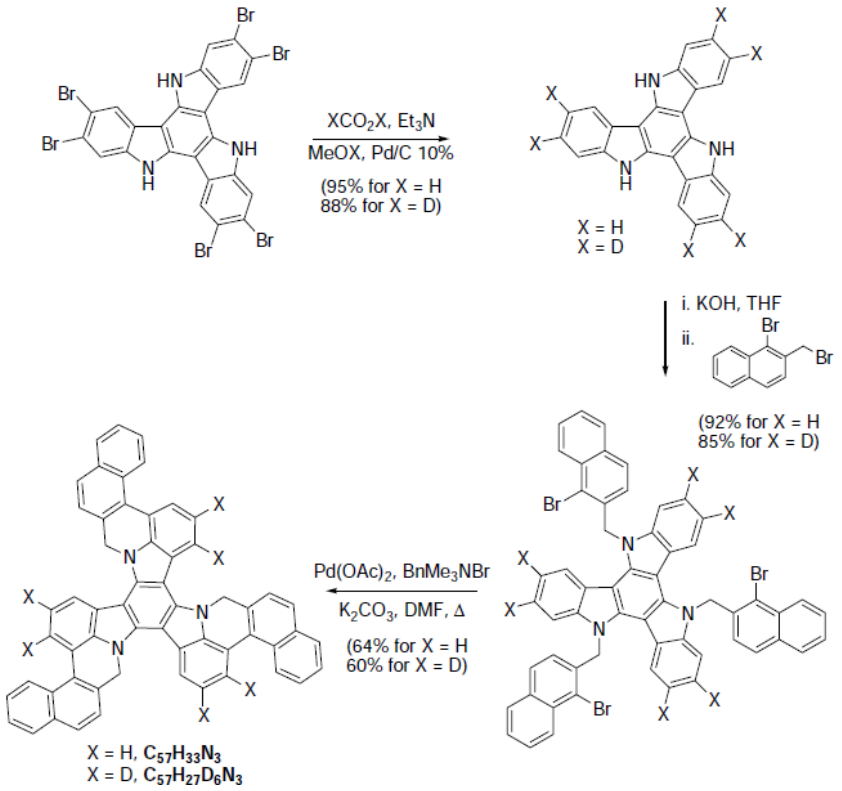

Figure 6.1: Chemical synthesis of deuterated $C_{57}H_{27}D_6N_3$

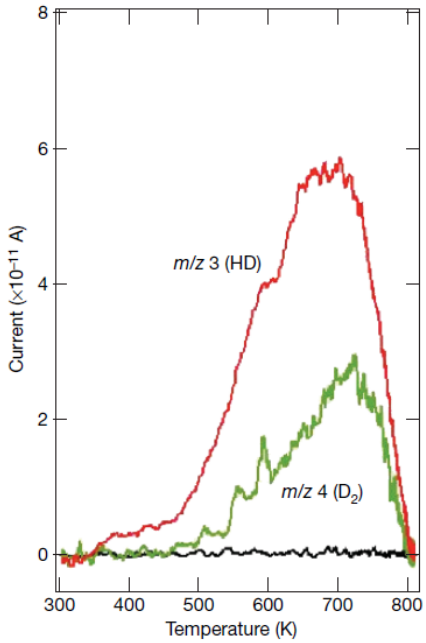

Figure 6.2: TPD experiment of the cyclodehydrogenation process. Temperature evolution of the masses corresponding to HD (*m/z* 3) and D_2 (*m/z* 4), recorded after depositing $C_{57}H_{27}D_6N_3$ on the surface. Thermal desorption takes place at around 500 K. The *m/z* 4 signal has been scaled by a factor of eight. The black line is the result of recording the HD signal without depositing molecules on the platinum surface.

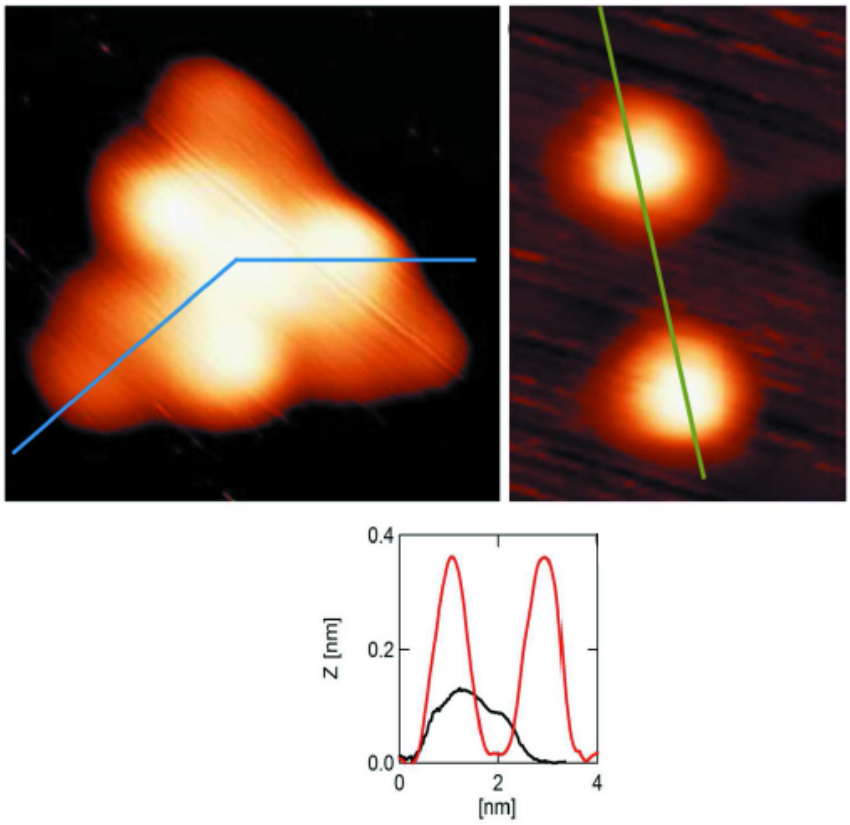

Figure 6.3: STM images and profiles of adsorbed polyarene and of two closed fullerenes.

surface different configurations are considered through geometrical relaxation and molecular dynamics.

Molecular dynamics (MD). This technique allows atoms and molecules to interact for a period of time by approximations of their motion. In the micro-canonical, or NVE, ensemble, an adiabatic process with no heat exchange is reproduced, maintaining constant the number of moles (N), the volume (V) and the energy (E). In the canonical ensemble or NVT, the number of moles (N), the volume (V) and the temperature (T) are conserved, and the energy of endothermic and exothermic processes is exchanged with a thermostat to control the temperatures. Such control can be implemented with velocity rescaling algorithm, the Nose-Hoover thermostat, Nose-Hoover chains, the Berendsen thermostat and Langevin dynamics.

The molecular dynamics simulations considered here are carried in canonical ensemble with velocity rescaling algorithm.

When no explicitly mentioned, the qualitative results shown for polyarene cyclization are equally valid for the doped heteropolyarene.

6.1.1 Geometries

The two polycyclic aromatic hydrocarbons considered, the polyarene $C_{60}H_{30}$[44] and the hetero-polyarene $C_{57}H_{33}N_3$[45] are structurally similar, fig. 6.4, and, as mentioned in chapters 3 and 4; composed by a central part, one hexagon and three pentagons, and three wings, at 120º. The labels given to the single elements (benzene like) are shown in the fig. 6.4 itself.

In chapter 4 two isomer of the heteropolyarene $C_{57}H_{33}N_3$ have been considered to understand nitrogen and hydrogen effects in the polycyclic aromatic hydrocarbon structure. For similar purposes, the same molecules are considered

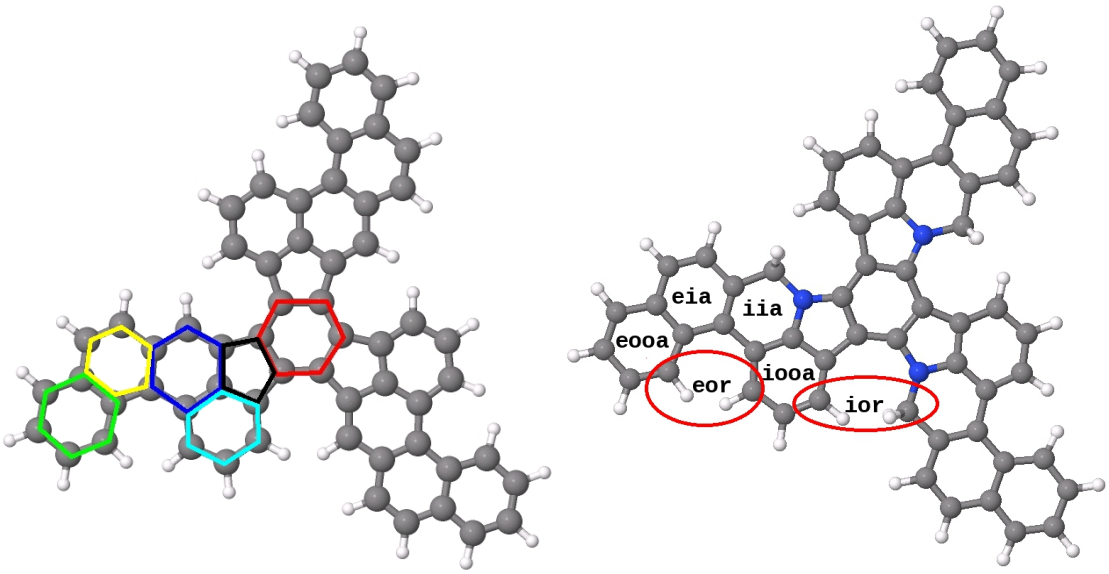

Figure 6.4: Polyarene (left) and hetero-polyarene (right). Components label: central hexagon (red), pentagon (black), internal in axis hexagon (blue), internal out of axis hexagon (cyan), external in axis hexagon (yellow) and external out of axis hexagon (green).

in this chapter for the cyclization processes in the gas phase. These two molecules differ from hI by the position of substituents and hydrogenation (fig. 4.4).

6.2 Cyclodehydrogenation in the gas phase

It is here assumed that the final cyclization occurs after the complete dehydrogenation. At experimental temperature no hydrate fullerene[96] are obtained, and in the gas phase no significant difference in the dehydrogenation energy barriers can be expected along the similar C-H bonds.

Therefore the dehydrogenation may be either 1) instantaneous and prior to cyclization or 2) progressive, and proceed along with enclosure. The first condition to be studied is the simplest situation: complete dehydrogenation.

6.2.1 Cyclization of complete dehydrogenated precursors

Considering the total dehydrogenation prior any cyclization, it means assuming that C-H dehydrogenation barriers are similar along all the molecule. Results obtained are qualitatively similar for both plane waves and LCAO methods and independent from the molecular precursor considered. To simplify, the results are shown only for the $C_{60}H_{30}$ when no otherwise explicitly stated.

The first step considers the simple geometrical relaxation of the fully dehydrogenated molecular precursor. The initial configuration is the ground state configuration obtained for relaxation in the gas phase and then dehydrogenated.

The obtained configuration, labeled *de1* and shown in fig. 6.5, is flat; in two wings two pentagons are formed in the *eor* and also bonded are the carbon atoms of the *ior* in the wing without the *eor* pentagon. Similar behavior is obtained for the fully dehydrogenated heteropolyarenes hI and hII (being the fully dehydrogenated hIII equivalent to hII); these results, independent from nitrogen doping and its position, prove once more that the helical shape of the hydrogenated molecules is caused by the steric congestion of their bay positions, that forces the more flexible aromatic ring of each wing to flip up respect to the plane of the less flexible ring.

The second initial configuration considered, labeled *de2* and show in fig. 6.6, has a slight central curvature, almost planar wings and one *ior* closed. Geometrical relaxation brings to a fully closed fullerene cage with no energy barriers. (fig. 6.7).

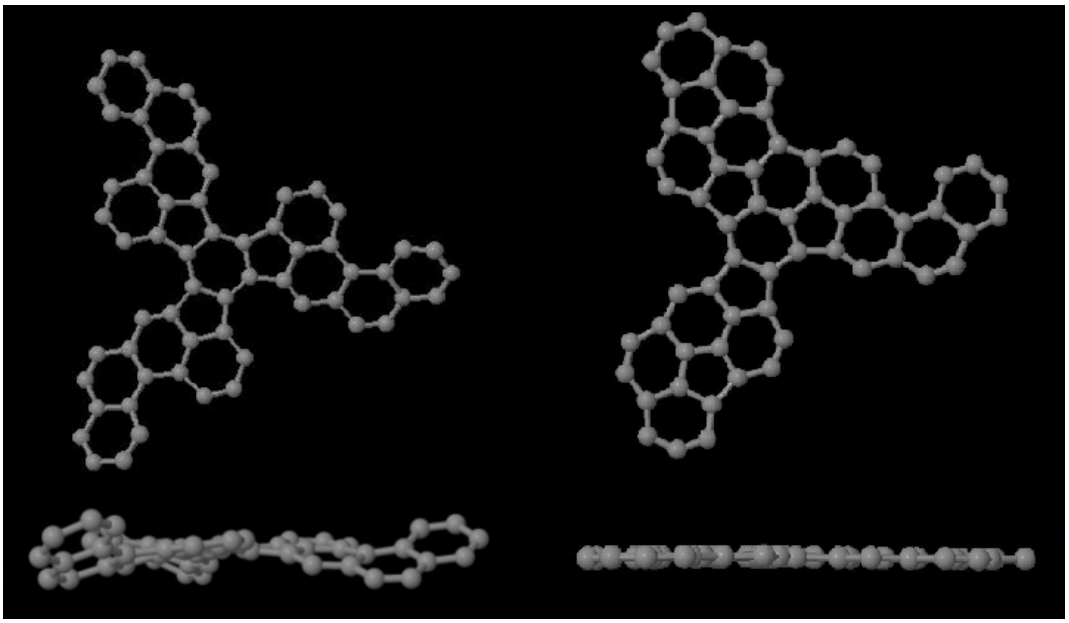

Figure 6.5: Fully dehydrogenated polyarene (*de1*). Initial (left) and final (right) configuration (frontal and side view).

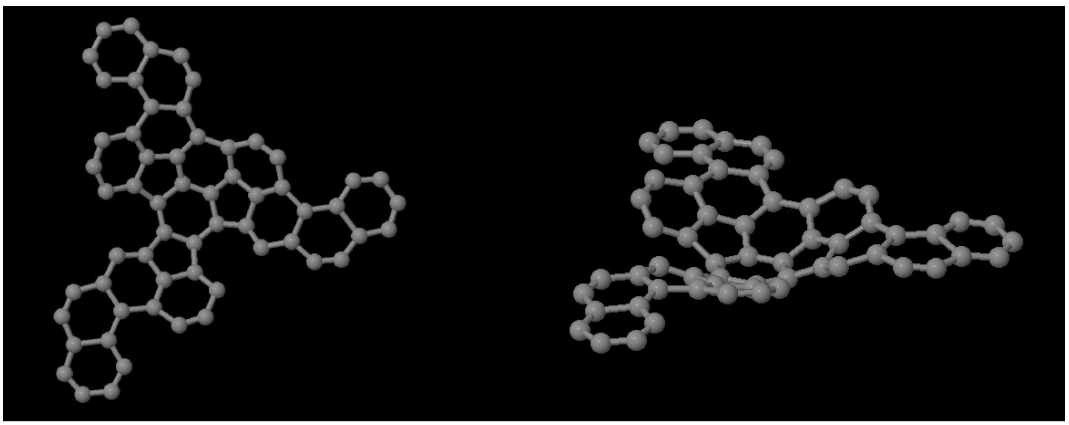

Figure 6.6: Fully dehydrogenated polyarene (*de2*) partially curved before pentagons formation

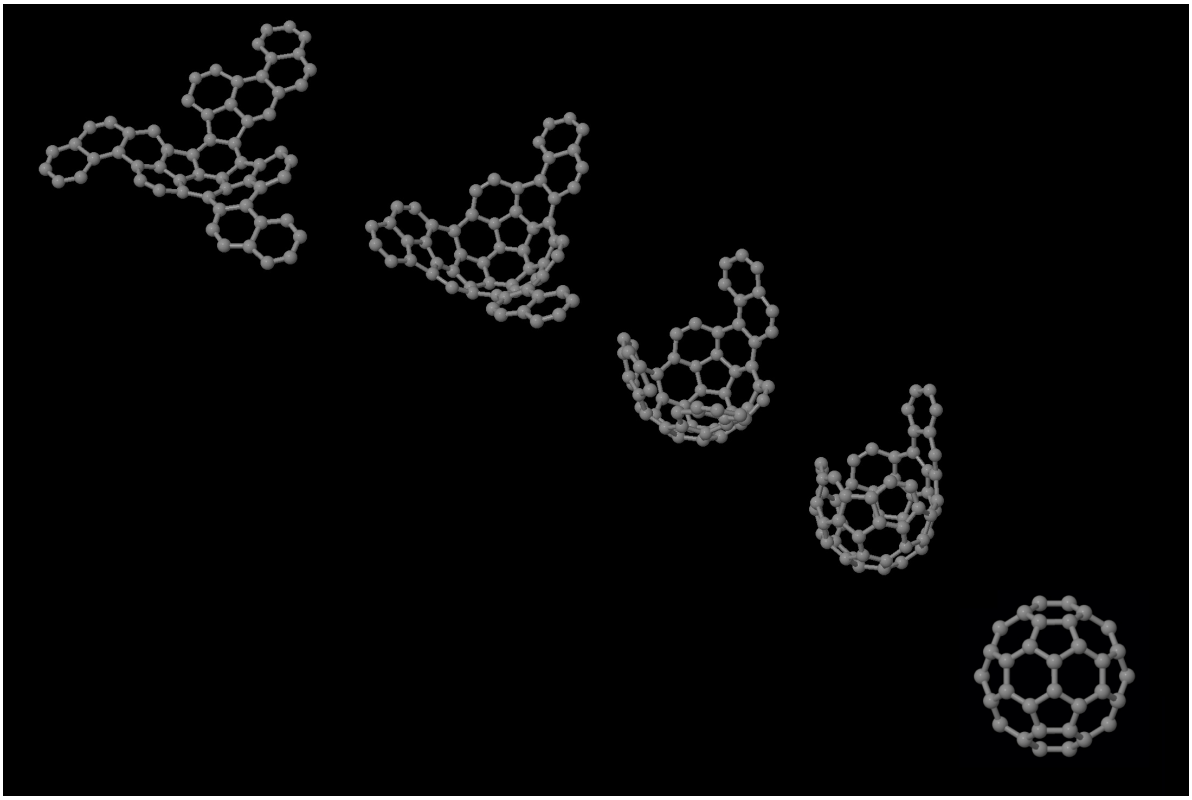

Figure 6.7: Cyclization of the fully dehydrogenated polyarene *de2* into fullerene

The process proceeds with cyclization of internal parts (*ior*) forming three corannulene like structures which, provide a significant curvature. This behavior induces the formation of pentagon through the bond formation in external parts (*eor*). Pentagons are then surrounded by almost complete corannulene like structures, which own curvatures induce the formation of the complete fullerene. No energy barriers are obtained for this process and is independent of presence of doping.

The curvature is then fundamental, occurring first internally to induce proper concavity direction in the external parts, in which pentagon formation occurs in a second stage.

Then the flat final configuration *de1* has been curved, asymmetrically in the three wings (fig. 6.8 left). In particular the concavity of the two wings with formed pentagons is opposite. After geometrical relaxation, such configuration does not converge to form fullerene. The final configuration achieved can be compared with a configuration of similar energy from cyclating *de2* (fig. 6.8); the same energy gained closing the two *eor* in *de1*, is gained in *de2* closing just the first internal bond *ior*. The bond formation in the *eor* position prevents cyclization while in the *ior* enhances it.

These results apparently contradict what obtained in Ref. [47], where the pentagon formation (*eor*) is energetically more favorable than hexagon (*ior*), and cyclization suggested occurring from external part to internal. The geometrical relaxations of *de1* configurations (flat and curved) show that the formation of two pentagons and one hexagon does not help cyclization.

Nonetheless the polyarene cyclization considered in Ref. [47], is analyzed considering independently the molecule parts with *eor* and *ior*. For this reason, conclusions on the appropriate cyclization path are misleading. Such cyclization order must be avoided, and is probably the reason of low efficiency reported in Ref. [30].

GGA GGA calculations confirm the LDA results, meanwhile some little additional barriers are encountered along the full enclosure process. As for LDA, instantaneous dehydrogenation and additional curvature to the planar converged structure, prevents the formation of the fullerene.

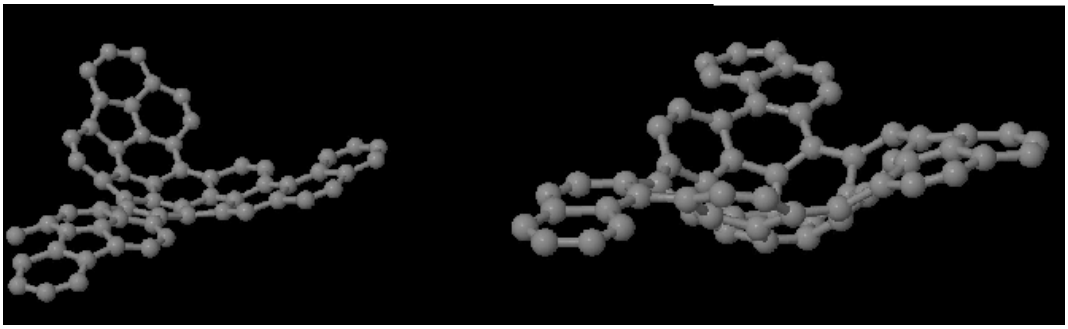

Figure 6.8: Similar energy configurations of fully dehydrogenated polyarene: artificially curved flat *de1* (left) and *de2* (right).

6.2.2 Molecular Dynamics on flat and dehydrogenated structures

Geometrical relaxation at 0 K have shown that fully dehydrogenated (hetero)polyarenes do not form fullerenes, forming instead flat hydrocarbons.

Instead, the fullerenes, and the triazafullerene, are obtained only when the concavities of the corannulene-like structures of the folding wings are analogous, and then not inversion barriers are present.

The corannulene inversion barrier is 0.46 eV[97], and therefore the bowl-to-bowl flip is rapid[98]. This fact suggests that experimental annealing temperature could be enough to change wings concavity and to form (triaza)fullerene.

To prove that the corannulene-like structures concavity is the key point to form fullerenes, molecular dynamics simulations has been performed in the canonical ensemble, at different temperatures (500 and 750 K), for both polyarene and heteropolyarene (hI and hII) from their flat fully dehydrogenated configurations (*de1*).

Molecular dynamics simulations progress almost identically in the three molecules considered: firstly the *eor* bonds close and then the remaining open *ior* (fig. 6.9). The curvature of the PAHs progresses with the wing folding, enhanced by the corannulene like structures. For t<450 femtoseconds, cyclization of heteropolyarenes is slightly faster. At 750 femtoseconds heteropolyarenes close last *ior* (fig 6.10 and 6.11), while polyarene does not. Cyclization is achieved firstly by heteropolyarenes and only later by polyarene. Enclosure from hI is slightly slower than the once coming from hII. Difference in time steps are anyway negligible as estimated in hundreds of femtoseconds.

The cyclization folding path is independent from doping, from its position in the central part of the molecule, and proceeds from central to external parts. The temperature of 500 K is already sufficient to allow the inversion barriers of the corannulene like structures to be overtaken.

6.2.3 MD at the experimental annealing temperature: formation of Stone-Wales like defect

When MD simulation temperature is increased to 750 K, during convergence, and only in the polyarene, the wing with unclosed *eor*, faces the weakening of the carbon bond between *eia* and *eooa*, with the formation of a 10 atoms ring; while in the heteropolyarenes, the *eor* closes and no defects are formed (fig 6.10 and 6.11).

Temperature becomes an important and sensitive parameter for the formation of defect-less fullerenes, because MD simulations show Stone Wales (SW) like defect in the fullerene at the experimental annealing temperature, while no defect is obtained for 500 K. In addition, if simulation is carried at 500 K until all *eor* are closed and then temperature is increased to 750 K no defect are formed. The formation of the defect is then related to the stability of the molecule itself.

The fig. 6.12 shows how the SW like defect is trapped into the fullerene cage as consequence of wrong “healing” and bonding of the 10 carbon atoms rings, which form the one pentagon and one heptagon instead of two hexagon and therefore additionally bond with a square. Generally, a SW defect form from one hexagon and one pentagon one heptagon and one square.

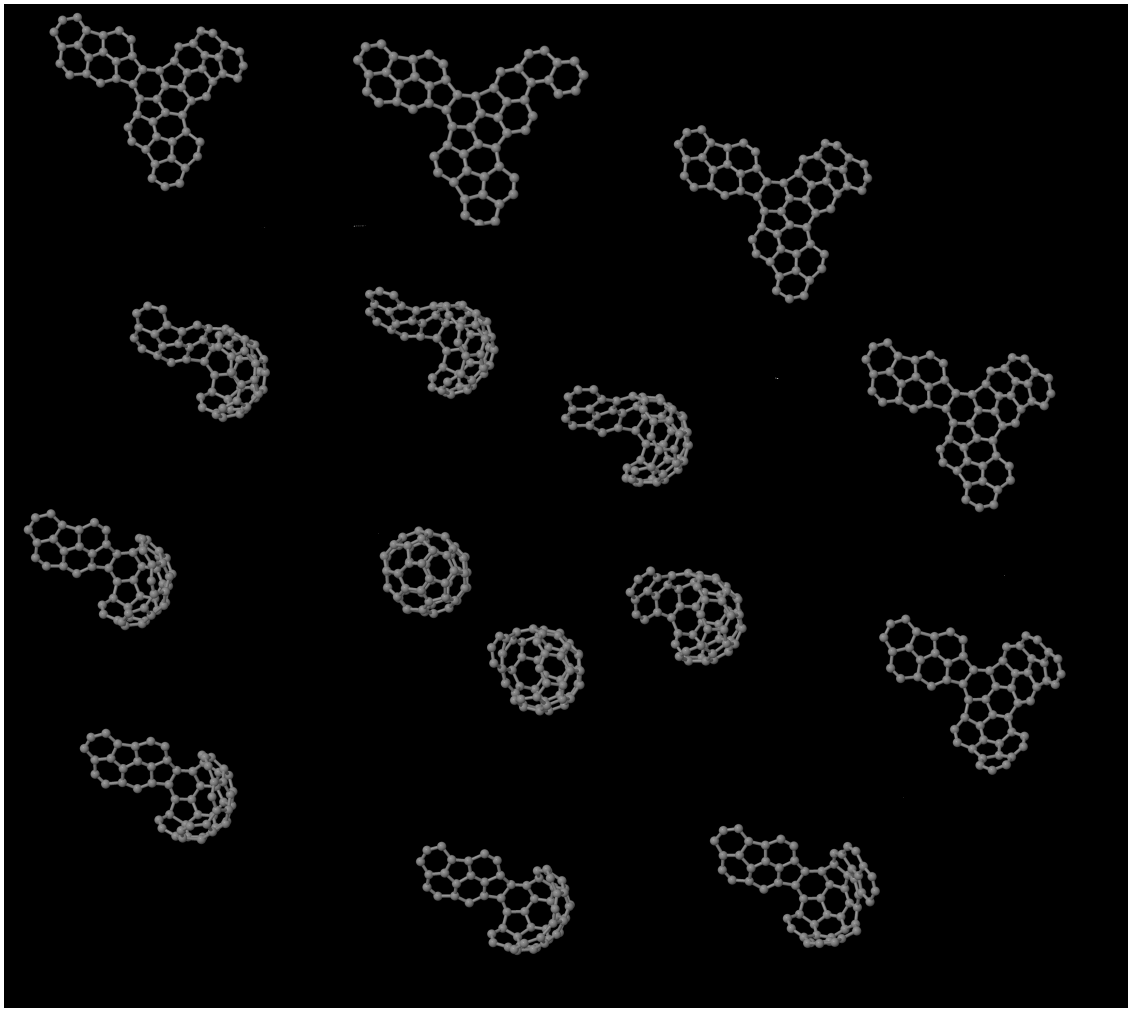

Figure 6.9: Molecular dynamics simulation for cyclization of fully dehydrogenated polyarene at 500 K.

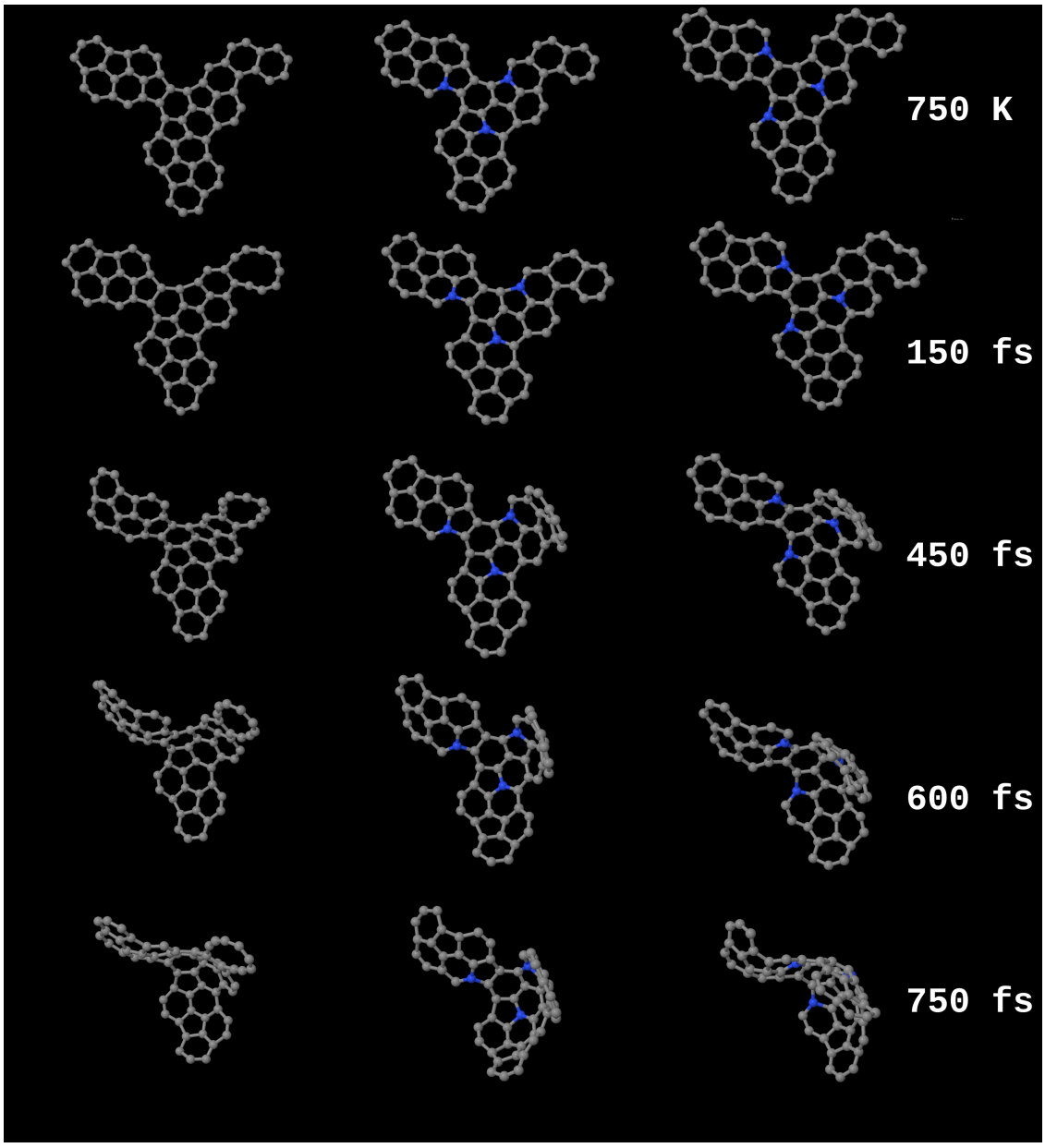

Figure 6.10: Molecular Dynamics for polyarene, heteropolyarene hI and hII at 750 K, between 0 and 750 fs

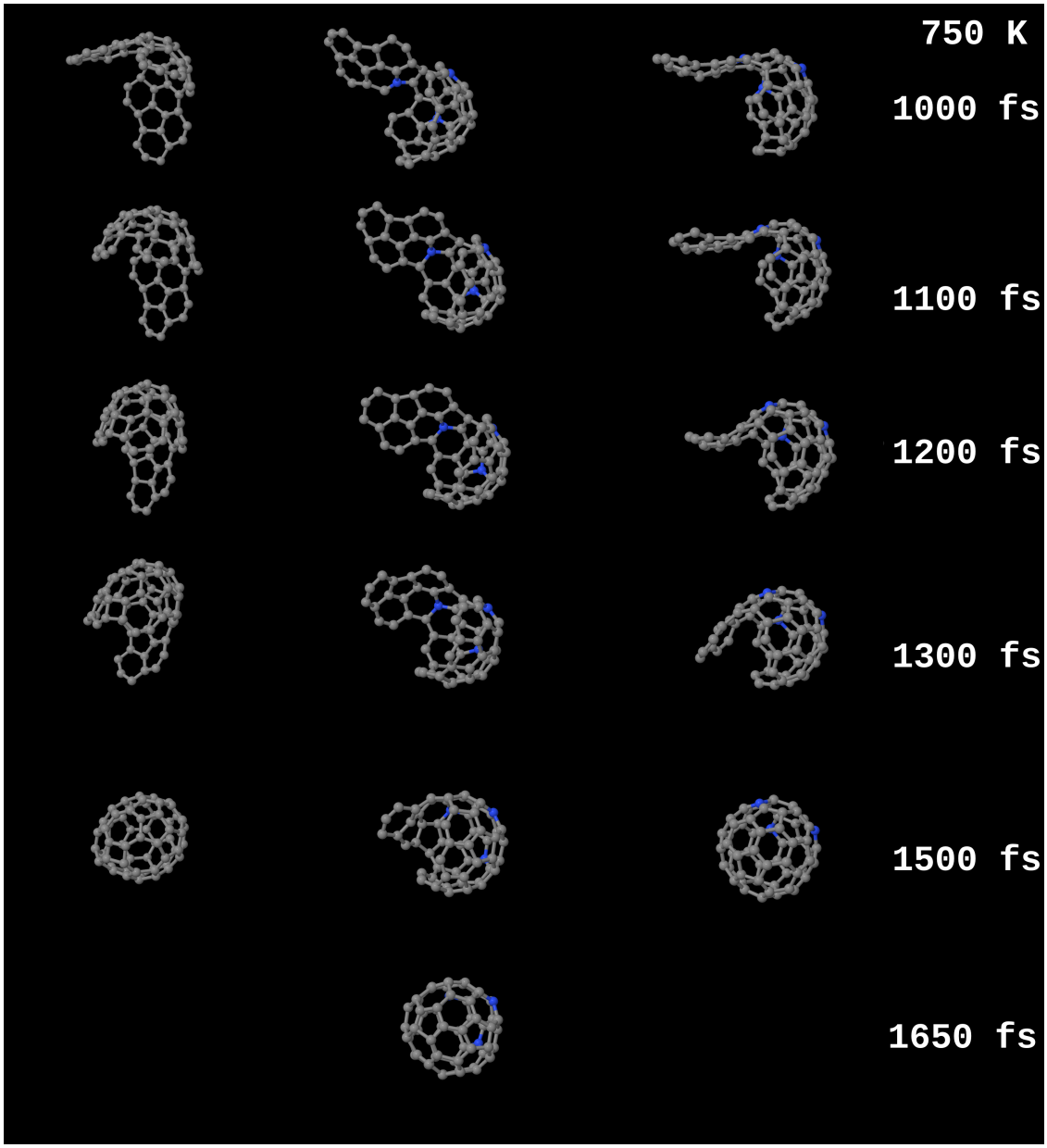

Figure 6.11: Molecular Dynamics for polyarene, heteropolyarene hI and hII at 750 K, between 1000 and 1650 fs

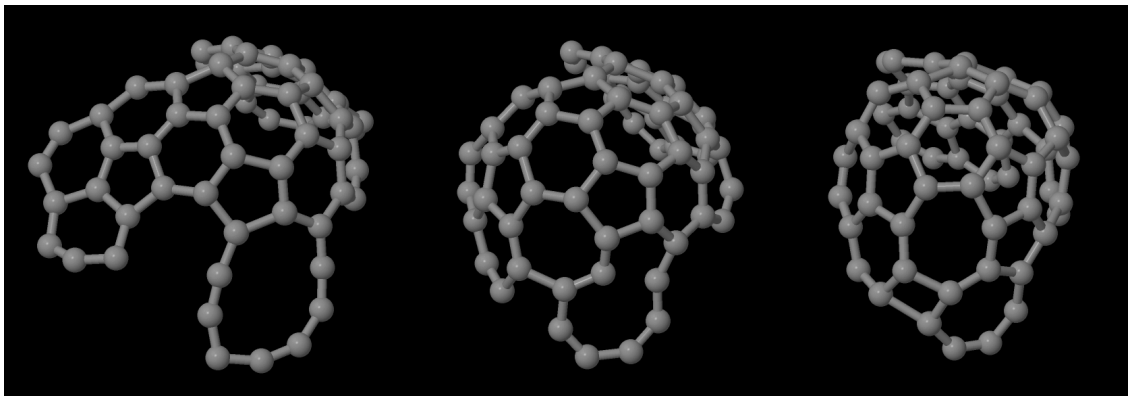

Figure 6.12: Trapping of the Stone-Wales like defect in the fullerene cage

The LDA energy difference between the fullerene and the fullerene with the SW like defect is 3.89 eV and homo-lumo gap passes from 1.79 eV to 0.60.

Doping effect on cyclodehydrogenation The MD simulations on heteropolyarene hI and hII show that cyclization proceeds with negligible time differences among them and respect to polyarene. Similar are also the folding paths. The only difference with carbon only precursor folding process is obtained at 750/800 K when the charge redistribution effect of nitrogen on first and second neighbors avoids the formation of the 10 atoms ring defect in one wing. Results obtained show that folding process is independent by doping and by its position in the molecular structure, in geometrical relaxation of partially internally curved *de2* configurations as much as in MD simulations up to 750 K.

6.2.4 NEB: quantitative estimation of the energy barriers

Self-healing Certain materials, due to lifetime or even to production procedures, can incur in micro/nano-scopic damages that cause problems to the devices/systems in which they are implemented. Subsequent growth of self-generated defects (cracks) can then cause the failure of the device. The development of a nanotechnology involving an own material property to partially (or fully) repair eventually occurring defects during device lifetime, is therefore a main issue of the frontier nanotechnology. Materials/devices that own such built-in ability to partially repair damages are called self-healing materials. They include an "active" phase to respond to the micro-damage, switching on repair mechanism. Therefore its importance is increasing, from bio-system regeneration, to the new C-based molecular nano-devices, in which self repairing could help to avoid problems of current leaks, defect formations etc, problems unfortunately common to most of Si-based technology. At micrometric scale, such behavior is known for liquid-based and solid-state healing agents (polymers), and, at nano-metric scale, such behavior can be found in some carbon rich materials[99, 100], but yet it has not been fully understood and therefore addressed to any specific carbon atom property, so that the triggers of such phenomena remain to be studied.

The simulations have shown that fully dehydrogenated molecular precursors may be object to formation of structural defects, which healing is also possible. The minimum energy path as described by the nudged elastic band (NEB), may offers a significant contribution, to evaluate the energy barriers among the configurations with and without defects and towards the formation of fullerene. This approach, implemented in the localized orbitals code Fireball allows explorations of the phase space between two known configurations and that generates the geometrical step between them.

To estimate the energy barriers, the basis set used in Fireball for the NEB method, has been tested, energetically with plane waves methods. As shown in table 6.1, the total energy differences are maintained between the four configurations in fig 6.14. These configurations represent the final (I.) and initial (II., III. and IV.) configurations of NEB calculations. The II. and III. are obtained through geometrical relaxation of dehydrogenated and differently initially curved fullerenes (the three *ior* are closed), The IV. is created breaking the bond between two hexagons in one of the to other wings and geometrically relaxed; this configurations is energetically, is the most favorable.

The NEB calculations, shown in fig. 6.15, show that in spite of the possible formation of structural defects (the merge of the two external hexagonal rings to form a 10 atoms ring has a small energy barrier, 5 meV, for the first defect) during the intermediate stages, the energy barriers leading to the final formation of a perfect fullerene (lower than 0.3 eV) can be easily overcome with the thermal energy available during the annealing.

The main energy barrier is always the first one, which value increases with the number of structural defects; the barrier configurations correspond to formation of bond in the first *eor*, which obtained concavity aids further folding. In all configurations the process proceed similarly and with full recover of the structural defect. The ability to control the last step of the process, through doping or with surface, may open possibility to inclusion of atoms or little molecules inside the cage (endohedral fullerenes). In such sense preliminary results confirm experimental findings that desired addition inside the cage are instead included in the cage if considered from beginning of the process (fig. 6.13).

The NEB barriers and convergence to appropriate minima, have been checked through geometrical relaxation of

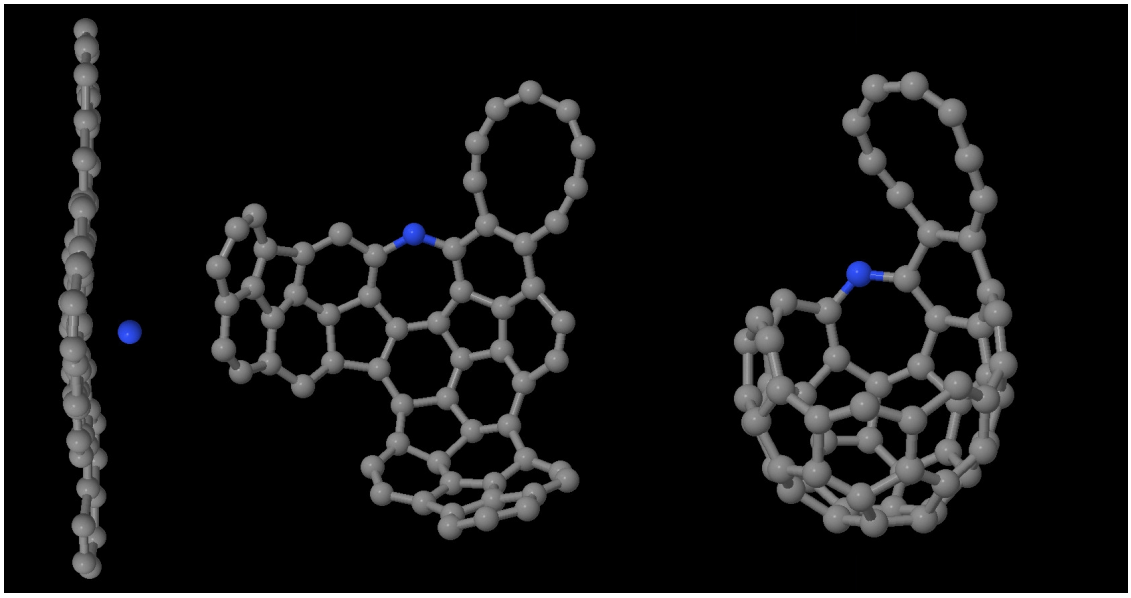

Figure 6.13: Inclusion of nitrogen in the folding dehydrogenated polyarene

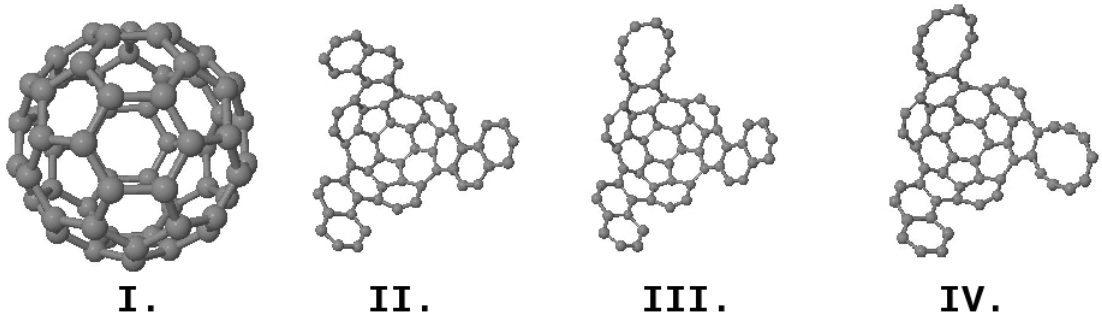

Figure 6.14: From left: fullerene, $C_{60}H_0$ with no wing defect, one and two.

near saddle point configurations. The self-healing of the structures depends directly on the reorganization of the bond in the formed half cage, their transition from one hybridization to another.

6.3 Full dehydrogenation on surface

Results in the gas phase suggest that, through aid of the temperature, the folding of the (triaza)fullerene is always possible as inversion barriers toward proper concavity of the corannulene like structures is low. The same conditions have been considered then for adsorbed molecular precursors.

$\triangle E$ (eV)		I.	II.	III.	IV.
VASP	LDA	0.00	+37.05	+38.10	+38.91
Openmx	LDA	0.00	+39.79	+40.66	+41.54

Table 6.1: Energy difference between the configurations in fig. 6.14. In parenthesis the relative energy difference.

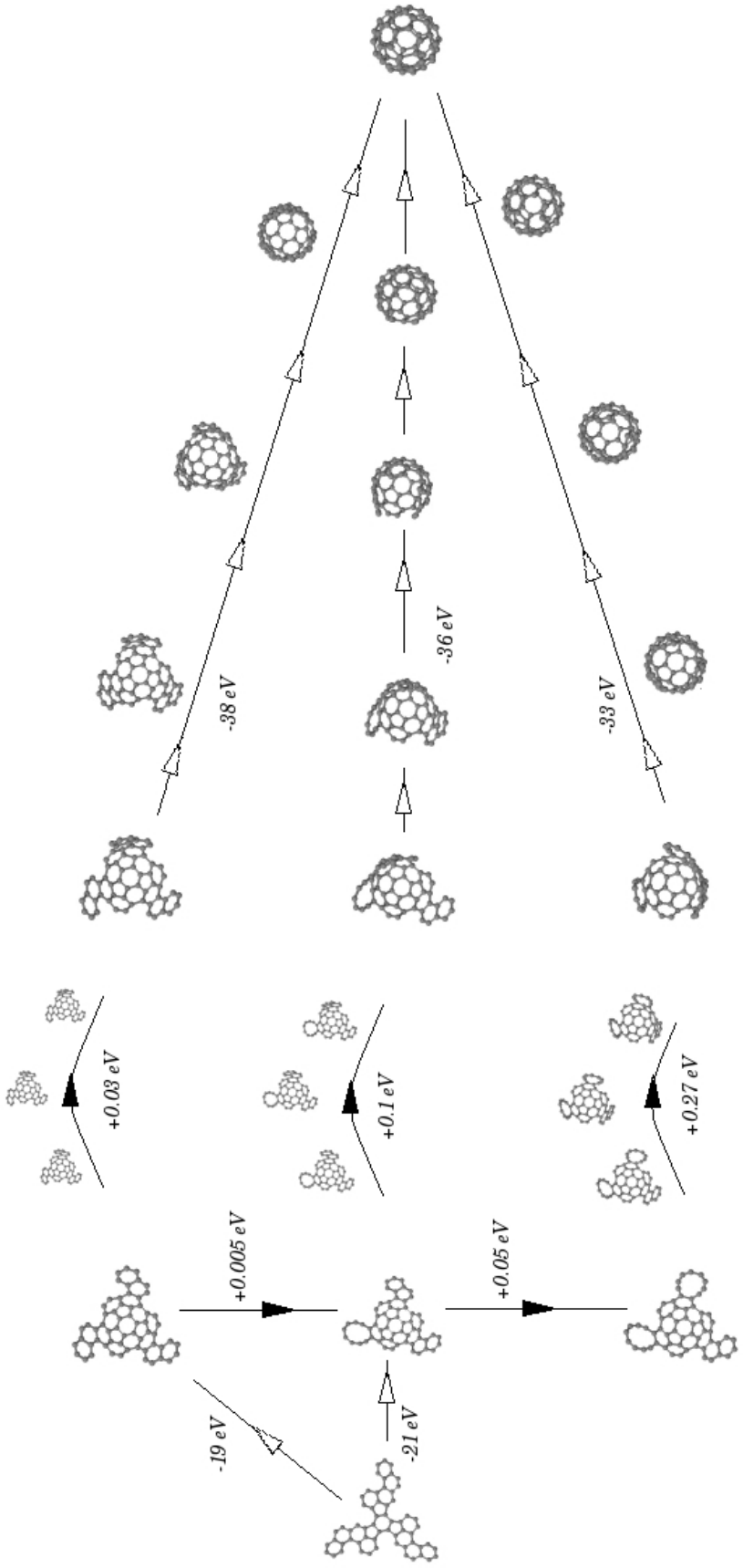

Figure 6.15: NEB calculations energy profile for polyarene to converge to fullerene.

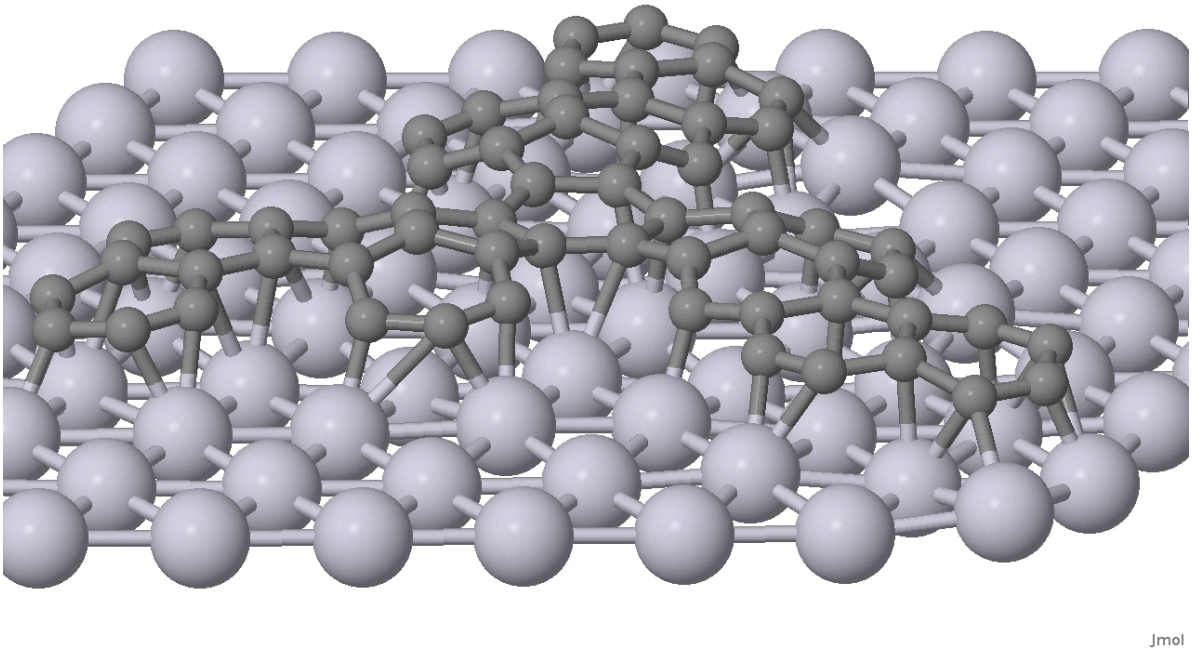

Figure 6.16: Adsorption of the fully dehydrogenated polyarene

6.3.1 Computational Approach to Large Scale Simulation on Surface

Nonetheless the cyclization on the surface may be considered itself a main computational challenge. The large systems considered for the adsorption, and the complexity of the process required further simplifications. The initial configurations considered are the ground states completely dehydrogenated, and the slab is instead reduced to only one layer, logically constrained. To validate the one layer approach, the geometrical adsorption has been calculated and compared with the adsorption on three layers. The difference in adsorbing structures are negligible. When no explicitly indicated the results shown for polyarene are to be considered valid for the heteropolyarene too.

6.3.2 Fully dehydrogenated molecule

Considering fully dehydrogenated molecule adsorption in the ground state configuration, implies that an instantaneous dehydrogenation occurred before any eventual desorption.

Both geometrical relaxation and molecular dynamics up to 1000 K show a strong C-Pt interaction and not even a partial desorption of any molecular part (fig. 6.16). These results suggest that the simultaneous dehydrogenation of adsorbate can be discarded, and formation of fullerenes considered from adsorbed precursors alternating dehydrogenation and cyclization process in order to avoid strong C-Pt interaction.

6.3.3 Partial dehydrogenation

Calculations have shown that fully dehydrogenated molecular precursor can cyclate in the gas phase with the kinetic energy contribution of the temperature to pass the inversion barriers of its folding components. Instead, on surface, the same molecule enhances its interaction with the substrate.

The following step considered, has been the cyclization of partially dehydrogenated molecular precursors, in both gas phase and on the surface. Nonetheless a partial dehydrogenation may be considered in different position,

then to restrict the possible configurations, the results of cyclization of fully dehydrogenated molecule have been considered. In the two environments, two possible initial dehydrogenated isomers are considered, labeled α and β, in which the hydrogen atoms eliminated are respectively in the *ior* (internal dehydrogenation) and in the *eor* (external dehydrogenation).

In the first case, α, the hydrogen atoms in the *ior* are eliminated from the ground state of the fully hydrogenated molecule in the gas phase.The geometrical relaxation brings to the spontaneous formation of C-C bonds in the *ior* and so of the half cage, fig. 6.17. No structural defects formation are observed as hydrogen stabilize the structure.

In the second case, β, the hydrogen atoms eliminated are in the *eor* of the ground state of the fully hydrogenated molecule in the gas phase. The geometrical relaxation is effected by the repulsive interaction between hydrogen atoms in the internal part of the molecule (*ior*) and the formation of pentagons (eor) can induce undesired concavity.

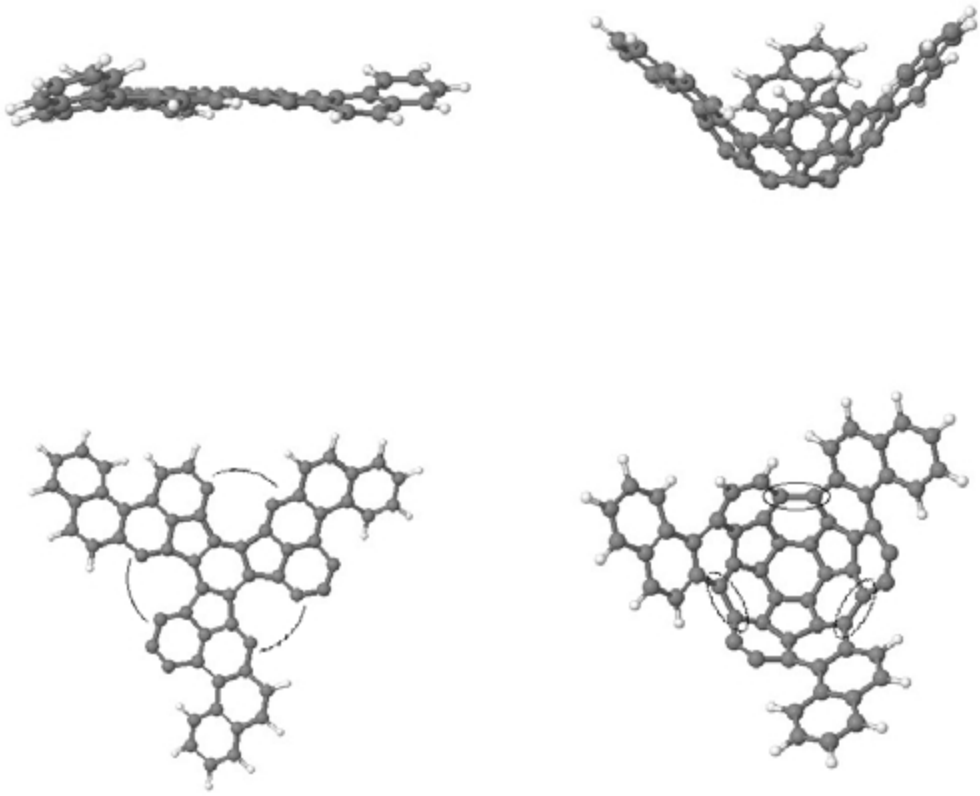

Figure 6.17: Partial dehydrogenated molecule (left) convergence to half cage (right). Side views (up) and frontal (down)

6.3.4 Surface

On the surface the approach considered the two dehydrogenated configurations α and β.

The initial configuration for the α isomer (fig. 6.18 left) is the (hetero)polyarene ground state to which three pairs of hydrogen atoms of the *ior* are eliminated. Geometrical relaxation shows no significant change in the adsorption geometry.

Similar procedure is followed for the β isomer (fig. 6.18 right): to the (hetero)polyarene ground state three pairs of hydrogen atoms are eliminated but in the *eor* positions, and the system geometrically relaxed.

No spontaneous dehydrogenation or cyclization of dehydrogenated bonds have been observed in both cases. The energy difference (0.96 eV) shows that the dehydrogenation of the α configuration is the most favorable.

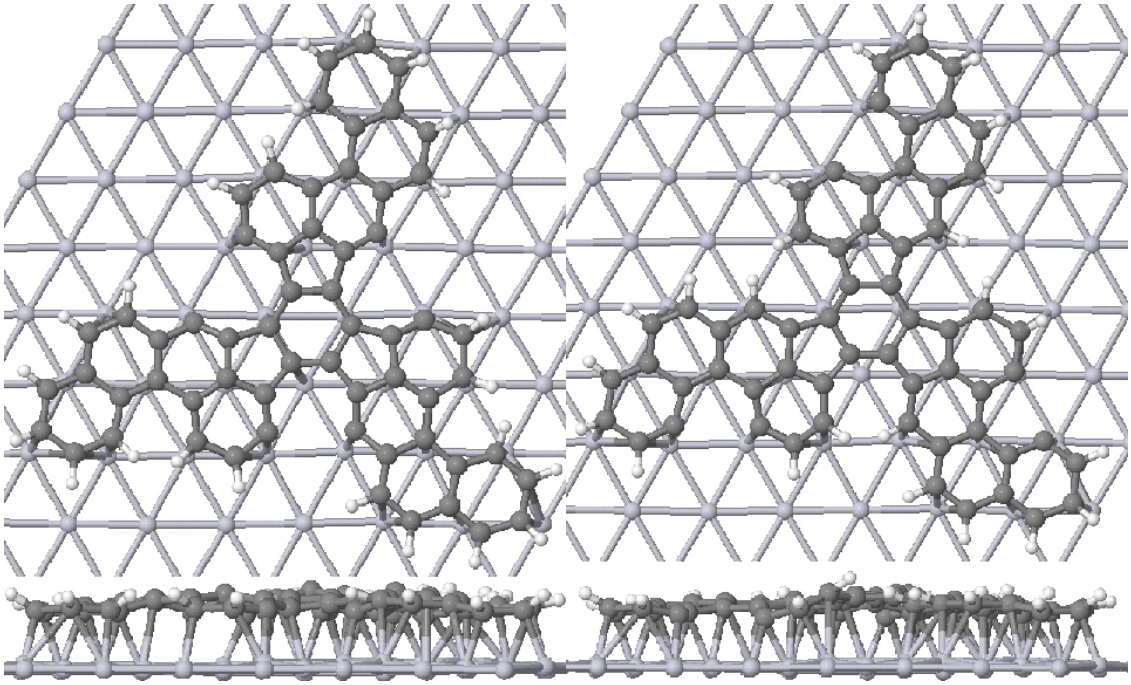

Figure 6.18: Ground state for adsorption of α (left) and β (right) polyarene.

6.3.5 Molecular dynamics of α isomer

In the gas phase and on surface, the effects of the temperature on the cyclization of the fully dehydrogenated molecular precursor, have been considered with MD simulations.

With the same idea, for the α isomer, MD simulations are carried at the experimental annealing temperature (750 K). These simulations show the bond formation between dehydrogenated atoms of *eor* labeled 13 and 32 (fig. 6.19). Along with the increase of the height on surface, their reciprocal distance decreases till the bond formation (at 2.3 Å on the surface) which generates further rise on the slab (3.0 Å).

While one dehydrogenated carbon height on surface is approximately constant ($\sim$ 2.1 Å) the other mostly varies from 1.4 to 1.8 Å and only once it is at 2.1 Å the C-C bond is formed if the carbon-carbon distance is small enough.

From graphic in fig. 6.19, it is also clear that bond formation is due to both mutual distance and height on surface. Meanwhile at proper mutual distance, an atom too low on surface would interact too strongly with the substrate, avoiding C-C bond formation.

To speed up the folding process and following geometrical relaxation behavior, the height on surface of the central part is increased artificially and the wings are moved inward. The central part increasing heights on surface for configuration different from ground state 3bri30-bri0 are in table 3.1 and 3.2.

During MD simulations bonds are formed as expected and further rise of centre observed and folding proceeds symmetric in the three wings. Temperature has also been increased up to 1000 K to fasten calculations, and in fig6.20 is shown the geometrical relaxation of a configuration obtained during MD simulations after cyclization of the three *ior* bonds.

These results allow a discrimination on the folding process of the α isomer on Pt(111). For such configuration two possible cyclization folding verses can be considered: upward and downward. In the first case the centre of the molecule is bonded with the substrate and the wings rise (flower, fig. 6.21 right), while in the second the centre rises and wings close moving on the surface toward the centre (octopus, fig. 6.21 left). The first folding way is discarded because all geometrical relaxations studied, show that the molecule centre tends to increase its height on the surface and because the kinetic energy necessary for the three wings to desorb and fold is high.

Complete dehydrogenation of one wing and then

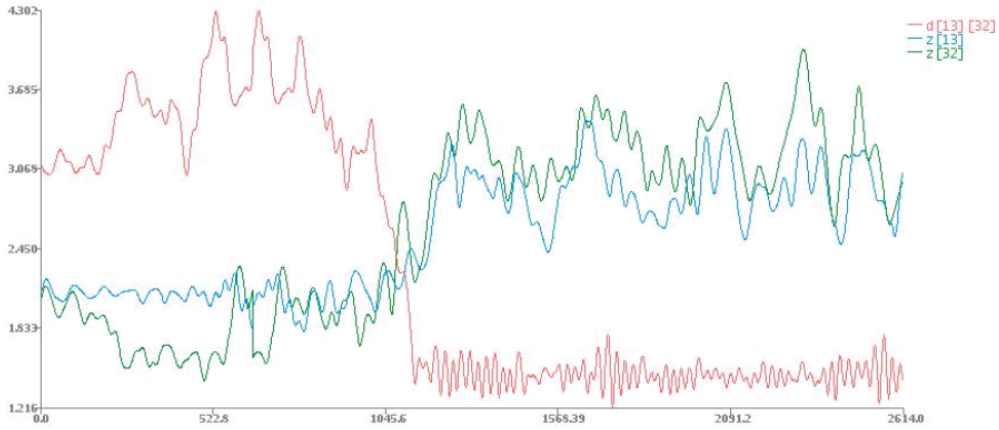

Figure 6.19: Bond formation in polyarene dehydrogenated carbon atoms

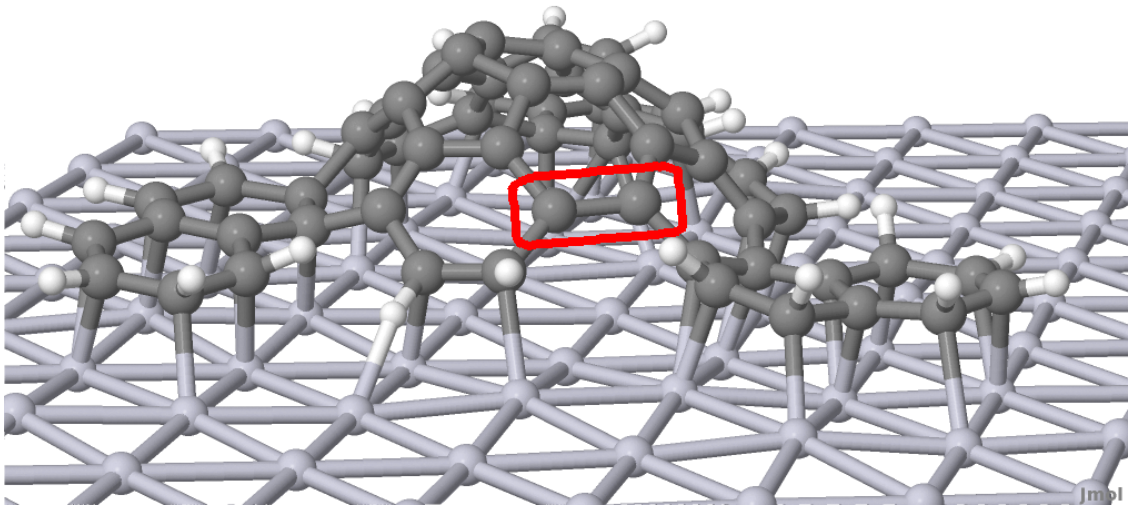

Figure 6.20: Molecular dynamics simulations of α configuration at 800 K. In the rectangle the closed bond in *ior* position.

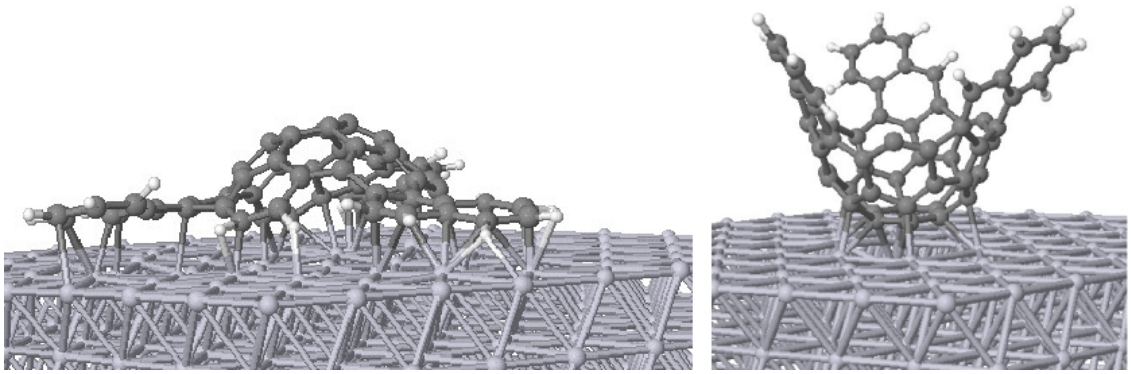

Figure 6.21: The two different folding process, octopus (left) and flower (right)

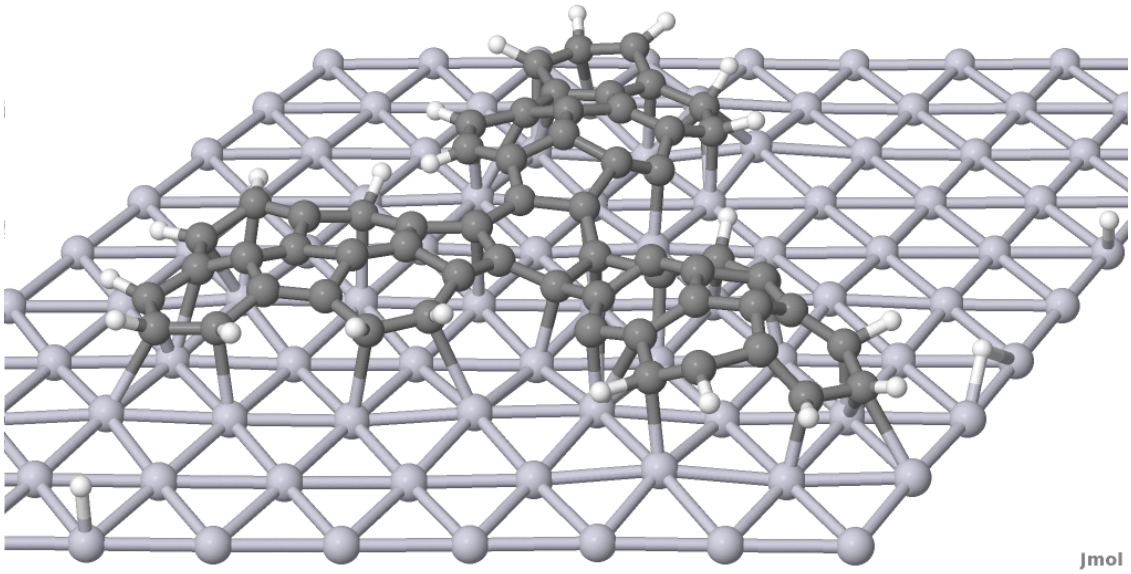

Figure 6.22: Molecular dynamics simulations of β configuration at 800 K.

The idea that cyclization may proceed symmetrically from internal part of a polycyclic aromatic hydrocarbon adsorbed on transition metal surface has also been observed in, at least, another system[53].

Molecular dynamics of β isomer When MD simulations are similarly carried on the β configuration, the formation of bond in the *eor* is obtained. The formation of pentagons induce a small curvature in all wings and a decrease on the central part of the molecule.

It is also obtained a spontaneous dehydrogenation of the carbon atom of the central part (*ior*), exactly those atoms that has been removed in the α configuration. These results provide an indirect confirmation that dehydrogenation on surface occurs from internal parts. Hydrogen atoms may then contribute to increase dehydrogenation through diffusion on Pt(111)

6.3.6 Further evolution of the α molecule

The study of cyclization of the α configuration, proceed with progressively dehydrogenated configurations. Each is obtained as follow: a molecule with a certain dehydrogenation is geometrically relaxed, MD calculations are done on such configuration and then one of the simulations step is geometrically relaxed. To such configuration, eventually, a certain number of hydrogen atoms is eliminated and the structure adjusted, if necessary, to increase its height and to move the wing inward; then this new structure is geometrically relaxed. The overall process of alternated dehydrogenation, geometrical relaxation, molecular dynamics in various configurations, show that molecule is progressively closing with rise of central part, that "drags" inward the wings so that they can cyclate (fig. 6.23)

6.3.6.1 Symmetric vs asymmetric folding

The symmetric folding from internal part to external, symmetrically in the three wings, shows that hydrogenation in external parts (*eooa* hexagons) is necessary to reduce C-Pt interaction so that central part can drag the wing breaking less energetic C-Pt bonds, making the surface more "slippery".

Instead the asymmetric folding must be discarded, because no further folding is obtained when two wings merge to form one curve part, excluding the third wing and the central part (fig. 6.24). Furthering MD up to 1200K, increasing

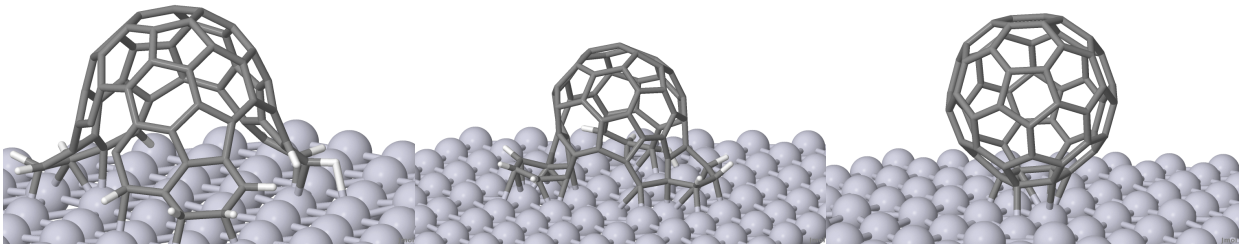

Figure 6.23: Perspective view of MD simulations steps for $C_{60}H_{12}$, $C_{60}H_9$ and $C_{60}H_0$.

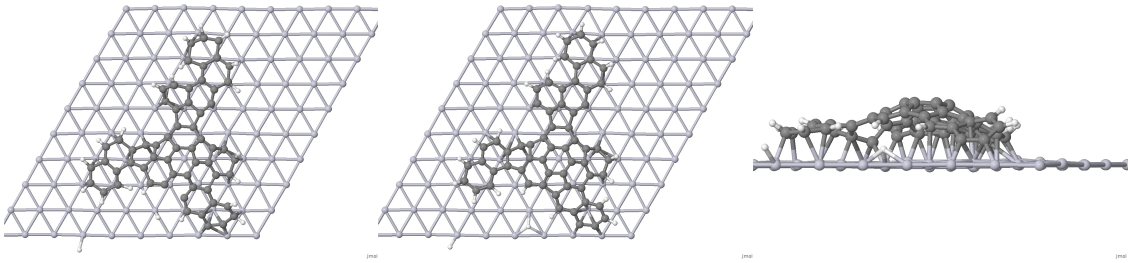

Figure 6.24: Asymmetric folding initial configuration (left) and final configuration upper (center) and side view (right)

dehydrogenation and also artificially increasing height of central part (fig. 6.25), no folding is obtained. This occur because along with inversion barriers, to decrease the C-C distances between the merged wings and the third one , a partial desorption is required, while C-H bonds should be broken in appropriate order to avoid increase of C-Pt interaction that strengthen the interaction with the substrate.

6.3.7 Cyclization and desorption

Along all this study, it has been shown that the interaction between molecule and substrate is important for anchoring the molecule to the substrate. Nonetheless, the experiments do not clarify if the molecules are desorbed during cyclization. In this last part such possibility is considered. If the molecule desorbes, at any stage, its cyclization would then resemble, structurally, the configurations obtained in the gas phase (section 6.2). Two configurations have been geometrically relaxed near the surface, in their gas phase geometry. These molecules tend to re-adsorb in configuration similar to their analogous obtained through progressive folding (fig. 6.26 and 6.27).

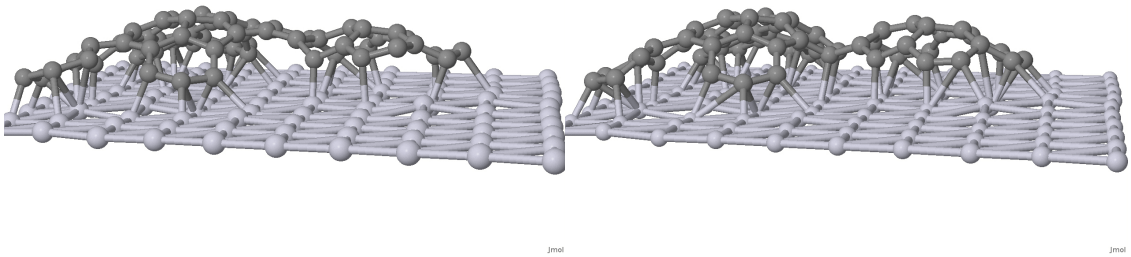

Figure 6.25: $C_{60}H_0$ in initial (left) and final (right) configurations.

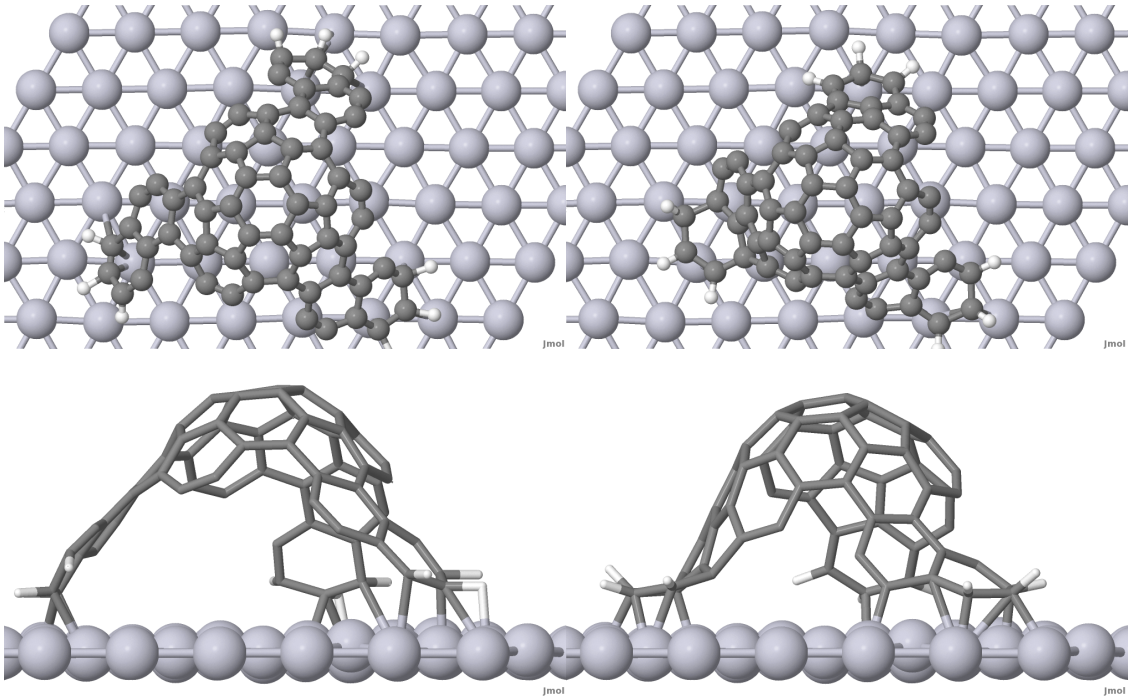

Figure 6.26: Initial and final configuration for $\alpha C_{60}H_9$ their side view (second line)

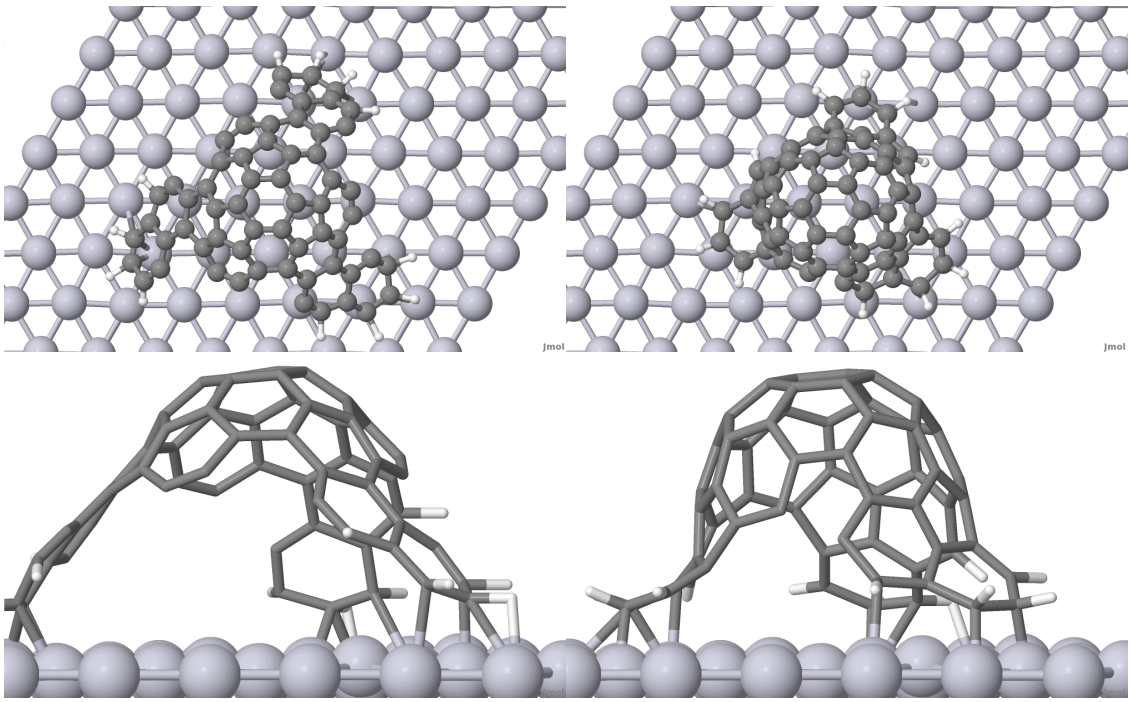

Figure 6.27: Initial and final configuration for $\alpha C_{60}H_{12}$ their side view (second line)

6.4 Conclusions

The cyclization of molecular precursors of fullerene and triazafullerene, has been analyzed here, in gas phase and on surface, at different stages of dehydrogenation.

In the gas phase, the cyclization of a fully dehydrogenated molecule depends on the curvature of the folding wings and therefore on their inversion barriers. MD simulations show that temperature helps to provide the required kinetic energy to pass the inversion barriers, but it may generates undesired defects. The overall cyclization process in the gas phase is not effected by nitrogen doping of considered heteropolyarene, but its folding via MD simulation does not present any structural defect. NEB calculations have shown the energy barriers required to the effective formation of fullerene and, along with them, that the formation of structural defect is self healed. On the surface, cyclization from fully dehydrogenated molecule is not obtained for the stronger C-Pt bonding.

When partial dehydrogenated molecule folding is considered, in both gas phase and on the surface, different dehydrogenated configurations show that cyclization (and then dehydrogenation) may occur closing progressively the bonds from internal part to the more external. On surface the hydrogenation of external part of the wing is also necessary to decrease C-Pt interaction and allow the inward movements that allow cyclization. Nonetheless only through the strong substrate molecule interaction is possible to obtain a progressive hydrogenation and cyclization without desorption. Doping and (de)hydrogenation are therefore important characteristics to be considered case by case in order to evaluate possible extension of the process to other systems.

Chapter 7

Conclusions

The efficient and controllable synthesis of (triaza)fullerene on Pt(111) have been discussed in this thesis in its three fundamental steps 1) the adsorption of molecular precursors, 2) the adsorption of the fullerene and triazafullerene obtained after experimental annealing on the same surface and 3) the cyclodehydrogenation process. The most important results and the future developments are here resumed.

Adsorption and Enantioselectivity of (hetero)fullerene molecular precursors The adsorption of fullerene and triazafullerene molecular precursors have been discussed both structurally and electronically. The two molecules, independently by presence of doping and hydrogenation in the central part (heteropolyarene) adsorb similarly and enantioselective respect to their adsorption side upon deposition. The adsorption is guided by the molecule external parts which behave like benzene. Theoretical results are in good agreement with experimental findings both structurally and electronically. For heteropolyarene, the electronic differences obtained between experimental and theoretical methods are consequence of dehydrogenation.

The enantiomeric selectivity observed is strictly connected to the surface (111) morphology and atomic distances, therefore it is expected to find enantiomeric adsorption of polyarene on Pd(111), which electronic and structural characteristics are similar to Pt(111), as much as similar is the benzene adsorption. Different adsorption is expected on other surfaces, like Cu(111) and Au(111) which lattice constants are either too small ($\alpha_{Cu} = 3.61$Å) or too large ($\alpha_{Au} = 4.08$Å), apart than being electronically less reactive. Furthermore both adsorption and enantioselectivity are connected to benzene moieties which interaction with substrate is almost identical on Pt and Pd, and radically different on Cu, Au and Ag. Theoretical findings suggest that similar behavior may be obtained in ad-hoc experiments on similar metallic surfaces for geometrical and electronic similarities, Pd ($\alpha_{Pd} = 3.90$ Å) and maybe Ir ($\alpha_{Ir} = 3.84$ Å) and exclude other metals such as Rh ($\alpha_{Rh} = 3.80$ Å) and Ag ($\alpha_{Ag} = 4.08$ Å). On other surfaces, eg Pt(110) or Pt(001), enantioselectivity of polyarene could still depends on specific benzene adsorption. Preliminary experiment carried on Cu(111) and Au(111) confirm theoretical predictions: the molecular diffusivity at RT is generally high and no STM images of adsorbed polyarene obtained. Depending on benzene adsorption other enantioselectivity angle could be a a priori defined on different surface geometries.

Fullerene and triazafullerene adsorption on Pt(111) Fullerene adsorption on Pt(111) has been extensively discussed on clean surface and with formation of surface vacancies in different positions and orientations. Good agreement with experimental findings is achieved in the description of the formation of domain with the increase of coverage and temperature. Lower adsorption height in hexagonal orientation is explained as consequence of vacancy formation in the surface. In small unit cell, mutual admolecule interaction energy is relevant. Triazafullerene adsorption has been analyzed for configurations similar to fullerene and main difference obtained is that it tends to rotate in order to bond one of the nitrogen with the substrate, in good agreement with experiments.

Deeper insight on the adsorption mechanism and charge transfer between N-doped fullerene in different coverage

conditions on different metallic substrate, with different functionals represents the next step of this part of the study. Fullerene and, especially, triazafullerene adsorption are of extreme interest for microelectronics, therefore the study of their conductivity properties at various condition is an essential step.

Cyclodehydrogenation The cyclodehydrogenation process of polycyclic aromatic hydrocarbons has been shown in both gas phase and on Pt(111). In the gas phase, the cyclization is strictly related to formation of corannulene like structures with proper curvature, which the inversion barriers can be easily passed at experimental temperature in the gas phase. Formation and self-heal of structural defects in the hexagonal structure is also observed. Cyclization is independent from doping, while formation of defect is avoided in the doped heteropolyarene.

On the surface cyclodehydrogenation proceeds symmetrically in the three wings from internal part to external, avoiding complete dehydrogenation and even dehydrogenation of surface interacting parts. The process is independent from doping that is localed in the the first to rise part of molecule.

In general, cyclodehydrogenation has shown a significant potential to form carbon nanostructures and always through catalytic effect of highly reactive metallic surfaces, Ru(0001)[53], Pt(111)[85], suggested on Pt(111)[94] and for larger fullerenes[101] etc[102]. Its extensibility to other systems and with other doping is then possible on surface as much as in gas phase through modulation of dehydrogenation barriers via doping.

Conclusiones

La síntesis, eficiente y controlable, de (triaza) fullerenos sobre Pt (111) ha sido discutida en esta tesis en sus tres pasos fundamentales 1) la adsorción de los precursores moleculares, 2) la adsorción del fullereno y triazafullerenos obtenidos después del annealing experimental y 3) el proceso cylodeshidrogenacion. Los resultados más importantes y la evolución futura se resumen aquí.

Adsorción y Enantioselectividad de precursores moleculares de (hetero)fullerenos La adsorción de los precursores moleculares de fullereno y triazafullerenos se han discutido tanto estructuralmente como electrónicamente. Las dos moléculas, de forma independiente del dopaje y de la hidrogenación en la parte central (heteropoliarene) adsorben de manera similar y enantioselectivamente con respecto a su lado de adsorción en deposición. La adsorción ocurre por las partes externas de la molécula, que se comportan como bencenos. Los resultados teóricos están en buen acuerdo con los resultados experimentales tanto estructuralmente como eletronicamente. Para el heteropoliarene, las diferencias obtenidas entre los métodos electrónicos experimentales y teóricos son consecuencia de la deshidrogenación.

La selectividad enantiomérica observada, es estrictamente vinculada a la superficie (111), sus distancias morfología y interatómica, por lo que se espera encontrar la adsorción enantomerica de poliarene sobre Pd (111), cuyas características electrónicas y estructurales son similares a Pt (111), tanto como similar es la adsorción de benceno. Adsorción que será diferente en otras superficies, como Cu (111) y Au (111), cuya constantes de red son demasiado pequeña ($\alpha_{Cu} = 3.61$Å) o demasiado grande ($\alpha_{Au} = 4.08$Å), además de ser electrónicamente menos reactivas. Por otra parte, tanto la adsorción y enantioselectividad están conectadas al benceno, desde luego la interacción con el sustrato es casi idéntico sobre Pt y Pd, y radicalmente diferente en Cu, Au y Ag. Resultados teóricos sugieren que el comportamiento similar puede obtenerse en experimentos similares en las superficies metálicas con similitudes geométricas y electrónicas, Pd ($\alpha_{Pd} = 3.90$ Å) y tal vez Ir ($\alpha_{Ir} = 3.84$ Å), y excluyen a otros metales como Rh ($\alpha_{Rh} = 3.80$ Å) and Ag ($\alpha_{Ag} = 4.08$ Å) En otras superficies, por ejemplo, Pt (110) o Pt (001), enantioselectividad de polyarene podría depender de la adsorción de benceno. Experimentos preliminares realizado en Cu (111) y Au (111) confirman las predicciones teóricas: la difusividad molecular a temperatura ambiente es generalmente alta y no se obtuvieron las imágenes de STM de polyarene adsorbido. Dependiendo del benceno, el ángulo de enantioselectividad de adsorción podría ser definida en la superficie de geometrías diferentes.

Fullereno y adsorción triazafullerene sobre Pt (111) La adsorción de fullereno sobre Pt (111) ha sido ampliamente discutida en la superficie limpia y con la formación de vacantes superficiales en diferentes posiciones y orientaciones, y obtenido un buen acuerdo con los resultados experimentales en la descripción de la formación de dominio con el aumento de la cobertura y la temperatura. La bajada de altura de la adsorción en la orientación hexagonal se explica como consecuencia de la formación de vacantes en la superficie. En la celda unidad mas pequeña, la energía de interacción mutua entre moleculas es relevante. La adsorción de triazafullerenos ha sido analizada para configuraciones similares a las del fullereno y la principale diferencia obtenida es que tiende a rotar con el fin que se forme un enlace del nitrógeno con el sustrato, en buen acuerdo con los experimentos.

Una visión más profunda sobre el mecanismo de adsorción y de transferencia de carga entre fullereno N-dopados en condiciones de cobertura diferentes de sustrato metálico diferentes, con diferentes funcionales rapresentan el sigu-

iente paso de esta parte del estudio. Fullereno y, especialmente, la adsorción triazafullerenos son de sumo interés para la microelectrónica, por lo tanto el estudio de sus propiedades de conductividad a varias condiciones es un paso esencial.

Cyclodehydrogenation El proceso de cyclodehydrogenation de hidrocarburos aromáticos policíclicos se ha demostrado, tanto en fase gas y sobre Pt (111). En la fase gaseosa, la ciclación es estrictamente relacionada con la formación de corannulene como la estructura con la curvatura adecuada, cuya barreras de inversión puede ser superada fácilmente a las temperaturas experimentales en la fase gaseosa. Se observa tambien la formación y el cierre de defectos estructurales en la estructura hexagonal. La ciclación es independiente de dopaje, mientras que la formación de defecto se evita en el heteropoliarene.

En la superficie la ciclodeshidrogenacion es simétrica en las tres alas desde la parte interna a las externas, evitando la deshidrogenación completa e incluso en su partes externas . El proceso es independiente del dopaje y de sus posicion en el interior de la molecula.

En general, se ha demostradoque la ciclodeshidrogenacion tiene un importante potencial para formar nanoestructuras de carbono y siempre a través de efecto catalizador de las superficies metálicas altamente reactivas, como Ru (0001)[53], Pt (111)[85], y se sugirió sobre Pt (111)[94] y para las grandes fullerenos[101, 102]. Su extensibilidad a otros sistemas y otros dopaje es entonces posible en la superficie tanto como en la fase gas, a través de la modulación de las barreras de deshidrogenación con el dopaje.

Bibliography

[1] H. W. Kroto, J. R. Heath, S. C. O Brien, R. F. Curl, and R. E. Smalley. C60: Buckminsterfullerene. *Nature*, 318:162, 1985.

[2] Ting Guo, Changming Jin, and R. E. Smalley. Doping bucky: formation and properties of boron-doped buckminsterfullerene. *Journal of Physical Chemistry*, 95 (13):4948–4950, 1991.

[3] T. Pradeep, V. Vijayakrishnan, A. K. Santra, and C. N. R. Rao. Interaction of nitrogen with fullerenes: nitrogen derivatives of c60 and c70. *Journal of Physical Chemistry*, 95 (26):10564–10565, 1991.

[4] Noriyuki Kurita, Kinya Kobayashi, Hiroki Kumahora, Kazutami Tago, and Kunio Ozawa. Molecular structures, binding energies and electronic properties of dopyballs c59x (x=b, n and s). *Chemical Physics Letters*, 198 (1-2):95–98, 1992.

[5] Han Ru-Shan Liu Jing-Nan, Gu Bing-Lin. Electronic structures of doped fullerenes with boron and nitrogen atoms. *Solid State Communications*, 84 (8):807–810, 1992.

[6] Yan Chai, Ting Guo, Changming Jin, Robert E. Haufler, L. P. Felipe Chibante, Jan Fure, Lihong Wang, J. Michael Alford, and Richard E. Smalley. Fullerenes with metals inside. *Journal of Physical Chemistry*, 95 (20):7564–7568, 1991.

[7] Stephen W. McElvany. Production of endohedral yttrium-fullerene cations by direct laser vaporization. *Journal of Physical Chemistry*, 96 (12):4935–4937, 1992.

[8] D. S. Bethune, R. D. Johnson, M. S. de Vries J. R. Salem, and C. S. Yannoni. Atoms in carbon cages: the structure and properties of endohedral fullerenes. *Nature*, 366:123–128, 1993.

[9] F. D. Weiss, J. L. Elkind, S. C. O'Brien, R. F. Curl, and R. E. Smalley. Photophysics of metal complexes of spheroidal carbon shells. *Journal of American Chemical Society*, 110 (13):4464–4465, 1988.

[10] L. M. Roth, Y. Huang, J. T. Schwedler, C. J. Cassady, B. Kahr D. Ben-Amotz, and B. S. Freiser. Evidence for an externally bound iron buckminsterfullerene complex, fec60, in the gas phase. *Journal of American Chemical Society*, 113 (16):6298–6299, 1991.

[11] Johannes Averdung, Heinrich Luftmann, Ingo Schlachter, and Jochen Mattay. Aza-dihydro[60]fullerene in the gas phase. a mass-spectrometric and quantumchemical study. *Tetrahedron*, 51:6977–6982, 1995.

[12] A. Huczko. Heterohedral fullerenes and nanotubes: Formation and characteristics. *Fullerene Science Technology*, 5 (6):1091 – 1131, 1997.

[13] Majid Keshavarz-K, Rosario Gonzalez, Robin G. Hicks, Gordana Srdanov, Vojislav I. Srdanov, Tasha G. Collins, Jan Cornelis Hummelen, Cheryl Bellavia-Lund, James Pavlovich, and Fred Wudl. Synthesis of hydroazafullerene c59hn, the parent hydroheterofullerene. *Nature*, 383:147–150, 1996.

[14] Iris Lamparth, Berthold Nuber, Georg Schick, Andreas Skiebe, and Thomas Grosser and. Andreas Hirsch. C59n and c69n: Isoelectronic heteroanalogues of c60 and c70. *Angewandte Chemie International Edition in English*, 3:2257–2259, 1995.

[15] Hummelen J. C., Knight B., Pavlovich J., Gonzalez R., and Wudl F. Isolation of the heterofullerene c59n as its dimer (c59n)2. *Science*, 269:1554, 1995.

[16] Berthold Nuber and Andreas Hirsch. A new route to nitrogen heterofullerenes and the first synthesis of (c69n)2. *Chemical Communications*, 12:1421–1422, 1996.

[17] Berthold Nuber. Facile synthesis of arylated heterofullerenes arc59n. *Chemical Communications*, 3:405–406, 1998.

[18] Cheryl Bellavia-Lund, Rosario Gonzalez, Jan Cornelis Hummelen, Robin G. Hicks, Angela Sastre, and Fred Wudl. Synthesis of c59(chph2)n from (c59n)2 and c59hn. the first derivatization of c59n. *Journal of American Chemical Society*, 119 (12):2946–1947, 1997.

[19] Francois Gygi Wanda Andreoni and Michele Parrinello. Impurity states in doped fullerenes: C59b and c59n. *Chemical Physics Letters*, 190 (3-4):159–162, 1992.

[20] Feng Chen, David Singh, and Susan A. Jansen. Electronic effects in metal complexation of fullerenes c60, c59n, and c59b. *Journal of Physical Chemistry*, 97 (42):10958–10963, 1993.

[21] Jinming Dong, Jie Jiang, Z. D. Wang, and D. Y. Xing. Structural and electronic properties of c59x (x=b,n): The extended su-schrieffer-heeger model. *Physical Review B*, 51 (3):1977–1980, 1995.

[22] Jinming Dong, Jie Jiang, J. Yu, Z. D. Wang, and D. Y. Xing. Nonlinear optical properties of the substituted fullerenes c59x (x=b,n). *Physical Review B*, 52 (12):9066–9070, 1995.

[23] Qiang Xu, Jie Jiang, Jinming Dong, and D. Y. Xing. Linear optical properties of the dopyballs c60-nxn (x = b or n; n = 1, 2). *Physica Status Solidi B*, 193 (1):205–212, 1996.

[24] D. Y. Xing Jie Jiang, Jinming Dong. Exciton effects on the optical properties of the substituted fullerenes c59x (x = b, n). *Solid State Communications*, 107 (7):537–540, 1997.

[25] S. Stafstrom, L. Hultman, and N. Hellgrenb. Predicted stability of a new aza[60]fullerene molecule, c48n12. *Chemical Physics Letters*, 340 (3-4):227–231, 2001.

[26] G. A. J. Amaratunga, M. Chhowalla, C. J. Kiely, I. Alexandrou, R. Aharonov, and R. M. Devenish. Hard elastic carbon thin films from linking of carbon nanoparticles. *Nature*, 383:321–323, 1996.

[27] N. Sano, H. Wang, M. Chhowalla, I. Alexandrou, and G. A. J. Amaratunga. Nanotechnology: Synthesis of carbon 'onions' in water. *Nature*, 414:506–507, 2001.

[28] Kratschmer and Huffman. *Production and discovery of fullerites: new forms of crystalline carbon*, chapter 2, pages 33–38. Cambridge U. Press., 1993.

[29] Andrey Chuvilin, Ute Kaiser, Elena Bichoutskaia, Nicholas A. Besley, and Andrei N. Khlobystov. Direct transformation of graphene to fullerene. *Nature Chemistry*, 2:450–453, 2010.

[30] L. T. Scott, M. M. Boorum, B. J. McMahon, S. Hagen, J. Mack, H. Wegner J. Blank, and A. de Meijere. A rational chemical synthesis of c60. *Science*, 295:1500–1503, 2002.

[31] G. Malloci, G. Mulas, G. Cappellini, V. Fiorentini, and I. Porceddu. Theoretical electron affinities of pahs and electronic absorption spectra of their mono-anions. *A&A*, 432:585–594, 2005.

[32] Miguel A. L. Marques, Alberto Castro, Giuliano Malloci, Giacomo Mulas, and Silvana Botti. Efficient calculation of van der waals dispersion coefficients with time-dependent density functional theory in real time: Application to polycyclic aromatic hydrocarbons. *Journal of Chemical Physics*, 127:014107, 2007.

[33] Atteye H. Abdourazak, Zbigniew Marcinow, Andrzej Sygula, and Peter W. Rabideau Renata Sygula. Buckybowls 2. toward the total synthesis of buckminsterfullerene (c60): Benz[5,6]-as-indaceno[3,2,1,8,7-mnopqr]indeno[4,3,2,1-cdef]chrysene. *J. Am. Chem. Soc*, 117 (23):6410–6411, 1995.

[34] Goverdhan Mehta and Gautam Panda. Buckybowls: a simple, conceptually new synthesis of c2v-semibuckminsterfullerene (c30h12, [5,5]-fulvalene circulene). *Chemical Communications*, 21:2081, 1997.

[35] Zbigniew Marcinow, Dennis I. Grove, and Peter W. Rabideau. Synthesis of a new c32h12 bowl-shaped aromatic hydrocarbon: Acenaphtho[3,2,1,8-ijklm]diindeno[4,3,2,1-cdef:1,2,3,4-pqra]triphenylene. *Journal of Organic Chemistry*, 67:3537–3539, 2002.

[36] Hidehiro Sakurai and Taro Daiko andToshikazu Hirao. A synthesis of sumanene, a fullerene fragment. *Science*, 301:1878, 2003.

[37] Mark D. Clayton and Peter W. Rabideau. Synthesis of a new c32h12 bowl-shaped aromatic hydrocarbon. *Tetrahedron Letters*, 38:741–744, 1997.

[38] K. Y. Amsharov and M. Jansen. Formation of fullerenes by pyrolysis of perchlorofulvalene and its derivatives. *Carbon*, 45:117–123, 2007.

[39] K.Yu. Amsharov, K. Simeonov, and M. Jansen. Formation of fullerenes by pyrolysis of 1,2-binaphthyl and 1,3-oligonaphthylene. *Carbon*, 45 (2):337–343, 2007.

[40] Konstantin Yu. Amsharov and Martin Jansen. A c78 fullerene precursor: Toward the direct synthesis of higher fullerenes. *Journal Organic Chemistry*, 73 (7):2931–2934, 2008.

[41] K. Amsharov and M. Jansen. C48 buckybowl and c60 fullerne precursors on the base of truxenone. *Z. Naturforsch. B*, 62:1497–1508, 2007.

[42] Kalin S. Simeonov; Konstantin Yu. Amsharov; Martin Jansen. A fast route toward the preparative isolation of fullerene isomers c78(1) and c78(2). *Fullerenes, Nanotubes and Carbon Nanostructures*, 17 (4):341–348, 2009.

[43] Colin Crowley, Harold W. Kroto, Roger Taylor, Matthew S. Bratcher David R.M. Walton, Pei-Chao Cheng, and Lawrence T. Scott. Formation of [60]fullerene by pyrolysis of corannulene, 7,10-bis(2,2-dibromovinyl)fluoranthene, and 11,12-benzofluoranthene. *Tetrahedron Letters*, 36:9215–9218, 1995.

[44] Berta Gomez-Lor, Oscar de Frutos, and Antonio M. Echavarren. Synthesis of crushed fullerene c60h30. *Chemistry Communications*, page 2431, 1999.

[45] Berta Gomez-Lor and Antonio M. Echavarren. Synthesis of a triaza analogue of crushed-fullerene by intramolecular palladium-catalyzed arylation. *Organic Letters*, 6 (17):2993, 2004.

[46] U.Deva Priyakumar, M. Punnagai, G.P. Krishna Mohan, and G.Narahari Sastry. A computational study of cation-pi interactions interactions in polycyclic systems: exploring the dependence on the curvature and electronic factors. *Tetrahedron*, 60 (13):3037–3043, 2004.

[47] Elena Bunuel, Juan Marco-Martinez, Sergio Diaz-Tendero, Fernando Martin, Manuel Alcami, and Diego J. Cardenas. Computational studies on the cyclization of polycyclic aromatic hydrocarbons in the synthesis of curved aromatic derivatives. *ChemPhysChem*, 7 (2):475–481, 2006.

[48] T. C. Dinadayalane and G. Narahari Sastry. Isolated pentagon rule in buckybowls: a computational study on thermodynamic stabilities and bowl-to-bowl inversion barriers. *Tetrahedron*, 59 (42):8347–8351, 2003.

[49] Andrzej Sygula and Peter W. Rabideau. Structure and inversion barriers of corannulene, its dianion and tetraanion. an ab initio study. *Journal of Molecular Structure: THEOCHEM*, 333 (3):215–226, 1995.

[50] G. Narahari Sastry. Computational studies on siblings en-route to fullerenes: Study of curved polycyclic aromatic hydrocarbons. *Journal of Molecular Structure: THEOCHEM*, 771 (1-3):141–147, 2006.

[51] Toru Amaya, Hiroyuki Sakane, Takuto Nakata, and Toshikazu Hirao. A theoretical study of the bowl-to-bowl inversion of sumanene derivatives. *Pure Applied Chemistry*, 82 (4):969–978, 2010.

[52] Brian D. Steinberg, Edward A. Jackson, Alexander S. Filatov, Atsushi Wakamiya, Marina A. Petrukhina, and Lawrence T. Scott. Aromatic pi systems more curved than c60. the complete family of all indenocorannulenes synthesized by iterative microwave-assisted intramolecular arylations. *Journal of American Chemical Society*, 131 (30):10537–10545, 2009.

[53] Kwang Taeg Rim, Mohamed Siaj, Shengwiong Xiao, Matthew Myers, Vincent D. Carpentier, Li Liu, Chaochin Su, Michael L. Steigerwald, Mark S. Hybertsen, Peter H. McBreen, George W. Flynn, and Colin Nuckolls. Forming aromatic hemispheres on transition-metal surfaces. *Angewandte Chemie International Edition*, 46:7891, 2007.

[54] Roberto Felici, Maddalena Pedio, Francesco Borgatti, Salvatore Iannotta, Mario Capozi, Giuseppe Ciullo, and Andreas Stierle. X-ray-diffraction characterization of pt(111) surface nanopatterning induced by c60 adsorption. *Nature Materials*, 4:688–692, 2005.

[55] P. Hohenberg and W. Kohn. Inhomogeneous electron gas. *Physical Review*, 136:B864, 1964.

[56] W. Kohn and L. J. Sham. Quantum density oscillations in an inhomogeneous electron gas. *Physical Review*, 137:A1697, 1965.

[57] Leonard Kleinman and D. M. Bylander. Efficacious form for model pseudopotentials. *Physical Review Letter*, 48 (20):1425–1428, 1982.

[58] David Vanderbilt. Soft self-consistent pseudopotentials in a generalized eigenvalue formalism. *Physical Review B*, 41 (11):7892–7895, 1990.

[59] P. E. Blochl. Projector augmented-wave method. *Physical Review B*, 50:17953–17979, 1994.

[60] G. Kresse and J. Furthmuller. Efficient iterative schemes for ab initio total-energy calculations using a plane-wave basis set. *Physical Review B*, 54:11169, 1996.

[61] G. Kresse and D. Joubert. From ultrasoft pseudopotentials to the projector augmented-wave method. *Physical Review B*, 59:1758, 1999.

[62] Alexander A. Demkov, Jose Ortega, Otto F. Sankey, and Matthew P. Grumbach. Electronic structure approach for complex silicas. *Physical Review B*, 52 (3):1618–1630, 1995.

[63] James P. Lewis, Kurt R. Glaesemann, Gregory A. Voth, Jurgen Fritsch, Alexander A. Demkov, Jose Ortega, , and Otto F. Sankey. Further developments in the local-orbital density-functional-theory tight-binding method. *Physical Review B*, 64 (19):195103, 2001.

[64] Pavel JelÃnek, Hao Wang, James P. Lewis, Otto F. Sankey, and Jose Ortega. Multicenter approach to the exchange-correlation interactions in ab initio tight-binding methods. *Physical Review B*, 71 (23):235101, 2005.

[65] J Harris. Simplified method for calculating the energy of weakly interacting fragments. *Physical Review B*, 31 (4):1770–1779, 1985.

[66] Otto F. Sankey and David J. Niklewski. Ab initio multicenter tight-binding model for molecular-dynamics simulations and other applications in covalent systems. *Physical Review B*, 40 (6):3979–3995, 1989.

[67]

[68] Taisuke Ozaki. Variationally optimized atomic orbitals for large-scale electronic structures. *Physical Review B*, 67:155108, 2003.

[69] T. Ozaki and H. Kino. Numerical atomic basis orbitals from h to kr. *Physical Review B*, 69:195113, 2004.

[70] Hendrik J. Monkhorst and James D. Pack. Special points for brillouin-zone integrations. *Physical Review B*, 13:5188–5192, 1976.

[71] D. J. Chadi and Marvin L. Cohen. Special points in the brillouin zone. *Physical Review B*, 8 (12):5747–5753, 1973.

[72] Greg Mills and Hannes Jonsson. Quantum and thermal effects in h2 dissociative adsorption: Evaluation of free energy barriers in multidimensional quantum systems. *Physical Review Letters*, 72 (7):1124–1127, 1994.

[73] C. Kittel. *Introduction to Solid State Physics*. Wiley New York, 1971.

[74] C. Morin, D. Simon, and P. Sautet. Chemisorption of benzene on pt(111), pd(111), and rh(111) metal surfaces: A structural and vibrational comparison from first principles. *Journal of Physical Chemistry B*, 108 (18):5653, 2004.

[75] Conrad Becker, Jan Haubrich, Klaus Wandelt, Franoise Delbecq, David Loffreda, and Philippe Sautet. Adsorption of simple alkenes on pt(111) and pt-sn surface alloys: Bond strength versus heat of adsorption. *Journal of Physical Chemistry B*, 112 (38):14693, 2008.

[76] Eveline Bus, David E. Ramaker, and Jeroen A. van Bokhoven. Structure of ethene adsorption sites on supported metal catalysts from in situ xanes analysis. *Journal of the American Chemical Society*, 129 (26):8094, 2007.

[77] Florian Mittendorfer, C. Thomazeau, P. Raybaud, and H. Toulhoat. Adsorption of unsaturated hydrocarbons on pd(111) and pt(111): A dft study. *Journal of Physical Chemistry B*, 107 (44):12287, 2003.

[78] Gianluca Santarossa, Marcella Iannuzzi, Angelo Vargas, and Alfons Baiker. Adsorption of naphthalene and quinoline on pt, pd and rh: A dft study. *A European Journal of Chemical Physics and Physical Chemistry*, 9:401, 2008.

[79] J. Michael Gottfried, Ebbe K. Vestergaard, Parthasarathi Bera, , and Charles T. Campbell. Heat of adsorption of naphthalene on pt(111) measured by adsorption calorimetry. *Journal of Physical Chemistry B*, 110 (35):17539, 2006.

[80] Marc-Andr Lalibert, Stphane Lavoie, BjÃžrk Hammer, Gautier Mahieu, and Peter H. McBreen. Activation in prochiral reaction assemblies on pt(111). *Journal of American Chemical Society*, 130 (16):5386, 2008.

[81] Ole Lytken, Wanda Lew, and Charles T. Campbell. Catalytic reaction energetics by single crystal adsorption calorimetry: hydrocarbons on pt(111). *Chemical Society Review*, 37:2172, 2008.

[82] Ole Lytken, Wanda Lew, Jonathan J. W. Harris, J. Michael Gottfried Ebbe K. Vestergaard, and Charles T. Campbell. Energetics of cyclohexene adsorption and reaction on pt(111) by low-temperature microcalorimetry. *Journal of American Chemical Society*, 130 (31):10247, 2008.

[83] Takashi Yamada, Masahiro Shibuta, Yohei Ami, Yasuhiro Takano, Akihiro Nonaka, Keisuke Miyakubo, and Toshiaki Munakata. Novel growth of naphthalene overlayer on cu(111) studied by stm, leed, and 2ppe. *Journal of Physical Chemistry C*, 114 (31):13334, 2010.

[84] Vincent Demers-Carpentier, Marc-Andr Lalibert, Stphane Lavoie, Gautier Mahieu, and Peter H. McBreen. Two-dimensional self-assembly and catalytic function: Conversion of chiral alcohols into self-assembled enols on pt(111). *Journal of Physical Chemistry C*, 114 (16):7291, 2010.

[85] G. Otero, G. Biddau, C. Sanchez-Sanchez, R. Caillard, C. Rogero M. F. Lopez, F.J. Palomares, N. Cabello, M.A. Basanta, J. Ortega, J. Mendez, A.M. Echavarren, R. Perez, B. Gomez-Lor, and J. A. Martin-Gago. Fullerenes from aromatic precursors by surface-catalysed cyclodehydrogenation. *Nature*, 454:865–869, 2008.

[86] G. Otero, G. Biddau, T. Ozaki, B. Gomez-Lor, J. Mendez, R. R. Perez, and J.A. Martin-Gago. Spontaneous discrimination of pah enantiomers on a metal surface. *Chemistry European Journal*, 2010.

[87] N. Troullier and Jose Luriaas Martins. Efficient pseudopotentials for plane-wave calculations. ii. operators for fast iterative diagonalization. *Physical Review B*, 43:8861, 1991.

[88] J. Donohue. *The Structures of the Elements*. Wiley New York, 1974.

[89] C. Morin, D. Simon, and P. Sautet. Trends in the chemisorption of aromatic molecules on a pt(111) surface: Benzene, naphthalene, and anthracene from first principles calculations. *Journal of Physical Chemistry B*, 108 (32):12084, 2004.

[90] J. Tersoff and D. R. Hamann. Theory of the scanning tunneling microscope. *Physical Review B*, 31 (2):805–813, 1985.

[91] Werner A. Hofer, Adam S. Foster, and Alexander L. Shluger. Theories of scanning probe microscopes at the atomic scale. *Review Modern Physics*, 75 (4):1287 – 1331, 2003.

[92] Manabu Kiguchi. Electrical conductance of single c60 and benzene molecules bridging between pt electrode. *Applied Physics Letters*, 95:073301, 2009.

[93] S. More, W. Berndt, A. M. Bradshaw, and Ronal Stumpf. Ordered phases of potassium on pt111: Experiment and theory. *Physical Review B*, 57 (15):9246–9254, 1998.

[94] Andreas Mueller, Konstantin Yu. Amsharov, and Martin Jansen. Synthesis of end-cap precursor molecules for (6, 6) armchair and (9, 0) zig-zag single-walled carbon nanotubes. *Tetrahedron Letters*, 51 (24):3221–3225, 2010.

[95] Herve Lesnard, Marie-Laure Bocquet, , and Nicolas Lorente. Dehydrogenation of aromatic molecules under a scanning tunneling microscope: Pathways and inelastic spectroscopy simulations. *Journal of American Chemical Society*, 129 (14):4298–4305, 2007.

[96] B. P. Tarasov, V. N. Fokin, A. P. Moravsky, Yu. M. Shul'ga, and V. A. Yartys. Hydrogenation of fullerenes c60 and c70 in the presence of hydride-forming metals and intermetallic compounds. *Journal of Alloys and Compounds*, 253-254:25–28, 1997.

[97] P. Ulrich Biedermann, Sergey Pogodin, and Israel Agranat. Inversion barrier of corannulene. a benchmark for bowl-to-bowl inversions in fullerene fragments. *Journal of Organic Chemistry*, 64 (10):3655–3662, 1999.

[98] Lawrence T. Scott, Mohammed M. Hashemi, and Matthew S. Bratcher. Corannulene bowl-to-bowl inversion is rapid at room temperature. *Journal of American Chemical Society*, 114 (5):1920–1921, 1992.

[99] Huang, J. Y., Ding, F., Yakobson, and B. I. Dislocation dynamics in multiwalled carbon nanotubes at high temperatures. *Phys. Rev. Lett.*, 100(3):035503–035507, 2008.

[100] Chen, Shuo, Ertekin, Elif, Chrzan, and D. C. Plasticity in carbon nanotubes: Cooperative conservative dislocation motion. *Phys. Rev. B*, 81(15):155417, 2010.

[101] Konstantin Amsharov and Martin Jansen. Synthesis of a higher fullerene precursor an unrolled c84 fullerene. *Chemical Communications*, pages 2691–2693, 2009.

[102] Tobias N. Hoheisel, Stephen Schrettl, Ruth Szilluweit, and Holger Frauenrath. Nanostructured carbonaceous materials from molecular precursors. *Angewandte Chemie International Edition*, 49 (37):6496–6515, 2010.